

Rydberg superatoms: An artificial quantum system for quantum information processing and quantum optics

Xiao-Qiang Shao,^{1, a)} Shi-Lei Su,^{2, a)} Lin Li,^{3, a)} Rejish Nath,^{4, a)} Jin-Hui Wu,^{1, a)} and Weibin Li^{5, a)}

¹⁾Center for Quantum Sciences and School of Physics, Northeast Normal University, Changchun 130024, China

²⁾School of Physics and Laboratory of Zhongyuan Light, Key Laboratory of Materials Physics of Ministry of Education, Zhengzhou University, Zhengzhou 450001, China

³⁾MOE Key Laboratory of Fundamental Physical Quantities Measurement, Hubei Key Laboratory of Gravitation and Quantum Physics, PGMF, Institute for Quantum Science and Engineering, School of Physics, Huazhong University of Science and Technology, Wuhan 430074, China

⁴⁾Indian Institute of Science Education and Research, Pune-411008, India

⁵⁾School of Physics and Astronomy, and Centre for the Mathematics and Theoretical Physics of Quantum Non-equilibrium Systems, The University of Nottingham, Nottingham NG7 2RD, United Kingdom

(Dated: 9 April 2024)

Dense Rydberg atom ensembles display intriguing collective behaviors mediated by their strong, long-range dipole-dipole interactions. These collective effects, often modeled using Rydberg superatoms, have gained significant attention across various fields due to their potential applications in quantum information processing and quantum optics. In this review article, we delve into the theoretical foundations of Rydberg interactions and explore experimental techniques for their manipulation and detection. We also discuss the latest advancements in harnessing Rydberg collective effects for quantum computation and optical quantum technologies. By synthesizing insights from theoretical studies and experimental demonstrations, we aim to provide a comprehensive overview of this rapidly evolving field and its potential impact on the future of quantum technologies.

Contents

I. INTRODUCTION	1
II. RYDBERG ATOMS AND RYDBERG SUPERATOMS	2
A. Characteristics of Rydberg atoms	2
B. Interaction potential between Rydberg atoms	4
C. Emergence of Rydberg superatom	5
III. EXPERIMENTAL TECHNIQUES AND ADVANCES	6
A. Coherent laser excitation of Rydberg atom	6
B. Preparation of Rydberg superatom: Many-body Rabi oscillation	8
C. Quantum interface and coherence property	9
IV. APPLICATIONS IN QUANTUM INFORMATION PROCESSING	12
A. Quantum logic gate	12
B. Quantum entanglement	14
C. Quantum simulation	16
V. APPLICATIONS IN QUANTUM OPTICS	18
A. Nonlocal nonlinear optics	18
B. Single-photon engineering	20
C. Hybrid Rydberg system	22

VI. CONCLUSION AND OUTLOOK

24

I. INTRODUCTION

Rydberg atoms exhibit striking properties that arise from their exaggerated atomic size and strong interatomic interactions.^{1–3} The large electric dipole moment couples with external electric fields, allowing the manipulation of the electronic as well as motional states of Rydberg atoms with laser and microwave (MW) fields. On the other hand, strong and long-range dipole-dipole or van der Waals interactions between Rydberg atoms are found even when they are separated by macroscopic distances.^{4,5} Such interactions, moreover, can be controlled additionally by laser or MW fields. This paves the way for realizing scalable quantum information processing architectures,⁶ and exploring novel many-body states⁷ and nonlinear quantum optics.⁸

At the heart of the Rydberg physics lies strong interaction-induced collective behaviors,^{9–11} such as the Rydberg blockade.¹² In high-lying Rydberg states, the interatomic interaction ($1 \sim 100$ MHz) can be much stronger than typical laser Rabi frequencies (tens of kHz \sim a few MHz). As a result, the laser excitation of one atom inhibits the excitation of neighboring atoms within a certain distance (i.e. blockade radius). Rydberg blockade becomes the foundation of many quantum gate schemes.^{3,6,12} Within the blockade radius, the many-body ground state and singly excited Rydberg state can be excited. The former consists of atoms in the electronic ground state, while the latter is a collective state where one atom is in the Rydberg state while all other atoms are in the electronic ground state. Dynamics of such collective states are conveniently described by an artificial *superatom*.¹² This description can be extended to many-atom

^{a)}Authors to whom correspondence should be addressed: shaoxq644@nenu.edu.cn; slsu@zzu.edu.cn; li_lin@hust.edu.cn; rejish@iiserpune.ac.in; jhhu@nenu.edu.cn; and weibin.li@nottingham.ac.uk

settings, where the collective effect allows for the creation of exotic many-body correlated states.^{13–18} These potentials make Rydberg atoms a leading candidate for implementing quantum simulation and quantum computing tasks. Moreover, strong Rydberg atom interactions can be mapped to optical fields, generating sizable optical nonlinearities.¹⁹ These have found wide usage in exploring nonlinear quantum optics^{8,20} and realizing optical quantum devices, such as single-photon sources,^{21–25} photonic quantum logic gates,^{26–28} photonic entanglement filter,²⁹ single-photon absorber,³⁰ single-photon switch,³¹ and transistors.^{31,32}

In this review article, we will delve into the theory underpinning of the Rydberg superatom, related collective effects and key experimental achievements. In particular, we will review the harness of Rydberg collectivity in two critical areas: quantum information processing and quantum optics. We start with the introduction of Rydberg atoms and Rydberg superatoms in Sec. II. The atomic properties and two-body interactions of Rydberg atoms, and the emergence of the collective states described by Rydberg superatoms, are discussed. In Sec. III, coherent laser excitation of Rydberg atoms and the preparation of Rydberg superatoms are given. Quantum interference of Rydberg superatoms is discussed. In Sec. IV, quantum information processing based on Rydberg superatoms and collective effects are discussed. We focus on the creation of quantum logic gates, entanglements, and simulations using Rydberg atoms. We describe the application of the Rydberg atom systems in quantum optics in Sec. V, including the demonstration and realization of strong nonlocal nonlinear optics, single-photon applications, and hybridizing quantum systems with Rydberg interactions and superatoms. Finally, we conclude in Sec. VI.

II. RYDBERG ATOMS AND RYDBERG SUPERATOMS

A. Characteristics of Rydberg atoms

In a broad sense, a Rydberg atom can be defined as an atom with one of its valence electrons in a highly excited state characterized by a large principal quantum number. The category of “atoms” that exhibit this characteristic includes alkali atoms,^{1,3,33} alkaline earth atoms,^{34–44} trapped ions,^{45–51} as well as solid state systems.^{52–54} Since alkali atoms possess only one valence electron, their properties in the Rydberg state closely resemble those of a hydrogen atom. This allows us to derive the distinctive properties of alkali Rydberg atoms using, for example, the quantum defect theory.^{1,2} The binding energy of the Rydberg states of alkali atoms (e.g., Rb and Cs) with the principal quantum number n , orbital angular momentum l , and total angular momentum $j = l \pm 1/2$ can be expressed as

$$E_{n,l,j} = -\frac{hcR_m}{(n - \delta_{n,l,j})^2}. \quad (1)$$

Here, $R_m = R_\infty/(1 + m_e/m_{\text{nucleus}})$ represents the mass-corrected Rydberg constant, where m_e denotes the electron

TABLE I. Quantum defect constants δ_0 , δ_2 , δ_4 , and δ_6 for different orbital angular momentum l of Rb and Cs extracted from Refs. 56, 58, 61, 66, 69, and 70.

Rydberg series	δ_0	δ_2	δ_4	δ_6
⁸⁵ Rb $nS_{1/2}$	3.1311804 ⁶¹	0.1784 ⁶¹	-1.8 ⁵⁶	
⁸⁵ Rb $nP_{3/2}$	2.64142 ⁶⁹	0.295 ⁶⁹	0.97495 ⁵⁶	14.6001 ⁵⁶
⁸⁵ Rb $nD_{5/2}$	1.3464572 ⁶¹	-0.596 ⁶¹	-1.50517 ⁵⁶	-2.4206 ⁵⁶
⁸⁵ Rb $nF_{7/2}$	0.016411 ⁶⁹	-0.0784 ⁶⁹	-0.36005 ⁵⁶	3.2390 ⁵⁶
¹³³ Cs $nS_{1/2}$	4.0493532 ⁶⁶	0.23915 ⁶⁶	0.06 ⁶⁶	11 ⁶⁶
¹³³ Cs $nP_{3/2}$	3.5590676 ⁶⁶	0.37469 ⁶⁶	-0.67431 ⁵⁸	22.3531 ⁵⁸
¹³³ Cs $nD_{5/2}$	2.4663144 ⁶⁶	0.01381 ⁶⁶	-0.392 ⁶⁶	-1.9 ⁶⁶
¹³³ Cs $nF_{7/2}$	0.0335646 ⁷⁰	-0.2052 ⁷⁰		

mass and m_{nucleus} refers to the atomic mass of the nucleus. The term $R_\infty = m_e e^4 / (8\epsilon_0^2 h^3 c)$ is the Rydberg constant, where e is the elementary charge, ϵ_0 denotes the permittivity of the vacuum, h represents the Planck constant, c stands for the speed of light in vacuum.^{2,55} Furthermore, the species-dependent quantum defect, denoted as $\delta_{n,l,j}$, can be approximated by the modified Rydberg-Ritz parameters

$$\delta_{n,l,j} = \delta_0 + \frac{\delta_2}{(n - \delta_0)^2} + \frac{\delta_4}{(n - \delta_0)^4} + \frac{\delta_6}{(n - \delta_0)^6} + \dots, \quad (2)$$

where the coefficients δ_0 , δ_2 , δ_4 , and δ_6 are primarily depends on l (while also being related to j) and remains non-negligible solely for states with $l \leq 3$.^{2,56} Precise understanding of the quantum defect is paramount for anticipating spectral lines, comprehending electron behavior in highly excited states, and probing the boundaries of quantum mechanics. This imperative has led researchers to pursue quantum defect parameters of Rydberg atoms with high precision through various methodologies.^{1,57–70} In Table I, we present a comprehensive compilation of modified Rydberg-Ritz parameters for low orbit states in Rb and Cs atoms. This compilation incorporates data from early seminal work and recent measurements. For additional orbitals or other alkali atoms, their quantum defects can be easily obtained using two recently released open-source software packages, pairinteraction⁷¹ and Alkali Rydberg Calculator (ARC) toolbox.⁷²

Starting from the expression for Rydberg’s binding energy, we can obtain a series of scaling laws that exhibit exaggerated characteristics concerning the principal quantum number n , or more precisely, the effective principal quantum number $n^* = (n - \delta_{n,l,j})$. The energy spacing between adjacent Rydberg levels is given by

$$\Delta E = E_{n+1,l+1,j} - E_{n,l,j} \approx \frac{2hcR_m[(\delta_{n,l,j} - \delta_{n,l+1,j}) + 1]}{n^{*3}}, \quad (3)$$

which follows a n^{*-3} scaling. The corresponding transition wavelength typically falls within the millimeter-wave band between 10 mm (30 GHz) and 1 mm (300 GHz). This feature offers exceptional precision in spectroscopic measurements,^{73,74} showing transient amplifiers of microwave radiation^{75–77} and contributing to the development of the fifth generation mobile communication network.^{78,79} It

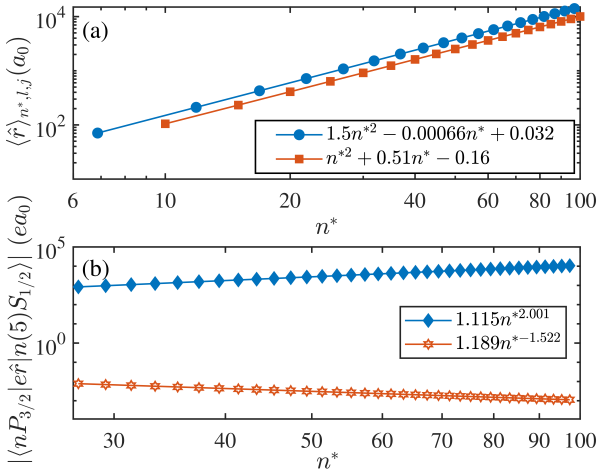


FIG. 1. (a) The numerical data demonstrates the scaling laws for the average orbit radius of Rydberg atoms in the S orbit (blue) and circular orbit (red), expressed in terms of the effective principal quantum number denoted as n^* for each case. (b) The scaling laws govern the radial dipole matrix elements for transitions between neighboring Rydberg states, denoted as $|\langle nP_{3/2} | \hat{e}r | nS_{1/2} \rangle|$ (blue), as well as for transitions between a low-lying state and a Rydberg state, represented as $|\langle nP_{3/2} | \hat{e}r | 5S_{1/2} \rangle|$ (red), where $n^* = n - \delta_{n,2,j}$ for the P orbit.

serves a crucial role in the advancement of atomic physics and quantum science research.^{80–87}

The average radius of the electron orbit, determined by the radial wave function for a Rydberg state, is given by,

$$\langle \hat{r} \rangle_{n^*,l,j} = \frac{1}{2}[3n^{*2} - l(l+1)]a_0, \quad (4)$$

where $a_0 \approx 5.29 \times 10^{-2}$ nm represents the Bohr radius.^{2,88} This formula offers an exact description of the radius of Rydberg atomic orbitals with high principal quantum numbers, as the Coulomb potential predominates in this regime. The Rydberg atomic-wave function, influenced by quantum defects, deviates from that of the hydrogen atom mainly by a phase shift. As a result, the average value of physical quantities can be directly derived from the hydrogen atom formula, with the only alteration being the substitution of the principal quantum number n with the effective principal quantum number n^* .^{52,54} For low l states, particularly $l = 0$ (S states), the average radius simplifies to be $3n^{*2}a_0/2$, but for the circular orbit with $l = n - 1$, where the quantum defect is zero, the value becomes $(n^2 + n/2)a_0$. For large n the radius of the Rydberg electron can be hundreds of nanometers. This permits the formation of ultra-long range Rydberg molecules,^{89–104} where ground state atoms are trapped within the Rydberg electron cloud. In Fig. 1(a), the ARC toolbox⁷² is used to perform numerical calculation of the average radii for the S and circular orbits of Rubidium, encompassing the principal quantum number n from 10 to 100. The data exhibit quadratic scaling with n^* , closely aligning with the analytical expression.

Electric dipole transitions $\langle n', l', j' | \hat{e}r | n, l, j \rangle$ between Rydberg atomic states are also characterized by elements of the

radial matrix $\int R_{n',l',j'}(r)erR_{n,l,j}(r)r^2dr$ together with the angular components.¹⁰⁵ These elements show a scaling of n^{*2} for adjacent Rydberg states ($n' \approx n$), consistent with the behavior of the orbital radius. Moreover, it scales with $n^{*-1.5}$ for transitions between a low-lying state and a Rydberg state ($n' \ll n$), due to the smaller overlap of the radial wave function, where low-lying states localize around the ion core.^{1,106} These scaling laws find an intuitive representation in Fig. 1(b), where we have specifically chosen the elements of the dipole radial matrix $|\langle nP_{3/2} | \hat{e}r | nS_{1/2} \rangle|$ and $|\langle nP_{3/2} | \hat{e}r | 5S_{1/2} \rangle|$ as illustrative examples. The other properties of the Rydberg states, such as their spontaneous decay rate and response to electric fields, are closely related to these dipole matrix elements.

The spontaneous decay rate from $|n, l, j\rangle$ to lower lying state $|n', l', j'\rangle$ considering the fine structure in SI units is governed by the Einstein coefficient:

$$A_{nlj \rightarrow n'l'j'} = \frac{2\omega_{n'l'j',nlj}^3}{3\epsilon_0 hc^3} (2j'+1)l_{\max} \left\{ \begin{array}{c} l, l', 1 \\ j', j, 1/2 \end{array} \right\}^2 \times |\langle n', l', j' | \hat{e}r | n, l, j \rangle|^2, \quad (5)$$

where $\omega_{n'l'j',nlj}$ designates the corresponding transition angular frequency, l_{\max} signifies the larger of the two values between l and l' , and the curly braces indicate a Wigner-6j symbol.^{107,108} For low angular momentum states, Rydberg states can decay to many low-lying states through dipole transitions. At zero temperature, the decay rate is proportional to n^{*-3} . However, in circular Rydberg states ($l = n - 1$), they can only undergo a transition to an adjacent Rydberg state via a dipole-allowed process.^{109,110} This leads to the spontaneous emission rate of the circular state being proportional to n^{*-5} . In all the situations, long lifetimes of Rydberg atoms are found, which are important for maintaining quantum coherence, a crucial factor for quantum computation and simulation.

Compared to the high l states, the quantum defects of the low $l \leq 3$ states have a greater impact on the energy levels correction. Consequently, the weak external electric field will not cause the Rydberg atom in the low orbit state to endure a direct transition between the adjacent orbits but will instead present the energy level shift as a second-order perturbation, which is in the form of a quadratic Stark effect¹¹¹

$$\Delta E_{\text{Stark}} = \sum_{n',l',j' \neq n,l,j} \frac{|\langle n', l', j' | \hat{e}r \cdot \mathbf{E} | n, l, j \rangle|^2}{E_{n',l',j'} - E_{n,l,j}} = \frac{1}{2} \alpha_0 E^2 \quad (6)$$

where we have assumed a static electric field E is applied along the z -axis creating off-diagonal couplings between states, with the selection rule $\Delta l = \pm 1$, $\Delta m_j = 0$. As determined by the Wigner-Eckart theorem,¹¹² the dipole matrix elements are linked to the radial matrix elements $\langle n', l', j' | \hat{e}r | n, l, j \rangle$ through coefficients independent of the principal quantum number. Therefore, the scalar polarizability α_0 scales with n^{*7} due to the combined scaling of the radial dipole matrix element and the energy spacing for neighboring Rydberg states in the denominator.^{113–117} It should be noted that states possessing quantum numbers of angular momentum $l > 3$ manifest degeneracy, leading to a linear Stark shift.

TABLE II. Scaling of various properties of Rydberg atoms with the effective principal quantum numbers n^* . The data in the parentheses are scaling in the circular state.

Property	Expression	n^* scaling
Binding energy	$E_{n,l,j} = -\frac{\hbar c R_m}{(n-\delta_{n,l,j})^2}$	n^{*-2}
Level spacing	$E_{n+1,l+1,j} - E_{n,l,j}$	n^{*-3}
Orbit radius	$\langle \hat{r} \rangle_{n^*,l,j} = \frac{1}{2} [3n^{*2} - l(l+1)]a_0$	n^{*2}
Dipole moment	$\langle nP_{3/2} e\hat{r} n(5)S_{1/2} \rangle$	$n^{*2} (n^{*-1.5})$
Transition rate	$A_{nlj \rightarrow n'l'j'} = \alpha_0$	$n^{*-3} (n^{*-5})$
Scalar polarizability		n^{*7}

For a more precise description of the Stark structure of the Rydberg states in alkali atoms, direct diagonalization of the energy matrix is required. The high polarizability of Rydberg atoms can be exploited as highly accurate sensors for electric fields^{118–132} and the nondestructive imaging of atoms and ions.^{133,134}

In Table II, a concise overview is presented, detailing the scaling behavior of various properties in Rydberg atoms with respect to the effective principal quantum number. A comprehensive exploration of additional Rydberg atom properties and associated mechanisms can be found in numerous recent review articles and references therein.^{3,7,135–145}

B. Interaction potential between Rydberg atoms

The interaction potential between Rydberg atoms manifests as an electrostatic interaction, which can be expressed as an infinite series of powers involving the inverse of the interatomic distance R .¹⁴⁶ The predominant component is represented by the lowest-order dipole terms^{6,147}

$$\hat{V}_{int} = \frac{1}{4\pi\epsilon_0} \left[\frac{\hat{d}_1 \cdot \hat{d}_2 - 3(\hat{d}_1 \cdot \mathbf{n})(\hat{d}_2 \cdot \mathbf{n})}{R^3} \right], \quad (7)$$

where $\hat{d}_i = -e\hat{r}_i$ is the electric dipole operator of atom i ($i = 1, 2$), and \mathbf{n} denotes the unit vector connecting the two atoms. Without loss of generality, the polar angle between the quantization axis z and \mathbf{n} is set to θ , and the azimuthal angle is ϕ . In the spherical basis, the electric dipole-dipole interaction can be expressed as

$$\begin{aligned} \hat{V}_{int} = & \frac{1}{4\pi\epsilon_0 R^3} \left[\frac{1-3\cos^2\theta}{2} (\hat{d}_1^+ \hat{d}_2^- + \hat{d}_1^- \hat{d}_2^+ + 2\hat{d}_1^0 \hat{d}_2^0) \right. \\ & + \frac{3}{\sqrt{2}} \sin\theta \cos\theta (\hat{d}_1^+ \hat{d}_2^0 e^{i\phi} - \hat{d}_1^- \hat{d}_2^0 e^{-i\phi} + \hat{d}_1^0 \hat{d}_2^+ e^{i\phi} \\ & \left. - \hat{d}_1^0 \hat{d}_2^- e^{-i\phi}) - \frac{3}{2} \sin^2\theta (\hat{d}_1^+ \hat{d}_2^+ e^{2i\phi} + \hat{d}_1^- \hat{d}_2^- e^{-2i\phi}) \right] \end{aligned} \quad (8)$$

where $\hat{d}^0 = \hat{d}^z$, $\hat{d}^+ = -(\hat{d}^x + i\hat{d}^y)/\sqrt{2}$, and $\hat{d}^- = (\hat{d}^x - i\hat{d}^y)/\sqrt{2}$, which correspond to changes in magnetic quantum number of $\Delta m_j = 0, +1$, and -1 , respectively, in the process of atomic transition. This formula enables us to construct typical interaction forms for the Rydberg atom system. In the

following, we will discuss different interaction types encountered in Rydberg atom experiments.

The spin-exchange interaction naturally occurs between two atoms in the quantum states of adjacent orbitals. As exemplified in Ref. 148, considering a pair of Rydberg states for ^{87}Rb atoms, denoted as $|\uparrow\rangle = |62D_{3/2}, m_j = 3/2\rangle$ and $|\downarrow\rangle = |63P_{1/2}, m_j = 1/2\rangle$, in the basis of two atoms $\{|\uparrow\uparrow\rangle, |\uparrow\downarrow\rangle, |\downarrow\uparrow\rangle, |\downarrow\downarrow\rangle\}$, only the first line of Eq. (8) is applicable due to the selection rules that govern the dipole operator. Consequently, the interaction Hamiltonian is,

$$\hat{H}_{\text{spin}} = \frac{(1-3\cos^2\theta)}{2} \frac{C_3}{R^3} (|\uparrow\downarrow\rangle\langle\downarrow\uparrow| + \text{H.c.}), \quad (9)$$

where H.c. stands for the Hermitian conjugate and the real coefficient $C_3 = \langle\uparrow\downarrow|\hat{d}_1^+ \hat{d}_2^-|\uparrow\downarrow\rangle/(4\pi\epsilon_0)$. This Hamiltonian was initially employed to examine the coherent dynamics of a spin excitation in a chain comprising three Rydberg atoms with $\theta = 0$.^{148,149} Subsequently, it was extended to simulate a topological model protected by symmetry in a zigzag configuration of Rydberg atoms, with the magic angle $\theta \approx 54.7^\circ$ governing the hopping direction along the next nearest neighbor atoms.¹⁸ Additionally, it was utilized to synthesize a density-dependent Peierls phase employing three Rydberg atoms arranged in an equilateral configuration with $\theta = \pi/2$.¹⁵⁰ Furthermore, this model finds application in the simulation of energy transport¹⁵¹ and various generic spin chain models.^{152–158}

The Förster resonance explores the resonant interaction between a pair of Rydberg states and other degenerate or quasi-degenerate energy levels under the dipole-dipole interaction described by Eq. (8). Even if a small energy defect exists, it can be mitigated by the differential Stark effect induced by external electric fields.^{159,160} The mathematical expression closely resembles Eq. (9), differing only in the composition of the bases. Experimental observations indicate that in the presence of a modest electric field ($F_{\text{res}} \approx 33$ mV/cm), resonance occurs between the state $|dd\rangle$ and the symmetric state $|pf_1\rangle_s = (|pf_1\rangle + |f_1p\rangle)/\sqrt{2}$ of two ^{87}Rb atoms,^{161,162} where $|d\rangle = |59D_{3/2}, m_j = 3/2\rangle$, $|p\rangle = |61P_{1/2}, m_j = 1/2\rangle$ and $|f_1\rangle = |57F_{5/2}, m_j = 5/2\rangle$. Therefore, this interaction channel is effectively isolated from other interaction channels at an interatomic distance $R = 9.1$ μm in the presence of a 3.3 G magnetic field. The corresponding Hamiltonian is given by

$$\hat{H}_{\text{Förster}} = \frac{(1-3\cos^2\theta)}{\sqrt{2}} \frac{C_3}{R^3} (|dd\rangle_s \langle pf_1| + \text{H.c.}), \quad (10)$$

with the measured $C_3/h = 2.39 \pm 0.03$ GHz μm^3 . A more systematic study of Förster resonance involving different atomic species can be found in Ref. 163, and the Stark-tuned three-body Förster resonances have been predicted¹⁶⁴ and observed.^{165,166} By integrating adiabatic rapid passage and Landau-Zener control with Förster resonance tuning, robust two-qubit quantum logic gates can be achieved.^{167–169} Additionally, a recent experimental breakthrough has demonstrated an ultrafast Förster oscillation capable of performing a conditional phase gate on nanosecond timescales.¹⁷⁰

In the absence of an external electric field, the energy difference defined by $\Delta_{r',r''} = E_{r'} + E_{r''} - 2E_r$ of the Rydberg

atom pair in the Förster resonance process greatly exceeds the strength of the dipole-dipole interaction when the atoms are at a significant distance from each other (perturbation theory is applicable). Here, E_r represents the energy of the Rydberg state $|r\rangle$ of interest, while $E_{r'}$ and $E_{r''}$ denote the energies of a pair of Rydberg states $|r'\rangle$ and $|r''\rangle$, whose symmetric state is dipole coupled to the Rydberg pair state $|rr\rangle$. This leads to a multichannel-induced Stark shift in the energy levels of the atom pair, resulting in the interaction between the atoms manifesting as a classical van der Waals interaction,^{3,171} represented by

$$\hat{H}_{\text{vdw}} = -\frac{C_6}{R^6} |rr\rangle\langle rr|. \quad (11)$$

Here, C_6 is defined as $C_6 = \sum_{r'r''} |\langle r'r''| \hat{V}_{\text{int}} |rr\rangle|^2 / \Delta_{r',r''}$, where in principle $|r'r''\rangle$ encompasses all pair states dipole coupled to $|rr\rangle$. However, for practical computational efficiency, focusing on quantum states within a specific range of energy differences allows one to obtain sufficiently accurate values C_6 . When the interatomic distance is not significantly large and perturbation theory is not applicable, it becomes crucial to perform the diagonalization of the Hamiltonian governing the pair-state interaction. Experimentally, the coefficients $|C_6|$ for $|nD_{3/2}, m_j = 3/2\rangle$ of the ^{87}Rb atom with $n = 53, 62$, and 82 are measured directly between two isolated single Rydberg atoms separated by a controlled distance of a few micrometers,¹⁷² and the angular dependence of the effective interaction energy of the two $82D_{3/2}$ ($82S_{1/2}$) atoms is also demonstrated.¹⁷³ Recently, with the advancement of experimental techniques enabling the precise arrangement of a large number of atoms in defect-free programmable geometric configurations across various dimensions, the van der Waals-type Rydberg interaction has found applications in simulating large-scale Ising-type quantum spin models,^{174–181} generating and manipulating Schrödinger cat states,¹⁸² designing frustrated magnets,^{183,184} and exploring nonequilibrium physics.^{185–188}

C. Emergence of Rydberg superatom

In the fields of chemistry and atomic physics, the concept of a superatom is used to characterize a cluster of atoms that exhibits collective behavior and possesses characteristics distinct from its constituents.^{189–191} These superatoms possess unique electronic structures and reactivity,^{192,193} making them highly compelling for a wide range of applications in materials science and nanotechnology.^{194–196} Similarly, a Rydberg superatom denotes a collectively excited state of an ensemble of N atoms, where the atoms exhibit such high correlation that only a single excitation is permitted, a phenomenon known as the Rydberg blockade.⁶ In a two-body system, this blockade effect can be achieved using either the Förster resonance or van der Waals interaction, as confirmed by experimental observations.^{4,5,197,198} However, in a many-body system, the construction of a Rydberg superatom is typically facilitated by the Rydberg interaction in the form of a pairwise additive van der Waals potential.^{9–11,199,200} This is particularly true for the

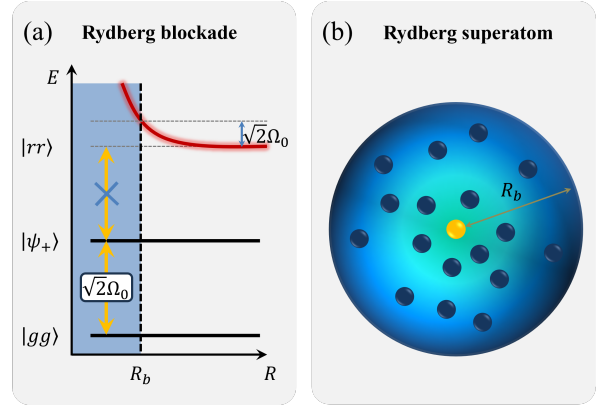


FIG. 2. (a) Rydberg blockade mechanism. The double excitation of the Rydberg state $|rr\rangle$ is inhibited within the blockade radius R_b owing to the large energy shift induced by the strong repulsive interaction. (b) Schematic view of a Rydberg superatom comprised of N atoms sharing a single Rydberg excitation enclosed within a blockade sphere.

Rydberg- S state, which possesses only one repulsive branch in its molecular potential, preventing a breakdown of the Rydberg blockade.^{159,176,201–203} Here, we will provide a concise theoretical analysis of the mechanism and associated properties of Rydberg superatoms. Detailed explanations of the experimental procedures and their applications in quantum information and quantum optics will be discussed in the following sections.

Consider an ensemble of N two-level atoms, with ground state $|g\rangle$ and Rydberg state $|r\rangle$, being illuminated by a resonant laser field characterized by a Rabi frequency Ω_0 . In the interaction picture, the Hamiltonian of the system reads

$$\hat{H}_I = \sum_{i=1}^N \frac{\hbar\Omega_0}{2} |g_i\rangle\langle r_i| + \text{H.c.} - \frac{1}{2} \sum_{i \neq j} \frac{C_6}{R_{ij}^6} |r_i r_j\rangle\langle r_i r_j|, \quad (12)$$

where a negative value of C_6 denotes repulsive van der Waals interactions, while a positive value signifies attractive interactions. At the same time, for the sake of simplification, we temporarily disregard the impact of atomic position and motion on the relative phase between individuals. Under the influence of Eq. (12), if all atoms in the ensemble are initially set in the ground state $|G\rangle = |g_1, g_2, \dots, g_N\rangle$, they will collectively transition to a symmetric single atom excitation state, assuming $C_6/R_{ij}^6 \gg \hbar\Omega_0$. The critical interatomic distance denoted the Rydberg blockade radius and expressed as $r_b = [C_6/(\hbar\Omega_0)]^{1/6}$,^{7,9} plays a crucial role. Within this range, a single excitation of a Rydberg atom can impede the excitation of a second atom, defining the upper limit of the blockade range. When considering the collective excitation of two atoms, as shown in Fig. 2(a), the associated collective blockade radius is defined as $R_b = [C_6/(\hbar\sqrt{2}\Omega_0)]^{1/6}$.²⁰⁴ Within this modified range, Rydberg atoms manifest a robust repulsive interaction, constraining excitation to a single excited symmetric state $|\psi_+\rangle = (|gr\rangle + |rg\rangle)/\sqrt{2}$ for the pair of atoms, assuming both atoms are driven with same Rabi frequency. An offset in Rabi frequencies of two atoms may freeze the dynamics in

a single atom, inhibiting the creation of the collective single excited state.²⁰⁵ Expanding the system to the collective excitation of N atoms, the collective blockade radius should be calculated as $R_b = [C_6/(\hbar\sqrt{N}\Omega_0)]^{1/6}$. The corresponding collective state is represented by

$$|R\rangle = \frac{1}{\sqrt{N}} \sum_{i=1}^N |g_1, g_2, g_3, \dots, r_i, \dots, g_N\rangle, \quad (13)$$

where all atoms share a single Rydberg excitation. Fig. 2(b) presents a schematic representation of a Rydberg superatom. This artificial atom comprises two effective levels: the ground state $|G\rangle$ and the collective excited state $|R\rangle$, connected by a coupling strength of $\sqrt{N}\Omega_0$. We note that the excited state of the Rydberg superatom is itself a multiparticle W state with maximum entanglement.²⁰⁶ This entangled state holds significant relevance in quantum information processing.^{207–209} Recent experiments have demonstrated its robustness to both particle loss and external electric field noise, particularly as a logical qubit.^{210,211} Therefore, the emergent properties of a Rydberg superatom are derived from the collective behavior of its constituent atoms rather than from the properties of individual atoms alone. These properties encompass enhanced nonlinear optical responses and strong light-matter coupling, both of which hold promise for applications in quantum information processing and quantum optics. As the Rydberg superatom system progresses to the forefront of quantum science, it demonstrates the potential to revolutionize various technological domains, including quantum computing and advanced materials engineering. Ongoing research in this field explores various experimental techniques and theoretical models to comprehend and manipulate the behavior of Rydberg superatoms.

In the context of the Rydberg atom system, along with the Rydberg blockade, phenomena such as the Rydberg antiblockade,^{116,212,213} Rydberg dressing,^{15,214–219} ground state blockade,^{220,221} and unconventional Rydberg pumping are encountered.^{222,223} While these approaches diversify how Rydberg atoms interact, they fall outside the purview of Rydberg superatoms and, therefore, lie beyond the scope of our discussion here.

III. EXPERIMENTAL TECHNIQUES AND ADVANCES

A. Coherent laser excitation of Rydberg atom

An essential step in Rydberg experiments is the preparation of Rydberg atoms. The utilization of lasers offers high-resolution, coherent, and efficient excitation of Rydberg states. After the invention of tunable dye lasers, Rydberg laser spectroscopy with resolution ~ 0.1 nm was demonstrated in 1973.^{224,225} The spectral resolution was improved to ~ 10 GHz in 1979. In 2003, Rydberg Autler-Townes spectra with MHz resolution were studied with narrow linewidth lasers.²²⁶

The laser fields used for Rydberg excitation must be intense enough to guarantee a fast excitation within the Rydberg lifetime and coherence time. The natural lifetimes of high-lying

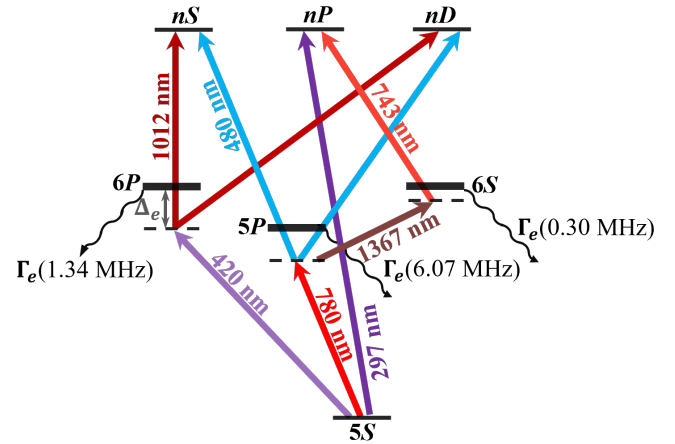


FIG. 3. Different Rydberg laser excitation schemes for ^{87}Rb atom. 297 nm UV laser can couple the ground state $5S$ and the Rydberg state nP . 780 nm (420 nm) and 480 nm (1012 nm) lasers can excite atoms from $5S$ to nS or nD via an intermediate state $5P$ ($6P$) with intermediate detuning Δ_e . Due to the finite lifetime of the intermediate states, atoms in these states decay with a rate of Γ_e , which is one of the main sources of error in the two-photon excitation scheme. Using the intermediate states $5P$ and $6S$, atoms can be excited to the nP Rydberg states using the 780 nm, 1367 nm, and 743 nm lasers.

Rydberg states are mainly limited by spontaneous emission and black-body radiation (BBR), and can last more than hundreds of microseconds. However, the Rydberg-ground coherence times are usually about a few to tens of microseconds, limited by many decoherence channels, such as the Doppler effect, density-dependent phase shift, fluctuating background electric fields, etc. Therefore, the Rabi frequencies of the excitation laser have to be large, usually on the orders of MHz, to ensure coherent excitations. Such large Rabi frequencies require intense light sources for highly excited Rydberg states since the dipole matrix elements between the ground and Rydberg states decrease with the principal quantum number as $n^{-1.5}$. In Rydberg tweezer array experiments, it has been shown that a larger Rabi frequency is crucial for high-fidelity operations within the finite ground-Rydberg coherence.²²⁷ In a Rydberg superatom containing N atoms, the effective ground-Rydberg Rabi frequency is improved by a factor of \sqrt{N} due to collective enhancement effects.

Given the considerable energy gaps between the ground and Rydberg states, direct ground-to-Rydberg transition frequencies typically fall within the ultra-violet (UV) range.²²⁸ Taking Rubidium atoms as an example, lasers with ~ 297 nm wavelength can promote atoms from the $5S$ ground state to the nP Rydberg states.²²⁹ Coherent manipulation between the ground and Rydberg states using a UV laser was demonstrated in Fig. 3, see Ref. 230. The single photon UV scheme is ideal for realizing the Rydberg dressing and has also been used in the Rydberg-ground state quantum memory.²³¹

To avoid the use of UV Rydberg lasers, a commonly adopted scheme involves an intermediate state and use two-photon Rydberg excitation, as shown in Fig. 3. With the 780 nm - 480 nm (420 nm - 1012 nm) two-photon scheme, the

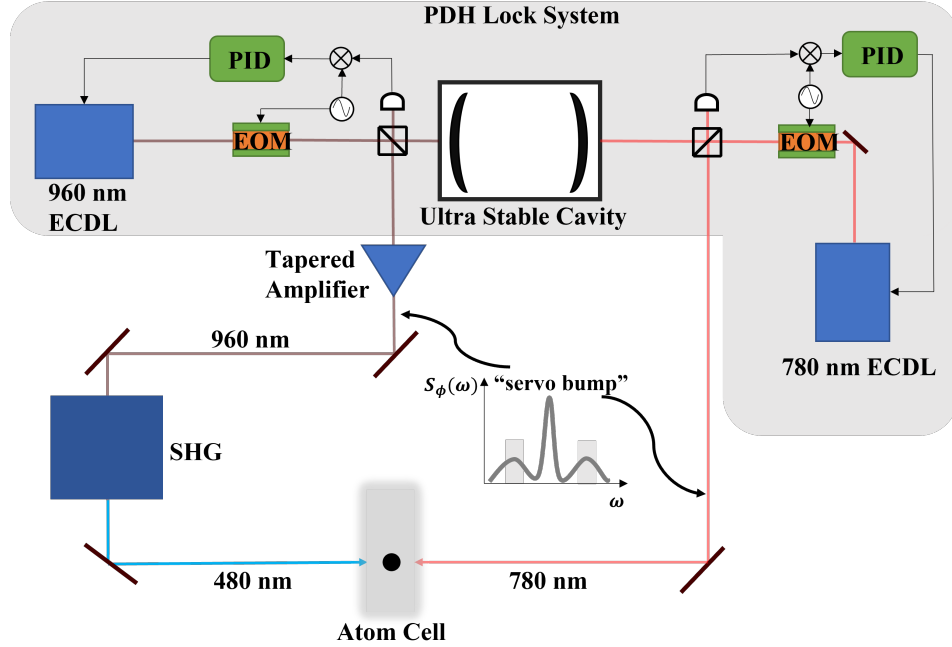


FIG. 4. Laser setup of 480 nm and 780 nm lasers used in ^{87}Rb Rydberg excitation. The 780 nm and 960 nm lasers are obtained from external cavity diode lasers (ECDLs). Both lasers are frequency locked to a high finesse, ultra-stable cavity using the Pound-Drever-Hall (PDH) locking technique, which generates “servo bump” due to the limited stabilization bandwidth. Frequency doubling of the power-amplified (using the tapered amplifier) 960 nm laser in the second harmonic generator (SHG) generates blue light at 480 nm. The 780 nm and 480 nm laser beams excite the atoms in a counterpropagating configuration to minimize the Doppler effect.

ground state Rb atom can be excited to the nS or nD Rydberg states. Fig. 4 shows the laser setup for the 780 nm - 480 nm scheme. The 780 nm light field can be easily obtained from a commercially available external cavity diode laser (ECDL), while the 480 nm light comes from a second-harmonic-generator (SHG) seeded by power-amplified 960 nm laser light. To achieve a strong blockade effect, the laser linewidth must be narrow enough compared to the Rydberg interactions. Therefore, both 780 nm and 960 nm ECDLs are frequency stabilized to an ultralow expansion cavity with high finesse to guarantee narrow linewidth. However, the Pound-Drever-Hall (PDH) laser locking technique leads to large “servo bumps” outside the stabilization bandwidth, which could cause severe decoherence during laser excitation. To suppress this noise, cavity-filtering²³² or active feedforward techniques²³³ can be used.

Besides the above-mentioned single and two-photon schemes, three-photon Rydberg laser excitation is also possible. A technical advantage of the three-photon protocol is that it is possible to choose certain intermediate states, such that all of the lasers involved in the excitation are in the near-infrared (NIR) regime. For ^{87}Rb , as shown in Fig. 3, lasers at 780 nm, 1367 nm, and 743 nm can be used for Rydberg excitation through two intermediate states $5P$ and $6S$. Furthermore, by carefully arranging the direction of the excitation lasers, Doppler-free Rydberg excitation can be achieved using the three-photon scheme.²³⁴

The Rydberg excitation fidelity is affected by various decoherence and loss mechanisms. For the single-photon scheme,

a major source of errors in coherent excitation between ground and Rydberg states is the Doppler effect due to atomic motions, which results in a random detuning $\delta = kv$, where v is the velocity of the atom along the wave vector of the laser beam k . Limited by the available UV laser power and the small dipole moment between the ground and Rydberg states, the Rabi frequency of the single-photon excitation Ω_{297} is on the order of a few MHz. As shown in Fig. 5(a), the ground-Rydberg states π -pulse excitation error exceeds a few percent for an atomic temperature of 50 μK and $\Omega_{297} \sim \text{MHz}$. Infidelity caused by the Doppler effect can be suppressed by lowering the temperature or increasing the Rabi frequency.

Compared to the UV laser in single-photon excitation, it is easier to achieve high power for the visible and near-infrared lasers used in two-photon schemes. Therefore, the Rabi frequency of the ground-Rydberg state $\Omega = \Omega_1 \Omega_2 / 2\Delta_e$ in two-photon excitation can reach tens or even hundreds of MHz, where Ω_1 (Ω_2) is the Rabi frequency for the ground-intermediate (intermediate-Rydberg) transition, and Δ_e is the intermediate-state detuning, as shown in Fig. 3.

In the two-photon scheme, if a counterpropagating excitation protocol is employed, the Doppler effect will be less severe than in the single-photon case. As shown in Fig. 4, by counterpropagating the two excitation beams, the Doppler effect can be minimized. It is also obvious that the 780 nm - 480 nm excitation scheme has a smaller Doppler-induced error than that of the 420 nm - 1012 nm scheme. However, regardless of the excitation approach used, achieving a Doppler-induced error well below 1% is achievable by either lowering

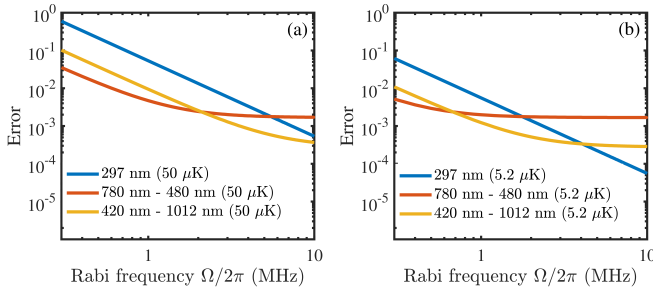


FIG. 5. Influence of Rabi frequency ($\Omega_1 = \Omega_2$ for two-photon excitation schemes) on Rydberg excitation error in different schemes for an atomic temperature of (a) $50 \mu\text{K}$ and (b) $5.2 \mu\text{K}$. The simulation is performed with intermediate detuning $\Delta_e = 2\pi \times 5687 \text{ MHz}$ in 780 nm - 480 nm scheme and $2\pi \times 7.6 \text{ GHz}$ in 420 nm - 1012 nm scheme.

the atomic temperature or applying a strong laser (large Rabi frequency).

Due to the finite lifetime of intermediate states, the Rydberg excitation fidelity is also affected by the spontaneous emission. The excitation error for a ground-Rydberg π pulse is $\sim \frac{\pi \Gamma_e}{4\Delta_e} (\frac{\Omega_1}{\Omega_2} + \frac{\Omega_2}{\Omega_1})$, where Γ_e is the spontaneous emission rate of the intermediate state. For a fixed detuning Δ_e , this error is minimized when $\Omega_1 = \Omega_2$. Since the dipole matrix element between the ground and intermediate states is orders of magnitude larger than that between the intermediate and Rydberg states, the two-photon Rabi frequency is limited by the achievable laser power for the intermediate-Rydberg transition. Recent developments in fiber lasers make it possible to achieve tens or even hundreds of watts of power at 1012 nm. Meanwhile, $6P_{3/2}$ has a lower spontaneous emission rate than $5P_{3/2}$. Consequently, the error caused by the spontaneous emission of the intermediate state in the 420 nm - 1012 nm scheme can be orders of magnitude lower than that in the 780 nm - 480 nm scheme.

As illustrated in Fig. 5, at $50 \mu\text{K}$ and $5.2 \mu\text{K}$, we conduct a comparative analysis of the errors using three different laser excitation schemes with varying Rabi frequencies. For the 780 nm - 480 nm excitation scheme, the intermediate state detuning is set at $2\pi \times 5687 \text{ MHz}$,²³⁵ while for the 420 nm - 1012 nm, it is $2\pi \times 7.6 \text{ GHz}$.²³⁶ From the simulation, it is evident that Doppler-induced infidelity can be effectively suppressed by increasing the excitation Rabi frequency.

In addition, laser phase noise and intensity noise also contribute to the Rydberg excitation error. Depending on the laser phase stability and the Rabi frequency, the contribution of phase noise to the excitation error could be more than a few percent²³⁷ without suppressing the servo bump. By using an optical cavity as a filter, as shown in Fig. 6(a), the servo bump, which is typically around MHz, is strongly suppressed by the cavity since its transmission bandwidth can be narrower than kHz.²³⁸ Moreover, Fig. 6(b) shows an alternative protocol, the feedforward technique, for suppressing the servo bump. A phase discrimination circuit based on the beat signal of the laser²³³ and the residual PDH error signal is used as the phase detector.²³⁸ The signal obtained from the phase

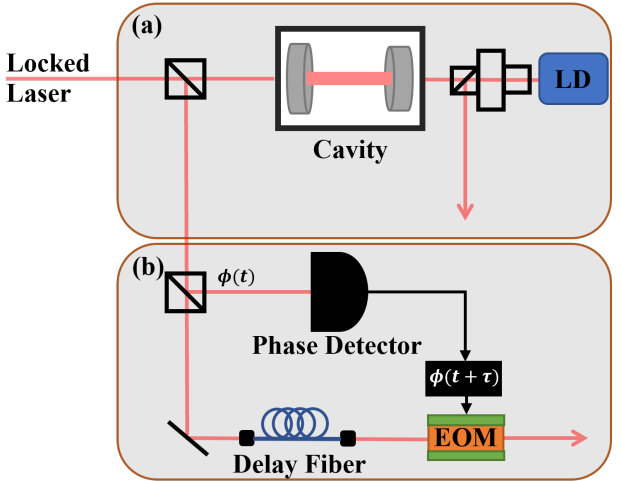


FIG. 6. Filtering Cavity and feedforward techniques for suppressing the “servo bump”. (a) The frequency-stabilized laser is sent to a narrow bandwidth optical cavity. The “servo bump” phase noise in the transmitted laser will be strongly suppressed, which is used for the injection lock of another laser diode (LD). (b) The phase information of the laser is obtained by a phase detector, which is then feedforward to an electro-optic modulator (EOM) to cancel the phase noise of the laser. The delay fiber is used to minimize the inherent delay time τ of the phase detector.

detector is then feedforward to an electro-optical modulator (EOM) with optimized modulation depth so the phase noise of the laser can be reduced. An appropriate length of delay fiber is used to overcome the frequency deviations caused by the inherent delay time of the phase detector. It is reported that after suppressing the servo bump, the fidelity after 9π pulse²³³ and the coherence time²³² can be significantly increased. The intensity noise largely depends on the lasers themselves. For example, the 297 nm laser used in the single-photon scheme in ^{87}Rb atoms can be obtained from the fourth harmonic generation seeded by a power-amplified 1188 nm laser. Using stimulated Raman scattering fiber amplifier technology, the amplified 1188 nm laser usually has a peak-to-peak intensity noise of a few percent. In addition, the cavities for frequency quadrupling will introduce additional intensity noise in the cavity locking. Considering the above noise sources, the resulting Rydberg excitation errors could be as large as a few percent.

B. Preparation of Rydberg superatom: Many-body Rabi oscillation

A major difference between a Rydberg superatom and a single atom is their Rabi oscillations.²³⁹ For a single atom, if the laser field is resonant with the $|g\rangle \leftrightarrow |r\rangle$ transition, the system will undergo Rabi oscillations between the two states with Rabi frequency Ω .²⁴⁰ In 1954, Dicke predicted that the atom-light coupling strength could be increased by a factor of \sqrt{N} in an ensemble.²⁴¹ Such a collective effect could lead to a many-body Rabi oscillation with an enhanced Rabi frequency of $\sqrt{N}\Omega$.²⁴² In 2001, Lukin *et al.* suggested that if

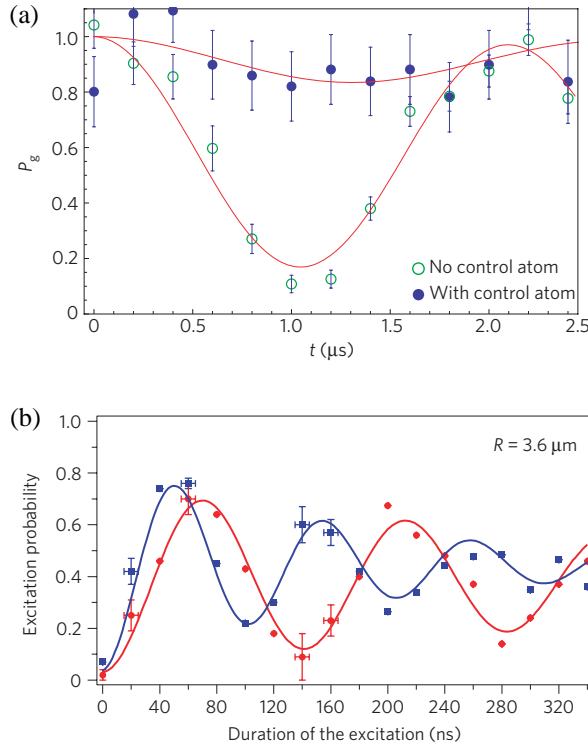


FIG. 7. (a) Rydberg blockade between two single atoms. Reprinted with permission from Urban *et al.*, *Nature Physics* **5**(2), 110-114 (2009). Copyright 2009 Springer Nature.⁴ (b) Rabi oscillations enhanced by two atoms. Reprinted with permission from Gaëtan *et al.*, *Nature Physics* **5**(2), 115-118 (2009). Copyright 2009 Springer Nature.⁵

an atomic ensemble is confined within the blockade radius,¹² many-body Rabi oscillation could be achieved by performing laser excitation between the ground state $|G\rangle$ and the Rydberg superatom state $|R\rangle$. Coherent many-body Rabi oscillation is not only conclusive evidence for the successful preparation of the Rydberg superatom but also the cornerstone for many Rydberg-atom-related quantum applications, such as deterministic quantum photonic state preparation and manipulation, quantum networks, and quantum simulations.

Although Rydberg interactions were already observed in the 1980s, Rydberg excitation blockade between two single atoms was not demonstrated until 2009.^{4,5} As illustrated in Fig. 7(a), the unfilled circles show the ground-Rydberg state Rabi oscillation of a single atom confined in μm sized far-off-resonance trap. When a control atom, which is $\sim 10 \mu\text{m}$ apart, is driven to the Rydberg state, the excitation of the target atom (filled circles) is suppressed due to a strong two-atom interaction shift of about 9.5 MHz.⁴ This conditioned Rydberg excitation blockade mechanism paves the way for the two-qubit quantum logic gate with neutral atoms.²⁴³

Fig. 7(b) demonstrates the first two-atom enhanced ground-Rydberg Rabi oscillation.⁵ To achieve a strong Rydberg blockade, two atoms are brought within a distance of 4 μm . Careful selection of Rydberg levels results in the Förster resonance, leading to a Rydberg-Rydberg interaction strength ~ 50 MHz. The Rabi oscillation of two atoms (blue squares)

is accelerated compared to the case of a single atom (red circles), by a factor of 1.38(3), close to the expected value of $\sqrt{2}$ in the two-atom blockade model.

In 2012, a coherent many-body Rabi oscillation was demonstrated in a mesoscopic ensemble containing a few hundred atoms.¹⁰ To achieve blockade over the entire ensemble, the atoms are confined within a region $\sim 6 \mu\text{m}$ and a highly-lying Rydberg state $|102S_{1/2}\rangle$ is used. As shown in Fig. 8(a), pronounced many-body Rabi oscillations are observed between the ground state $|G\rangle$ and the Rydberg superatom state $|R\rangle$ under different effective atom numbers N_e . From the oscillation dynamics, the collective enhancement factor can be extracted and compared with the atom number N_a . The observed $\sqrt{N_e}$ enhancement behavior agrees with Dicke's prediction. The detection of the Rydberg state is accomplished by converting the superatom state into a single photon. Therefore, this work provides the basis for high-quality Rydberg single-photon source and related quantum optics research.

Several experiments conducted on atomic ensembles have also confirmed a similar many-body Rabi oscillation phenomenon. Fig. 8(b) shows the many-body Rabi oscillations where the number of atoms ranges from 1 to 15.²⁴⁴ After the preparation of the Rydberg superatom $|R\rangle$, it can be transferred to a ground state superatom $|G'\rangle$. The above protocol can be repeated to deterministically prepare the atomic Fock state $|G'\rangle^n$. Fig. 8(c) displays the many-body Rabi oscillation under strong dissipation,²⁴⁵ which facilitates the realization of a Rydberg-based single-photon absorber.³⁰

In addition to atomic ensembles, many-body Rabi oscillations have also been observed in atom array settings. In 2015, Zeiher *et al.* demonstrated the preparation of a scalable Rydberg superatom in a quantum gas microscope [Fig. 9(a)].¹¹ The \sqrt{N} scaling in many-body Rabi oscillation was observed from one to a few hundred atoms. Related advances have also been made in reconfigurable tweezer arrays. Figs. 9(b) and 9(c) show the many-body Rabi oscillation with high contrast in one- and two-dimensional atomic arrays.^{174,246}

C. Quantum interface and coherence property

One of the most prominent features of Rydberg superatoms is their excellent matter-light quantum interface,^{12,247,248} as shown in Fig. 10. When a single atom absorbs and re-emits a single photon in free space, it is dominated by the spontaneous emission process, and the photon is ejected into 4π solid angles. In stark contrast, a Rydberg superatom can emit single photons into a highly directional spatial mode, as a result of the collective enhancement. Fig. 10(b) illustrates the single photon storage-and-retrieval protocol using a Rydberg superatom. Using a control laser connecting the intermediate state $|e\rangle$ and a Rydberg state $|r\rangle$, Rydberg EIT storage can be performed, and a single photon resonant with the $|g\rangle \leftrightarrow |e\rangle$ transition can be coherently transferred to a Rydberg superatom.

$$|R\rangle = \frac{1}{\sqrt{N}} \sum_{j=1}^N e^{i(\mathbf{k}_{in} + \mathbf{k}_c) \cdot \mathbf{x}_j} |g_1, g_2, \dots, r_j, \dots, g_N\rangle \otimes |0\rangle. \quad (14)$$

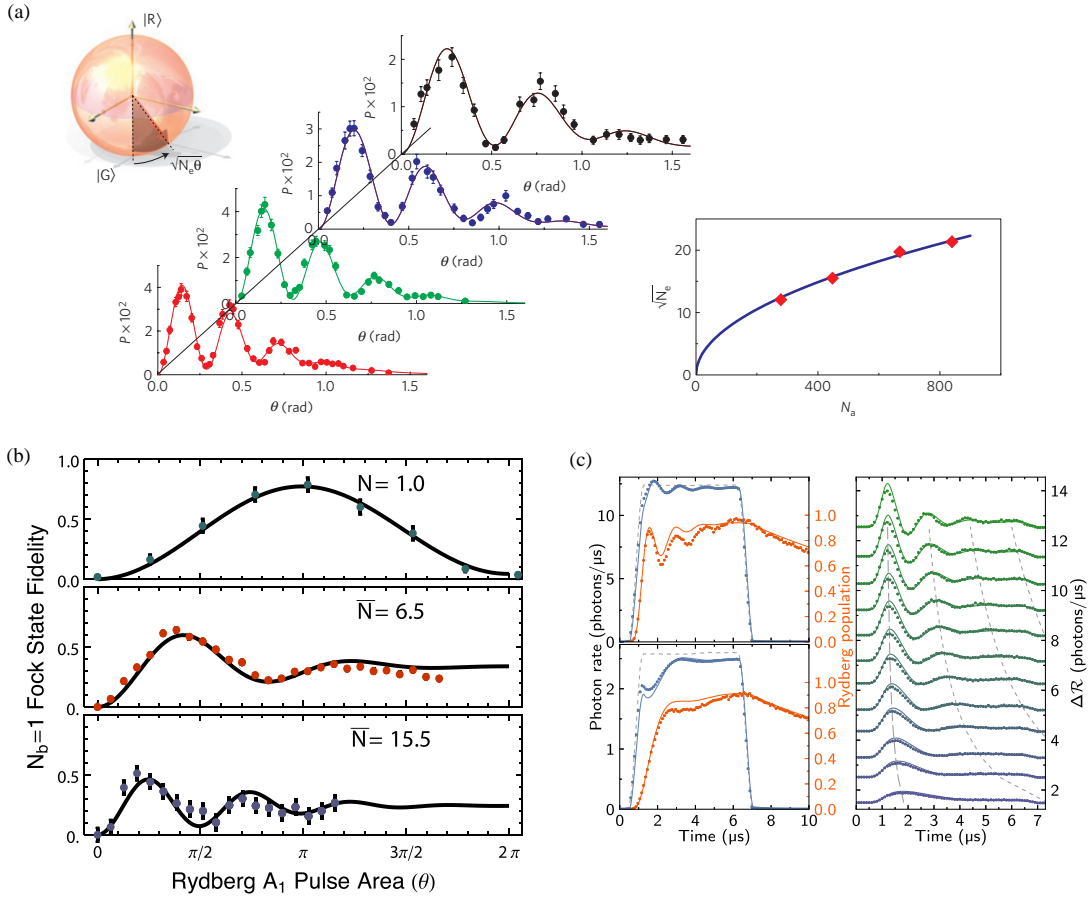


FIG. 8. Many-body Rabi oscillations in atomic ensembles. (a) Coherent many-body Rabi oscillations of a mesoscopic atomic ensemble. Reprinted with permission from Dudin *et al.*, *Nature Physics* **8**(11), 790-794 (2012). Copyright 2012 Springer Nature.¹⁰ (b) Rabi oscillation between the ground state and superatom state for various atom number distributions. Reprinted with permission from Ebert *et al.*, *Phys. Rev. Lett.* **112**(4), 043602 (2014). Copyright 2014 American Physical Society.²⁴⁴ (c) Time evolution of the photon signal and the Rydberg population. Reprinted with permission from Paris-Mandoki *et al.*, *Phys. Rev. X* **7**(4), 041010 (2017). Copyright 2017 American Physical Society, licensed under a Creative Commons Attribution 4.0 International license.²⁴⁵

Here, x_j is the position of the j -th atom, and $\mathbf{k}_{in}, \mathbf{k}_c$ are the wave vectors of the input photon and the control laser, respectively. $|0\rangle$ is the vacuum state of the photon field. This Rydberg EIT light storage process efficiently converts a photon into a single Rydberg excitation collectively shared among the atoms inside the Rydberg blockade radius.

Within the coherence time of the Rydberg superatom, the stored excitation can be transferred back to a single photon, with a read-out laser field. The read-out laser transfers the collective excitation from the Rydberg superatom state to the intermediate state,

$$|E\rangle = \frac{1}{\sqrt{N}} \sum_{j=1}^N e^{i(\mathbf{k}_m + \mathbf{k}_c - \mathbf{k}_r) \cdot x_j} |g_1, g_2, \dots, e_j, \dots, g_N\rangle \otimes |0\rangle, \quad (15)$$

where \mathbf{k}_r is the wave vector of the readout laser. Due to the finite lifetime in the intermediate state $|e\rangle$, the collective state

$|E\rangle$ soon radiates into a new state,

$$\frac{1}{\sqrt{N}} \sum_{j=1}^N e^{i(\mathbf{k}_m + \mathbf{k}_c - \mathbf{k}_r - \mathbf{k}_{out}) \cdot x_j} |g_1, g_2, \dots, g_j, \dots, g_N\rangle \otimes |1\rangle_{\mathbf{k}_{out}}, \quad (16)$$

where the atoms are back in the ground state $|g\rangle$ and a single photon is emitted into the direction defined by its wave vector \mathbf{k}_{out} . The probability of emitting a single photon into a certain mode \mathbf{k}_{out} is given by²⁴⁷

$$P(\mathbf{k}_{out}) \propto \frac{1}{N} \left| \sum_j e^{-i(\mathbf{k}_m + \mathbf{k}_c - \mathbf{k}_r - \mathbf{k}_{out}) \cdot \mathbf{x}_j} \right|^2. \quad (17)$$

Assisted by the collective enhancement of the Rydberg superatom, this emission pattern is highly directional: for mode $\mathbf{k}_{out} = \mathbf{k}_m + \mathbf{k}_c - \mathbf{k}_r$, each atom shares the same phase, and the emission amplitude is maximally enhanced. In single photon storage-and-retrieval experiments, the control laser and the read-out laser are often chosen to have the same mode $\mathbf{k}_c = \mathbf{k}_r$, so the retrieved single photon will propagate along the same mode as the input, $\mathbf{k}_{out} = \mathbf{k}_{in}$.

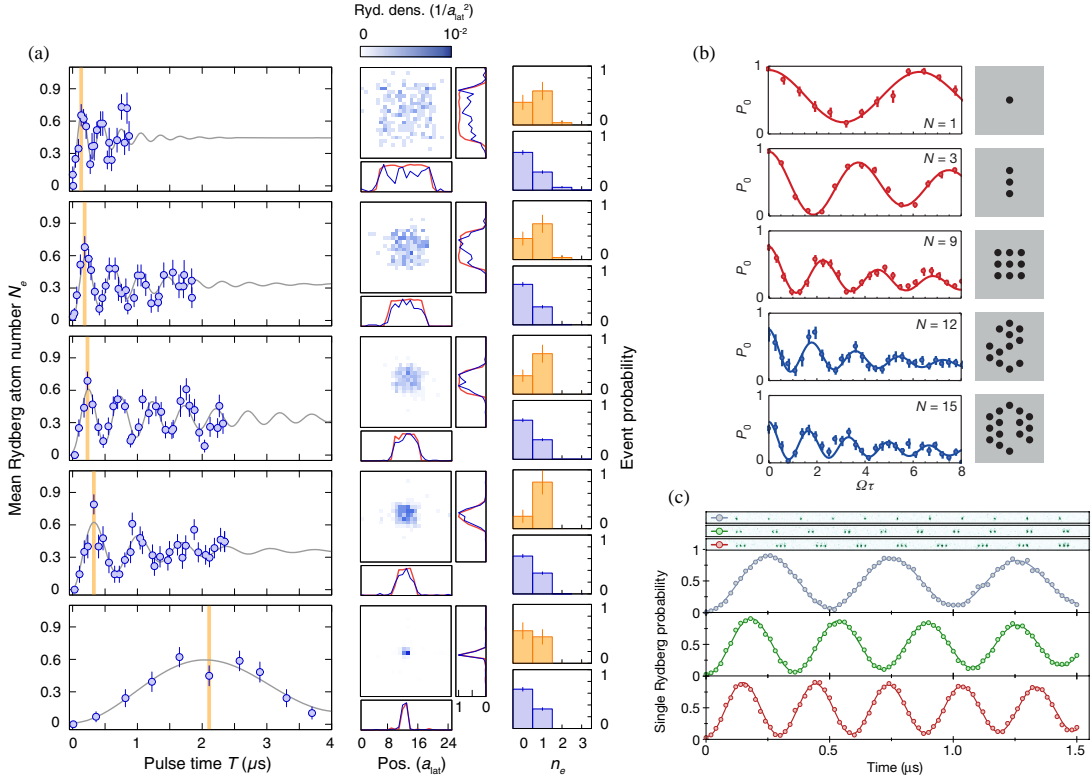


FIG. 9. Many-body Rabi oscillations in atom array experiments. (a) Collective Rabi oscillations in a quantum gas microscope. Reprinted with permission from Zeiher *et al.*, Phys. Rev. X **5**(3), 031015 (2015). Copyright 2015 American Physical Society, licensed under a Creative Commons Attribution 3.0 License.¹¹ (b) Collective Rabi oscillation in two-dimensional atomic arrays. Reprinted with permission from Labuhn *et al.*, Nature **534**(7609), 667-670 (2016). Copyright 2012 Springer Nature.²⁴⁶ (c) Collective Rabi oscillation in one-dimensional atomic arrays. Reprinted with permission from Bernien *et al.*, Nature **551**(7682), 579-584 (2017). Copyright 2012 Springer Nature.¹⁷⁴

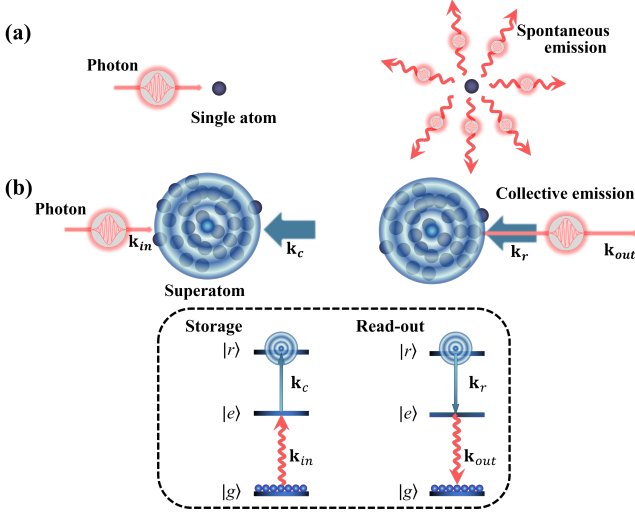
The efficient matter-light interface makes the Rydberg superatom a promising candidate for photonic quantum memory. Unlike their ground state counterpart, Rydberg quantum memories interact strongly, providing new possibilities for realizing deterministic quantum photonic devices, such as conditional phase shifter,^{26,249,250} entangling gate,^{27,28} and entanglement filter.²⁹

Rydberg superatom also differs from a single atom in terms of its coherent properties. As a collective excitation, Rydberg superatom is the superposition of each microstate: $\sum_{j=1}^N e^{i\phi_j} |g_1, g_2, \dots, r_j, \dots, g_N\rangle$. Therefore, the coherence of the Rydberg superatom largely depends on how well the relative phases ϕ_j between each microstates are maintained. Any effect that smears the relative phases will cause superatom decoherence.

One of the dominant Rydberg superatom decoherence mechanisms is motional dephasing.²⁵¹ After the preparation of the Rydberg superatom, the excitation lasers imprint an effective phase pattern, so-called spin wave, onto the atoms: $\phi_j = \Delta\mathbf{k} \cdot \mathbf{X}_j$. Here $\Delta\mathbf{k}$ is the differential wavevector from the excitation lasers, which corresponds to a spatial phase grating with period $\lambda_{\text{spinwave}} = 2\pi/|\Delta\vec{k}|$ along the direction of $\Delta\mathbf{k}$. For a gas of atoms with mass m and temperature T , the atomic speed can be described by the Maxwell-Boltzmann distribution, $f(v) = (m/2\pi k_B T)^{-3/2} e^{-mv^2/2k_B T}$.

For an atom with velocity \vec{v}_j , the motion-induced phase accumulates as $\phi_j = \Delta\vec{k}\vec{v}_j t$. During the read-out process, the probability η of converting the Rydberg superatom into the mode-matched direction is proportional to:²⁵² $|\sum_j f(v_j) e^{i\phi_j}|^2 \sim \left| \int e^{-mv^2/2k_B T} e^{i\Delta k v t} dv \right|^2 \sim e^{-t^2/\tau^2}$. Here, the motional dephasing time $\tau = \sqrt{m/k_B T}/\Delta k = \lambda_{\text{spinwave}}/(2\pi\sqrt{k_B T/M})$. For two-photon Rydberg excitation schemes, counter-propagating lasers schemes have larger spin wave periods, thus alleviating the motional superatom dephasing. For ⁸⁷Rb, counter-propagating 780 nm - 480 nm excitation scheme has a spin wave period of $\lambda_{\text{spinwave}} = 2\pi/|\Delta\vec{k}| = 1.25 \mu\text{m}$, leading to a coherence time of $\sim 6 \mu\text{s}$, for 10 μK atomic temperature.

To suppress motional dephasing, an effective technique is to confine the atoms within spatial regions that are much smaller than the spin wave period. For ground states superatom, a one-dimensional optical lattice along the direction of the spin wave can be used to overcome the motional dephasing and extend the coherence time to minutes scale.²⁵³ However, while red-detuned far-off-resonance optical traps are attractive for ground atoms, they are generally repulsive for Rydberg atoms. Therefore, traps that could simultaneously confine ground and Rydberg states are essential for extending motional decoherence times. To this end, optical traps with “magic” wave-



lengths are proposed^{254,255} and demonstrated.²⁵⁶ In ground-Rydberg state insensitive lattices, the Rydberg superatom storage times and many-body Rabi oscillation coherence times have been extended to tens of microseconds.^{257,258}

In addition to the ground-Rydberg-state magic trapping lattice, progress in extending the superatom coherence times was also made using other approaches. Using 297 nm single-photon Rydberg excitation, the quantum state shelving between Rydberg and ground states superatom was demonstrated.²³¹ The relatively short-lived Rydberg superatom can be coherently transferred to the ground state superatom, whose coherence time can be orders of magnitude longer. Furthermore, atomic samples prepared at lower temperatures also help to mitigate motional dephasing.²⁵⁹ In addition, it was recently shown that Rydberg spin wave motional dephasing can also be suppressed by introducing another spin wave using off-resonant ac-Stark lattice modulation.²⁶⁰

Due to their collective nature, the coherence properties between two Rydberg superatoms also differ from those of two single atoms. Multiple collective Rydberg excitations (multiple Rydberg superatoms) can be prepared for ensembles separated by a distance larger than the block radius. After the preparation of two Rydberg superatoms, the interaction between the pair of Rydberg atoms leads to the accumulation of phases over time,

$$|RR\rangle \sim \sum_{j,j' \neq j}^N e^{i \frac{V_{jj'}}{\hbar} t} |g\rangle_1 \dots |r\rangle_j \dots |r\rangle_{j'} \dots |g\rangle_N. \quad (18)$$

Here, $V_{jj'} = C_6/x_{jj'}^6$ is the vdW interaction between the Rydberg atom pair separated by $x_{jj'}$. Since the interaction is distance-dependent, the accumulation of random phases over time leads to a collective two-body dephasing.²⁶¹ To reduce such a dephasing mechanism, the interaction disorder between Rydberg superatoms needs to be suppressed, for instance, by

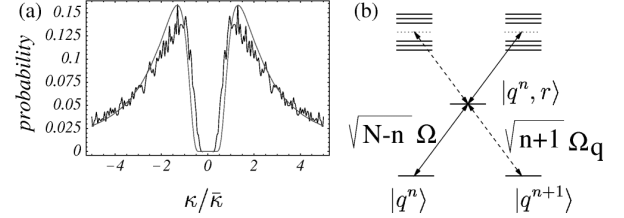


FIG. 11. (a) The displayed outcome presents both the results of Monte Carlo simulations and analytical approximations for a random gas in a finite volume, illustrating the probability distribution for frequency shifts of doubly excited Rydberg states. (b) Dipole blockade facilitates the generation of successive Fock states. Reprinted with permission from Lukin *et al.*, Phys. Rev. Lett. **87**(3), 037901 (2001). Copyright 2001 American Physical Society.¹²

making the superatom size much smaller than the separation between superatoms.

Notably, the Rydberg interaction-induced decoherence mechanism can be harnessed for the effective preparation and manipulation of photonic quantum states.^{261,262} For example, interaction dephasing-based Rydberg single-photon source,^{263,264} non-local quantum optics,²⁶⁵ and dissipative entanglement creation²⁹ have been experimentally demonstrated.

IV. APPLICATIONS IN QUANTUM INFORMATION PROCESSING

A. Quantum logic gate

The strong and long-ranged interactions furnish a direct pathway for the realization of two-qubit gates within Rydberg superatoms. The pioneering gate protocol, as delineated in Ref. 12, entails a Rydberg superatom blockade gate. In an ensemble comprising N identical atoms, each atom has the opportunity to be excited with equal probability, leading to the excitation of symmetric collective states exclusively starting from the ground state. However, the presence of resonant dipole-dipole interactions introduces a spectrum of doubly excited states, each state being separated by an energy gap of approximately $\hbar\bar{\kappa}$ in ensembles confined within a finite volume. Should the energy gap exceed the linewidth of the Rydberg state, resonant excitations from singly to doubly excited states experience significant suppression. Fig. 11 illustrates the probability distribution for frequency shifts of doubly excited Rydberg states by Monte Carlo simulations of 3×10^4 positions within a rectangular box along with the corresponding analytical approximations for a random gas. The strength of the interaction κ between any pair of atoms exceeds $\bar{\kappa}$, dominating most of the probability. This inhibition facilitates the production of collective spin states, enhancing the spectroscopic sensitivity beyond the standard quantum limit. It also aids in the preparation of a qubit that exhibits superpositions between the ground state and the single-excited storage state. This capability proves valuable for generating entanglement between two groups of atoms, drawing on principles similar to those described in Ref. 6. This regime sets the ground-

work for the emergence of superatoms in atomic gases, encompassing the Rydberg dressing, and opens avenues to scalable quantum logic gates within optical or magnetic trap arrays.^{15,266,267} Subsequently, experimental demonstrations of superatom gates have been achieved,²⁶⁸ along with the proposal of a scheme combining electromagnetically induced transparency (EIT) and Rydberg blockade in an atomic ensemble.²⁶⁹

To streamline operational steps and address practical applications, a single-step multiatom entanglement scheme based on individual atoms within an ensemble has emerged. Müller *et al.* proposed a scheme to achieve a high-fidelity gate of many particles using Rydberg interactions and combining EIT,²⁷⁰ which can be applied to multiparticle interferometry measurements.^{271,272} In this work, a short π pulse has no effect when the control atom is in the $|0\rangle$ state because it is decoupled from dynamics. The laser with Rabi frequency Ω_c between the intermediate state $|P\rangle$ and the Rydberg state $|R\rangle$ of the ensemble atoms is stronger than Ω_p between $|P\rangle$ and the ground states $|A\rangle, |B\rangle$, resulting in the EIT phenomenon when considering $\sqrt{2}\Omega_p/\Omega_c \ll 1$. The two ground states are decoupled, and the ensemble atoms always remain in the initial state $|A\rangle_k$. When the pulsed laser Ω_p is applied to the k th atom in the ensemble and undergoes adiabatic evolution along the dark state $|d\rangle_k$, causing decoupling of states $|A\rangle$ and $|B\rangle$ and achieving $|0\rangle|A^N\rangle \leftrightarrow |0\rangle|A^N\rangle$. However, when the control atom initially stays at $|1\rangle$ and is excited to $|r\rangle$ by the laser with Rabi frequency Ω_r , resulting in a shift of $|R\rangle$ because there is a blockade effect for the ensemble atoms so that $|P\rangle$ cannot couple with $|R\rangle$. Although $|A\rangle, |B\rangle$, and $|P\rangle$ remain non-resonantly coupled, $|1\rangle|B^N\rangle \leftrightarrow |1\rangle|A^N\rangle$ can be achieved. Based on this model, the fidelity of the C–NOT^N logic gate can reach 99%. Similar structures can also be used for nonadiabatic geometric quantum computation to reduce evolution time and mitigate decoherence.^{273–276} In 2018, nonadiabatic geometric quantum computation based on superatoms was proposed,²⁷⁴ and can be extended to the 3-qubit case with two species of superatoms in a two-mode cavity.²⁷⁵ Guo *et al.* utilized dynamical invariant and ZZS methods to reverse design gate pulses,²⁷⁶ optimizing gate fidelity and robustness against control errors. The average fidelity of the two-qubit controlled-NOT gate in their scheme is 0.9971.

For multiatom ensemble qubits, Saffman's group demonstrates coherence control between two ensemble qubits and achieves Rydberg blockade between them with a fidelity of 0.89(1).²⁷⁷ However, fluctuations in the collective Rabi frequency could greatly affect the ensemble qubits operation fidelity. Thus, a scheme is proposed to simulate quantum process tomography to characterize Rydberg gates based on collective states using optimal stimulated Raman adiabatic passage pulses.²⁷⁸ Recently, significant progress has been made in achieving entanglement gates through coherent manipulation of deterministically assembled arrays, employing local optical control to achieve entanglement using interatomic interactions, although individual addressing of atoms remains a challenge experimentally.^{198,236,279,280} Additionally, due to the excellent transmission characteristics of photons but the lack of strong interactions, entangling gate schemes for

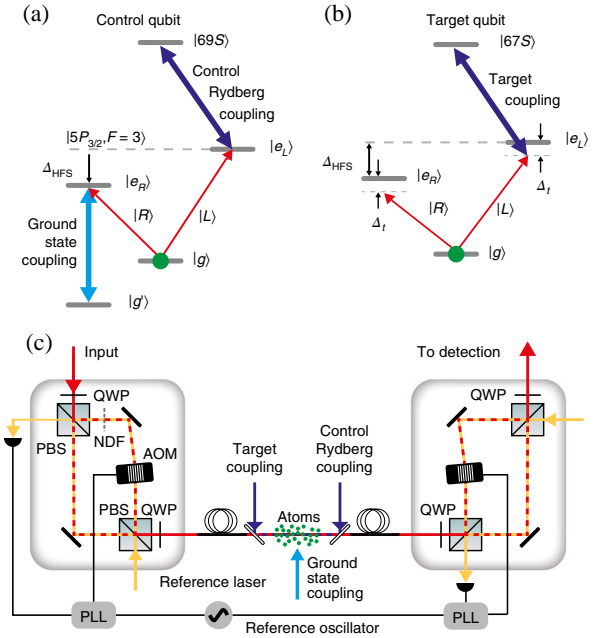


FIG. 12. Level scheme for EIT storage of the control qubit (a) and target qubit (b). (c) The schematic of the experimental setup. Reprinted with permission from Tiarks *et al.*, Nature Physics **15**(2), 124–126 (2019). Copyright 2019 Springer Nature.²⁷

photon-atom hybridization have been proposed.^{281–285} Specifically, the combination of a Rydberg blockade and optical cavities effectively enhances the gate robustness,²⁸⁴ while a two-photon interference through virtual photon exchanges renders the internal state dynamics of two Rydberg atomic qubits insensitive to the thermal photon state.²⁸⁵

Tiarks *et al.* achieved the first experimental realization of a photon-photon quantum gate using Rydberg interactions, as documented in their study.²⁷ By harnessing both EIT and Rydberg interactions within an ultracold atomic ensemble, they effectively encoded quantum information carried by photons into specific atomic states, as depicted in Fig. 12(a). This mapping facilitates the control of photon loss through post-selection, thereby mitigating its detrimental impact on quantum information and ensuring resilience against errors stemming from photon loss. Notably, the photon interaction occurs exclusively when they share the same polarization $|L\rangle$ due to the Rydberg component, and their interaction during temporal and spatial overlap results in the accumulation of a conditional phase shift, thus realizing a controlled phase flip gate, as illustrated in Fig. 12(b). By altering the basis, this gate can be converted into a controlled-NOT (CNOT) gate. The fidelity of the controlled-NOT truth table and the entangling-gate fidelity, post-selected upon the detection of control and target photons, are reported to be 70(8)% and 63.7(4.5)%, respectively. This technique employs effectively Rydberg interactions and EIT, allowing for strong, long-range interactions between photons while also solving the difficulty of restricted photon interactions. By mapping Rydberg interactions onto photons, this gate approach stores and manipulates quantum information, demonstrating high fidelity and potential advances in quan-

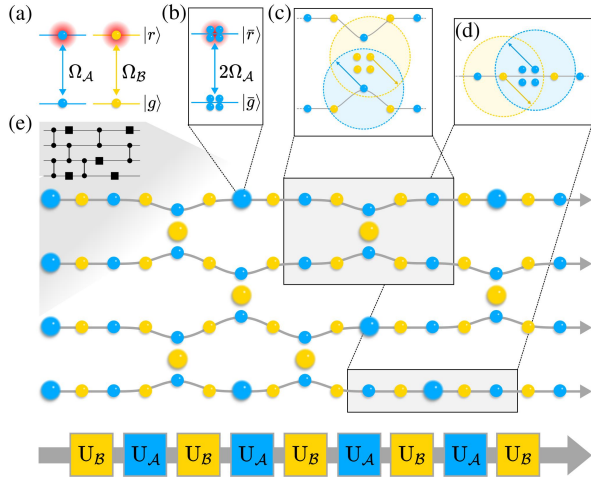


FIG. 13. Schematic diagram of converting a circuit into an atomic arrangement, which consists of two types of atoms, and superatoms are used as impurities. Reprinted with permission from Cesa *et al.*, Phys. Rev. Lett. **131**(17), 170601 (2023). Copyright 2023 American Physical Society.²⁸⁶

tum communication systems and quantum networking applications.

Recently, the Rydberg superatoms were utilized in a model for quantum computation using dual-species Rydberg atom arrays,²⁸⁶ which relies solely on global driving [see Fig. 13], thus eliminating the requirement for local addressing of the qubits. Cesa and Pichler introduce two distinct constructions: One imprints the circuit within the trap positions of the atoms, executed by pulses; the other encodes the algorithm within the global driving sequence, making the atom arrangement circuit independent. Central to this scheme is the concept of information flow, specifically focusing on the ability of qubits to propagate described by $|\Psi(k+1)\rangle = U_{\mathcal{B}}U_{\mathcal{A}}U_{\mathcal{B}}|\Psi(k)\rangle$, achieved under the conditional occurrence of the Rydberg blockade. Furthermore, the initialization of the circuits must align with the information flow. For the basic requirements of quantum computation, the construction of single- and two-qubit gates requires the assistance of impurity superatoms [see Figs. 13(c) and 13(d)]. Arbitrary single-qubit gates, including the Hadamard gate, are realized by using superatoms \mathcal{A} within the wires to enhance the Rabi frequency, facilitating collective phase gates $\mathcal{Z}_{\text{tot}} = \bigotimes_Q Z_Q$. Additionally, for two-qubit entangling gates, another superatom \mathcal{B} placed between the wires can induce a CZ gate. The study demonstrates that a quadratic increase in atom number is sufficient to eliminate the need for local control, thereby achieving a universal quantum processor. The authors also provide explicit protocols for all stages of arbitrary quantum computations and discuss error suppression strategies tailored to their model. Although the scheme is grounded in dual-species processors adhering to Rydberg blockade constraints, it holds potential for adaptation to alternative setups. This study opens new avenues for universal quantum computation with Rydberg superatoms.

B. Quantum entanglement

Quantum entanglement plays a crucial role in quantum computing and quantum information processing. Early experiments of entangled states have focused on photons and ions.^{287–289} However, these schemes face challenges in scaling to multiqubit entanglement and have a low success probability. Rydberg ensembles offer a promising solution to overcome these limitations and realize scalable entanglement of neutral atoms. Atom vapors serve not only as quantum memory, but also as “good” qubits due to strong Rydberg interactions. High-efficiency cluster states have been created via single-qubit measurements with Rydberg ensembles.²⁹⁰ Utilizing a fast entanglement generation scheme with a Lipkin-Meshkov-Glick-type Hamiltonian, a 700-atom cat state has been generated with a 50-fold improvement in the size of the entangled state.²⁹¹ To further enhance fidelity, Gärttner proposes a scheme to herald the entangled state by detecting an ion, achieving near-unity fidelity.²⁹² Additionally, addressing decoherence concerns, one can combine Zeno dynamics and shortcuts to adiabaticity with Rydberg superatoms, encoding quantum information in the collective state of superatoms to rapidly realize entangled states, including Bell states and W states.²⁹³ Similarly, fast conversion of three-particle Dicke states to four-particle Dicke states with Rydberg superatoms can be implemented based on Zeno dynamics and shortcuts to adiabaticity, offering high fidelity and robustness against decoherence.²⁹⁴ In Rydberg ensembles, large-scale entangled states can also be prepared by sending two Rydberg superatoms belonging to two different atomic W states into a cavity without qubit loss.²⁹⁵

Photons are excellent carriers for quantum information, and the entanglement between atom and photon holds promise for achieving long-range quantum information distribution. Most ensemble-based atom-photon entanglement schemes are probabilistic and suffer from limited scalability. In 2013, Li *et al.* introduced a new protocol to generate entanglement between light and optical atomic excitations with intrinsic determinism.²⁵⁶ In this scheme, the dephasing of optical atomic coherence is suppressed by state-insensitive confinement of ground and Rydberg states of ultra-cold atomic gas trapped in a one-dimensional optical lattice at 1004 nm. This confinement eliminates the differential energy shift between the ground state and the Rydberg state $\delta U = U_r(r) - U_g(r)$ and maintains coherence between them. Such a scheme has significant implications for extending the ground-Rydberg coherence and building functional Rydberg quantum networks. Fig. 14(a) illustrates the three-step process for the entanglement protocol: (i) Excitation of the Rydberg atomic ensembles from the ground state $|G\rangle$ to the single excited state $|R\rangle$. (ii) Generation of the entanglement state $|R\rangle \rightarrow |R\rangle|0\rangle_A + |G\rangle|1\rangle_A$ through a retrieval field Ω_A . (iii) Verification of the atom-photon entanglement by analyzing the correlations of photoelectric detection events. This scheme is compatible with quantum logic operations and long-term storage of quantum information, paving the way for quantum networks that enable secure communication and distributed quantum computing.

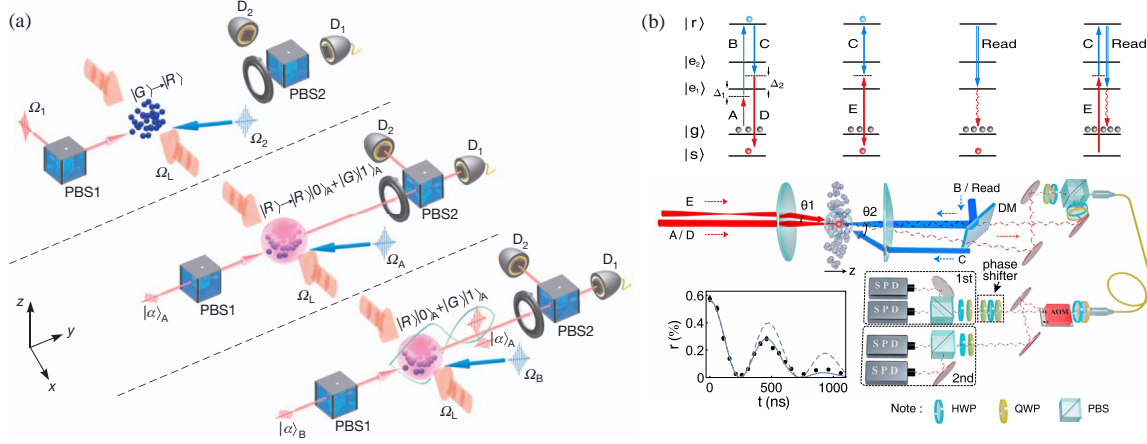


FIG. 14. Entanglement between Rydberg superatom and photon. (a) Schematic diagram of the entanglement of light with optical atomic excitation. Mapping the collective atomic excitation into quantum fields $|\phi\rangle_{A,B}$ by implementing resonance on the $|r\rangle$ and $|e\rangle$ used laser fields $\Omega_{A,B}$. Reprinted with permission from Li *et al.*, *Nature* **498**(7455), 466-469 (2013). Copyright 2013 Springer Nature.²⁵⁶ (b) Experimental preparation of semideterministic atom-photon entanglement. Reprinted with permission from Li *et al.*, *Phys. Rev. Lett.* **123**(14), 140504 (2019). Copyright 2019 American Physical Society.²⁹⁶

In 2019, an alternative atom-light entanglement protocol was experimentally demonstrated, leveraging Rydberg blockade and Raman coupling techniques.²⁹⁶ The manipulation of atoms within a confined volume of approximately $10 \mu\text{m}$ in all three dimensions ensures high effectiveness of Rydberg blockade, with an atomic density of approximately $10^{11}/\text{cm}^3$. In the schematic depicted in Fig. 14(b), the atomic ensemble is initially prepared in a ground state $|g\rangle$, following which Rydberg blockade is employed to sequentially generate two collective excitations—one in a ground state $|s\rangle$ and the other in a Rydberg state $|r\rangle$. These collective excitation states, referred to as two superatoms, possess distinct momenta, are then entangled by incorporating the momentum degree of freedom and interfering them through Raman coupling. Finally, one excitation is retrieved using a read beam, converting the momentum-entangled atomic state into entanglement between the polarization of the single photon and the momentum of the remaining atomic excitation, thereby achieving atom-photon entanglement. The high fidelity measurement of entanglement between the polarization of the single photon and the momentum of the atomic excitation underscores the practicality of employing this approach for quantum information processing tasks like quantum repeaters and networks. Although this scheme is semi-deterministic compared to the approach in Ref. 256, it remains immune to phase fluctuations and is devoid of high-order or vacuum components, which are essential for remote entanglement generation. After that, the same group presented a report detailing the deterministic creation of entanglement between an atomic ensemble and a single photon.²⁹⁷ This achievement was accomplished through a cyclical process termed “retrieving and patching”, which was applied sequentially to the Rydberg levels. By leveraging the Rydberg blockade effect, they ensured that a full excitation was generated only if a preceding excitation existed in one of the Rydberg levels. This process led to the creation of a

photon in a delayed temporal mode, entangled with the Rydberg levels hosting the collective excitation. Verification of the entanglement between the atomic ensemble and the single photon was conducted by retrieving the atomic excitation as a second photon and performing correlation measurements. The results yielded an entanglement fidelity of 87.8%.

The entanglement between photons holds tremendous potential across various fields, such as metrology and quantum computing. However, the direct interaction between photons is inherently weak, necessitating certain processing steps to induce their interaction.^{249,265,298} Numerous schemes have been proposed for the preparation of multiphoton entanglement, including spontaneous parametric downconversion^{299,300} and the entangling of single photons through atom-photon interactions.^{301,302} However, these schemes often suffer from drawbacks such as poor scalability of the photon number, complex setups, and other requirements on the system. Recently, Yang *et al.* proposed a novel scheme to generate multiphoton entanglement with a Rydberg superatom.³⁰³ In their approach, an atomic ensemble is used, where an atomic entanglement state $|\Psi\rangle_a$ is prepared by applying collective pulses with the Rydberg blockade mechanism. Subsequently, a “retrieving and patching” sequence is applied to $|r_1\rangle$, causing the Rydberg superatom to emit a photon and recreate the excitation. This sequence is repeated for $|r_2\rangle$, resulting in the creation of the entanglement state $(|0\rangle_1|1\rangle_2|L\rangle + |1\rangle_1|0\rangle_2|R\rangle)/\sqrt{2}$. By iterating these processes $m-1$ times and retrieving the two atomic qubits, the GHZ-type multiphoton entanglement $(|L\rangle^{\otimes m} + |R\rangle^{\otimes m})/\sqrt{2}$ can be obtained, where $|L\rangle$ and $|R\rangle$ represent a photon in the late and early modes, respectively. To enhance the performance of multiphoton entanglement, the scheme employs a low-finesse cavity to improve photon collective efficiency and polarizing beamsplitters with a Pockels cell in measurement to minimize exposure. The fidelity of the final prepared three- and six-

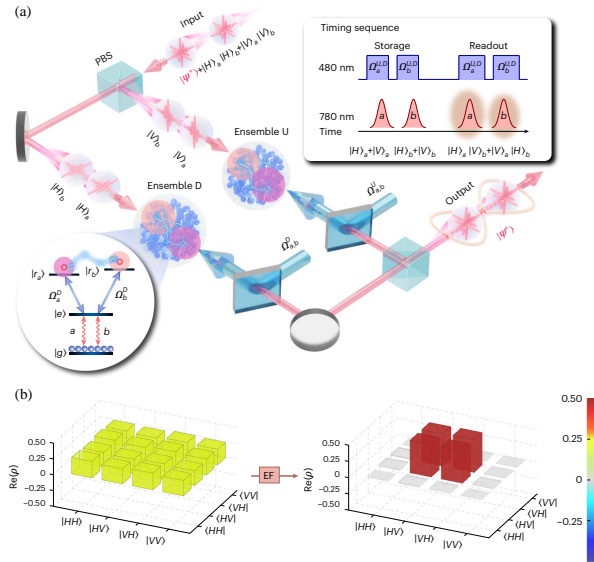


FIG. 15. Photonic entanglement filter with Rydberg superatoms. (a) Illustration of Rydberg entanglement filter protocol. (b) Extracting high-fidelity entangled state from input state with low fidelity. Reprinted with permission from Ye *et al.*, *Nature Photonics* **17**(6), 538–543 (2023). Copyright 2023 Springer Nature.²⁹

photon GHZ states is $82.9 \pm 0.3\%$ and $61.8 \pm 2.6\%$, respectively.

Strongly interacting Rydberg superatoms play a crucial role not only in generating entanglement but also in enabling deterministic manipulation of entangled photonic states. In Ref. 29, a novel photonic entanglement filter was realized using two Rydberg superatoms. The demonstrated entanglement filter transmits the desired photonic entangled state and blocks unwanted ones. As illustrated in Fig. 15(a), to achieve quantum state filtering, the undesired photonic components, $|HH\rangle$ and $|VV\rangle$ states, are converted into double Rydberg excitations in the same atomic ensemble via EIT photon storage. These double excitations can be eliminated using either Rydberg blockade or interaction-induced dephasing. On the other hand, the target entangled state, $|H\rangle|V\rangle + |V\rangle|H\rangle$ is protected in a decoherence-free subspace and can pass through the entanglement filter. Compared to prior repeat-until-success approaches based on probabilistic linear-optical systems, the Rydberg entanglement filter harnesses the strong atomic interaction and is, therefore, inherently deterministic. As shown in Fig. 15(b), photonic entanglement with fidelity $\sim 99\%$ can be extracted from an input state even when the initial fidelity is low. Such an entanglement filter opens new possibilities for scalable photonic quantum information processing with Rydberg superatom arrays.

The overall outlook for creating quantum entanglement using Rydberg superatoms is very positive. Areas including quantum computing, quantum communication, and basic quantum physics stand to benefit from further research and development in this field. These upgrades might pave the way for ground-breaking discoveries with far-reaching consequences in various science and technology areas.

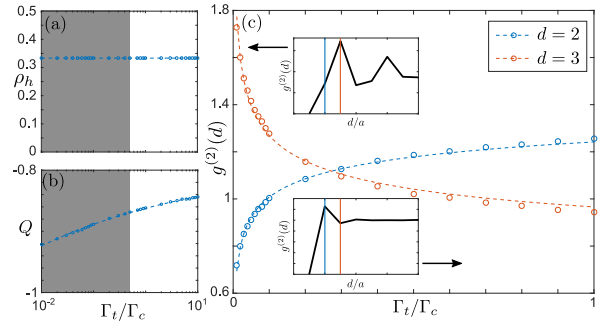


FIG. 16. Average density of holes ρ_h , Mandel Q parameter for the total number of holes, and amplitudes of the density–density correlation function $g^{(2)}(d)$ for the periods of $d = 2a$ (blue circles) and $d = 3a$ (red circles), versus the hopping rate Γ_t . Reprinted with permission from Letscher *et al.*, *New J. Phys.* **19**(11), 113014 (2017). Copyright 2017 Institute of Physics, licensed under a Creative Commons Attribution 3.0 licence.³¹⁰

C. Quantum simulation

Quantum simulation serves as a powerful tool for understanding and predicting many-body dynamics, allowing access to a wide range of phenomena, including thermal equilibrium relaxation in closed systems and non-thermal behavior in integrable and disordered systems. A particularly promising platform for investigating the dynamics of strongly interacting many-body quantum systems is provided by coherent laser-driven Rydberg atomic gases.^{304–306} Currently, spin systems based on Rydberg atoms have emerged as a promising platform for quantum simulation because of their superior interaction flexibility and strength, high controllability, and effective isolation from the environment.

One strategy suggested by Sun and Robicheaux involves simulating Rydberg gases and exploring two-body correlation by driving the superatoms, which can be subdivided into smaller regions called pseudoatoms, with a laser having a Rabi frequency following a Poissonian distribution.³⁰⁷ This method incorporates the classical correlation and provides a more accurate depiction of the Rydberg gas compared to the mean field approximation. Using the superatom picture, Olmos and colleagues conducted extensive research on fermionic collective excitations and thermalization in a symmetric quasi-one-dimensional ring lattice gas of Rydberg atoms.^{14,308} In the study of Refs. 13 and 309, the Rydberg superatoms serve as building blocks for the creation of Rydberg crystals using tailored laser excitation schemes. These crystals are used as representations of dilute metallic solids with tunable lattice parameters, allowing access to a wide range of fundamental phenomena in condensed matter physics.

In 2017, researchers explored the intricate dynamics of holes within a chain of Rydberg superatoms, exploring their behavior under the influence of driving forces and dissipation.³¹⁰ The study introduces an effective model depicting these holes as hard rods with a length of $2a$, providing insights into their creation, annihilation, and spatial correlations within the lattice. These holes stem from the spontaneous de-

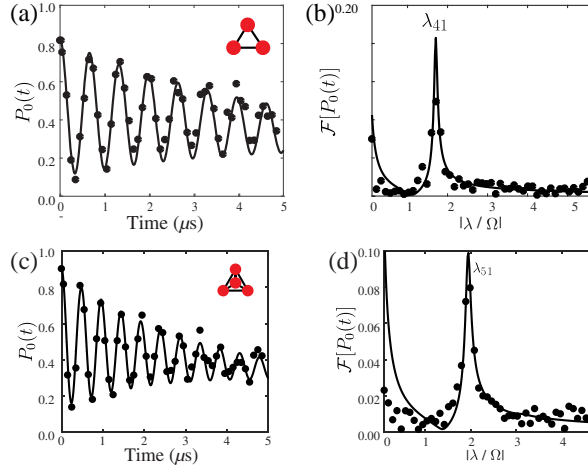


FIG. 17. Ground state population and corresponding Fourier transform in N -body ($N = 3, 4$) configuration. Reprinted with permission from Kim *et al.*, PRX Quantum **1**(2), 020323 (2020). Copyright 2020 American Physical Society, licensed under a Creative Commons Attribution 4.0 International license.³¹¹

decay of excited superatoms and can be annihilated when two holes are separated by an excited superatom, thereby influencing the equilibrium dynamics of the system. The steady-state distribution of holes converges to a density of 1/3 when the detuning of the laser matches the interaction strength between neighboring superatoms, showcasing the intricate interplay between excitation processes and decay mechanisms. Spatial correlations among holes exhibit liquid-like behavior, characterized by a length scale of $2a$ and decay over distances comparable to the lattice constant. An effective model for describing holes is established, offering an intuitive explanation by examining the influence of the hopping rate on the many-body steady state. As depicted in Fig. 16, increasing the hopping rate Γ_t renders the holes mobile, gradually reducing the peak of the correlation function $g^2(d)$ at $d = 3a$, while for a large hopping rate, the correlation function $g^2(d)$ exhibits a period $d = 2a$. The Mandel Q parameter describes the number fluctuations of holes, indicating significantly suppressed fluctuations attributed to pair annihilation processes. These findings yield valuable insights into the collective behavior of holes within the driven, dissipative spin chain of Rydberg superatoms, highlighting the pivotal role of hole dynamics in shaping the overall equilibrium phase of the system. The study contributes to the understanding of many-body dynamics in quantum systems, offering a comprehensive analysis of hole interactions and their implications for the spin dynamics of Rydberg superatom chains.

The scheme outlined in Ref. 311 suggests the continuous tuning of the quantum Ising Hamiltonian of Rydberg atoms arranged in three dimensions. In this arrangement, the atoms and pairs of Rydberg blockaded atoms are depicted as vertices and edges, respectively, as illustrated by the geometric red configuration in Fig. 17. Consequently, various connected graphs of N body configurations of Rydberg atoms are constructed, and their eigenenergies, along with different geomet-

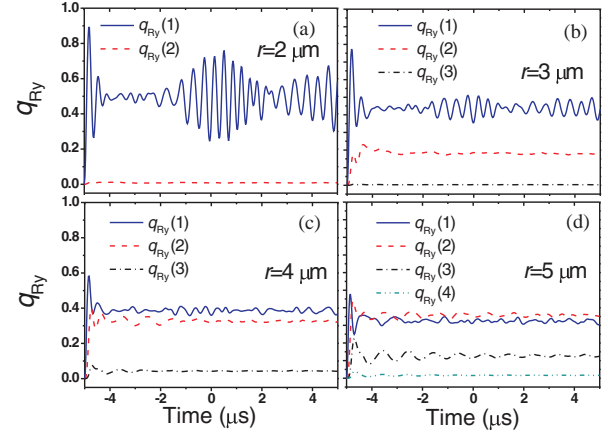


FIG. 18. The numerically calculated probabilities $q_{Ry}(n)$ to excite n Rydberg atoms in the mesoscopic atomic ensemble with $\bar{N} = 7$ atoms, randomly distributed in the optical dipole trap with different radius r . Reprinted with permission from Beterov *et al.*, Phys. Rev. A **90**(4), 043413 (2014). Copyright 2014 American Physical Society.³¹⁴

ric intermediates, are explored during the structural transformation process. The ground state population and the corresponding Fourier transform of the configurations in the superatom regime are depicted in Fig. 17 for $N = 3, 4$. Remarkably, the experimentally measured graph-dependent eigenspectra (represented by filled circles) align well with the model calculations of the few-body quantum Ising Hamiltonian (illustrated by lines). This high-dimensional programming of qubit connectivity demonstrated in the study represents a significant step toward the application of programmable quantum simulators.^{312,313}

One of the challenges in observing the Rydberg blockade is to obtain a precise measurement of the quantity of Rydberg atoms. Due to low detection efficiencies, accurately determining the number of excited Rydberg atoms becomes problematic, which is essential for exploiting the Rydberg blockade in quantum information applications. Beterov *et al.* investigated the complex dynamics of Rydberg excitations in atomic ensembles influenced by a classical electromagnetic field.³¹⁴ They demonstrated the observation of collapses and revivals in the average count of Rydberg excitations, resembling the behavior predicted by the Jaynes-Cummings model. Through the analysis of randomly loaded optical dipole traps, they predicted the occurrence of collapses and revivals in Rabi oscillations, emphasizing how the oscillation frequency depends on the number of interacting atoms. Moreover, the study examines the impact of finite interaction strengths and laser linewidth on the detectability of the revivals. Considering a randomly loaded optical dipole trap with an average atom number of $\bar{N} = 7$, data in Fig. 18 illustrate the excitation dynamics in a Rydberg state in the ensemble. In Fig. 18(a), the simulated dynamics of the probability of single-atom Rydberg excitation $q_{Ry}(1)$ for $r = 2 \mu\text{m}$ show collapses and revivals, while $q_{Ry}(2)$ approaches zero, indicating an effective Rydberg blockade. However, with increasing radius of the opti-

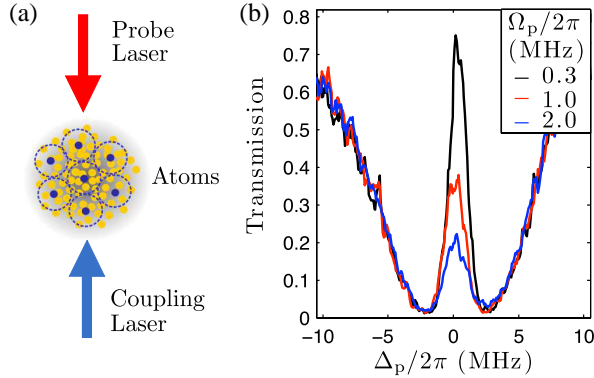


FIG. 19. (a) Schematic of a Rydberg EIT experiment with cold ^{87}Rb atoms driven by a probe field on the lower $|g\rangle \leftrightarrow |e\rangle$ transition and a coupling field on the upper $|e\rangle \leftrightarrow |r\rangle$ transition in the ladder configuration. (b) Nonlinear EIT spectra of the probe field where the transmission peak on resonance ($\Delta_p = 0$) reduces as probe Rabi frequency Ω_p increases. The experiment is done for the $|r\rangle = |60S_{1/2}\rangle$ state at atomic density $\rho = 1.2 \pm 0.1 \times 10^{10} \text{ cm}^{-3}$. Reprinted with permission from Pritchard *et al.*, Phys. Rev. Lett. **105**(19), 193603 (2010). Copyright 2010 American Physical Society.¹⁹

cal dipole trap, the revivals in $q_{Ry}(1)$ are diminished, and the probability of exciting two Rydberg atoms $q_{Ry}(2)$ increases, suggesting the breakdown of the Rydberg blockade. These results provide valuable insights into Rydberg blockade phenomena, reducing the need for precise quantification of Rydberg atoms and offering potential applications in quantum information processing and the investigation of sub-Poissonian atom-number fluctuations in mesoscopic atomic ensembles.

V. APPLICATIONS IN QUANTUM OPTICS

In this section, we first present a brief review of recent experimental and theoretical progress focusing on the nonlocal nonlinear responses, as induced by the dipole-dipole interactions and related to the dipole blockade effect, of cold Rydberg atoms driven into the EIT regime.³¹⁵ Then we look back at some important proposals and schemes for achieving efficient nonlinear quantum optics³¹⁶ by considering hybrid systems with Rydberg atoms restricted in cavities, placed close to waveguides, or trapped above atomic chips.

A. Nonlocal nonlinear optics

Typical EIT experiments are performed with atoms in low-lying states driven into the three-level Λ configuration involving an intermediate short-lived excited state and two long-lived ground states. When a ground state is replaced with a Rydberg state, it is viable to realize an intriguing transfer from the linear EIT in the Λ configuration to the nonlinear EIT in the ladder configuration, as a result of both long-lifetime and strong-interaction features of highly excited Rydberg atoms.

In 2010, Adams' group observed in ^{87}Rb atoms a coopera-

tive optical nonlinearity arising from Rydberg interactions and manifested itself as a gradual reduction of the probe transmission in the EIT window when the probe intensity increases¹⁹ as shown in Fig. 19. This is studied considering a ladder EIT system involving ground $|g\rangle$, intermediate $|e\rangle$, and upper $|r\rangle$ levels and is explained by a simple two-atom model where one atom contributes to the three-level EIT system while the other acts as a two-level absorbing system due to dipole blockade. This fascinating experiment soon is better explained by a mean-field superatom model where the collective states of $n_{SA} = \frac{4}{3}\pi\rho R_{SA}^3$ atoms within a blockade sphere of radius $R_{SA} = (C_6\gamma/\Omega_c^2)^{1/6}$ are considered but appropriately truncated³¹⁷ as shown in Figs. 20(a) and 20(b). This truncation is done based on two facts: i.e., (i) at most one atom is allowed to be in the upper Rydberg state and (ii) the excitation to the intermediate state $|e\rangle$ is well suppressed due to quantum destructive interference. Then it is appropriate to consider only the three lowest-order collective states $|G\rangle = |g_1, g_2, \dots, g_{n_{SA}}\rangle$, $|E^{(1)}\rangle = \frac{1}{\sqrt{n_{SA}}} \sum_j^{n_{SA}} |g_1, \dots, e_j, \dots, g_{n_{SA}}\rangle$, and $|R^{(1)}\rangle = \frac{1}{\sqrt{n_{SA}}} \sum_j^{n_{SA}} |g_1, \dots, r_j, \dots, g_{n_{SA}}\rangle$ for each superatom as one attempts to estimate the Rydberg excitation probability Σ_{RR} . With Σ_{RR} , it is easy to calculate the conditional polarizability $\alpha = \Sigma_{RR}\alpha_{TLA} + (1 - \Sigma_{RR})\alpha_{EIT}$ with α_{TLA} and α_{EIT} being the polarizabilities for the two-level absorbing and ladder EIT systems, jointly determining the probe field propagation in the Rydberg medium. Such a computationally efficient model is in quantitative agreement with the experimental results and also predicts in Fig. 20(c) a remarkable antibunching effect in terms of the intensity correlation function $g_p^{(2)}(L)$ observed at the sample exit, accompanied by the transmission reduction due to cooperative optical nonlinearity.

Through the utilization of Rydberg EIT, Vuletić and his colleagues showcased their ability to manipulate light fields at the level of single quanta. In their work Ref. 20, strongly interacting Rydberg states play a crucial role in generating quantum nonlinearity via the photon-photon blockade mechanism, as shown in Fig. 21. This blockade prevents the transmission of multi-photon states by precluding the simultaneous excitation of two Rydberg atoms within the blockade radius r_b . When an incident single photon is converted into a Rydberg polariton inside the medium under EIT conditions, the Rydberg blockade prevents a second polariton from traveling within the blockade radius of the first one, leading to the destruction of EIT. The interaction between Rydberg atoms creates a strong nonlinearity that results in the attenuation of a second photon approaching the single Rydberg polariton. This phenomenon is based on the physical principle that when the blockade radius exceeds the resonant attenuation length of the medium in the absence of EIT, two photons in a tightly focused beam cannot pass through each other or propagate close to each other inside the medium. By utilizing Rydberg states of $|100S_{1/2}\rangle$, the researchers were able to realize blockade radii $r_b = 13 \mu\text{m}$, effectively creating a quantum nonlinear absorption filter that converts incident coherent field into a train of non-classical, anti-bunched light pulses. The demonstration of quantum-by-quantum control over light fields in this research opens up new possibilities for non-linear quantum optics based on interact-

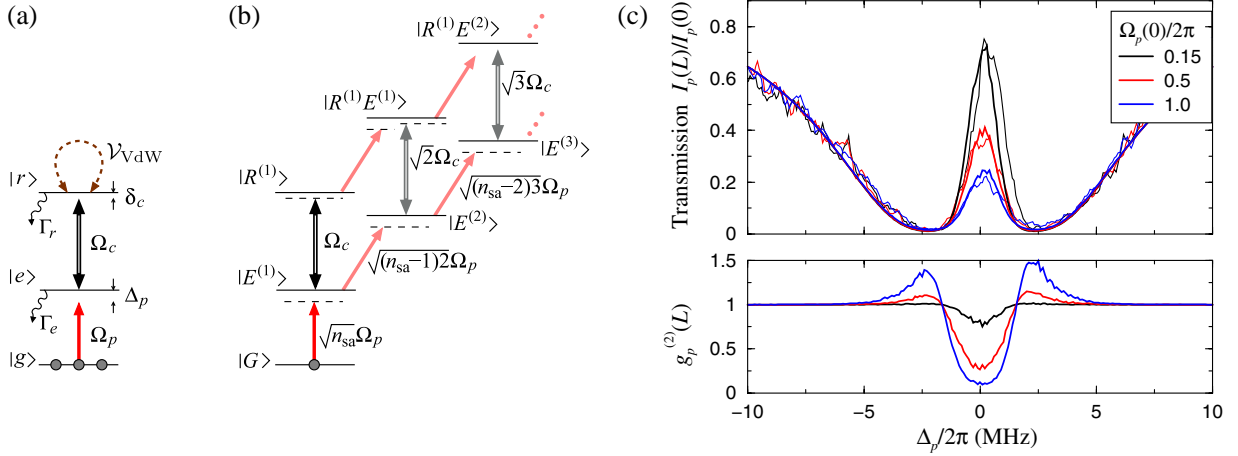


FIG. 20. (a) A ladder scheme of three-level atoms that interact with a probe and a coupling field. \mathcal{V}_{vdW} denotes the vdw interaction between two atoms in the Rydberg state $|r\rangle$. (b) Truncated level scheme of a superatom composed of n_{SA} atoms, with collectively enhanced transition amplitudes involving different numbers of probe and coupling photons. (c) Top: Probe field transmission against detuning Δ_p for different input probe Rabi frequencies. The thin lines are experimental curves from Ref. 19 while thick lines are numerical simulations based on the superatom model. Bottom: Corresponding intensity correlation function of the transmitted probe field at the end of the sample. Reprinted with permission from Petrosyan *et al.*, Phys. Rev. Lett. **107**(21), 213601 (2011). Copyright 2011 American Physical Society.³¹⁷

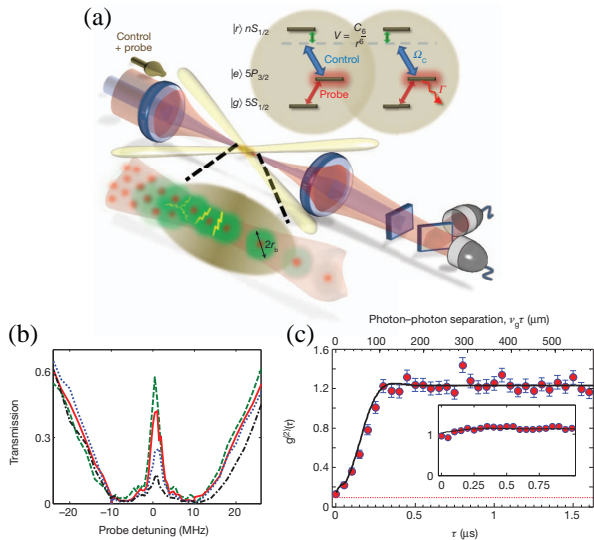


FIG. 21. (a) Rydberg-blockade-mediated interaction between slow photons. (b) Transmission versus probe detuning at various incoming photon rates. (c) Data points show photon–photon correlation function $g^{(2)}(\tau)$ at EIT resonance. Reprinted with permission from Peyronel *et al.*, Nature **488**(7409), 57–60 (2012). Copyright 2012 Springer Nature.²⁰

ing Rydberg atoms.

Soon afterward, higher-order collective states are included in an improved superatom model by going beyond the weak-probe approximation, which just results in quantitative differences, especially as the probe and coupling fields are off two-photon resonance, yet without changing main conclusions.³¹⁸ Such a superatom model has been further extended to realize the polarization-selective nonlinearity and cooperative nonlinear grating unattainable in normal atoms.^{319–321} A semianalyt-

ical rate-equation model has also been developed for revealing a universal relation between the nonlinear optical susceptibility and the Rydberg excitation density as interatomic coherences are well suppressed due to strong dephasing effects or very different Rabi frequencies of the probe and coupling fields.³²² Moreover, we note that a many-body iterative approach has been developed to account for the interparticle Rydberg correlations, though it is applicable only for dilute samples with less than one atom inside a superatom so that Rydberg interactions between different superatoms become dominant to reduce the many-body computational complexity. This alternative approach allows one to separate a local linear susceptibility and a nonlocal nonlinear susceptibility comparable in magnitude, hence achieving huge nonlocal optical nonlinearities beneficial, e.g., to largely enhance the Goos–Hanchen lateral shift and correlated biphoton generation.^{323–326}

An important application of the linear EIT in normal atoms is to realize the dynamically reversible storage and retrieval of a (classical or quantum) probe pulse by adiabatically switching off and on a control field. Such an important coherent control of the slow-light propagation and storage dynamics has been extended to Rydberg atoms exhibiting nonlocal nonlinear EIT responses. Many experiments show that storing an input probe pulse as a collective Rydberg excitation strongly enhances the Rydberg-mediated interaction compared to that in the slow-light dark-state polariton (DSP) case. For example, Distante *et al.* observed a strong enhancement of interatomic interactions due to the largely reduced polariton group velocity for short storage times while a weak enhancement dominated by Rydberg-induced dephasing of the polariton’s multiparticle components for longer storage times.³²⁷ This conclusion is supported by Fig. 22 where the output photon number N_{out} depends on the input photon number N_{in} clearly in a nonlinear way and becomes saturated for a sufficiently large N_{in} as described by the input-output relation

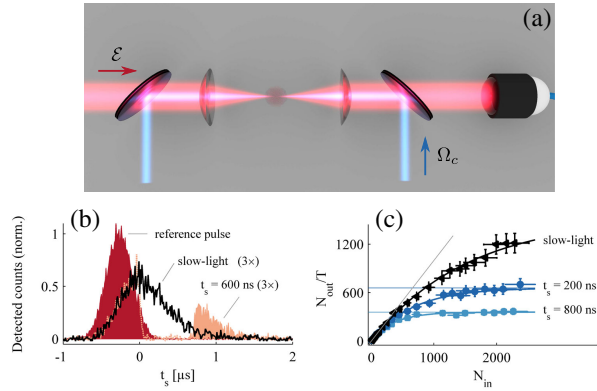


FIG. 22. (a) A light storage and retrieval experiment based on the nonlinear Rydberg EIT technique. (b) Normalized and background subtracted counts of an input probe pulse when slowly propagating or stored for $t_s = 600$ ns. (c) Output photon number normalized by linear process efficiency T against input photon number for the slow-light case and two storage times. Straight lines represent the linear behavior (oblique) and the saturation level (horizontal). Reprinted with permission from Distante *et al.*, Phys. Rev. Lett. **117**(11), 113001 (2016). Copyright 2016 American Physical Society.³²⁷

$N_{\text{out}} = N_{\text{max}} T (1 - e^{-N_{\text{in}}/N_{\text{max}}})$ with T being the linear process efficiency for small N_{in} . This nonlinear light storage experiment can be well explained by extending the superatom model from its steady-state solutions to the dynamic evolution case³²⁸ which further predicts an inhomogeneous nonclassical antibunching feature of the retrieved light signal. Another effective method has also been developed to reveal the correlated photon dynamics in dissipative Rydberg media valid in the limit of a large optical depth per blockade radius.^{329,330}

Even in the absence of a common medium, creating effective photon-photon interactions remains feasible.³³¹ Busche *et al.*'s study delved into a novel approach to such photon interactions utilizing Rydberg interactions.²⁶⁵ As depicted in Fig. 23, photons stored as collective Rydberg excitations in spatially separated optical media interact through van der Waals interactions, inducing non-uniform phase shifts that alter the retrieval modes of the photons. These interaction-induced phase shifts are pivotal in shaping the overall interaction between the photons, resulting in observable effects like reduced retrieval in the photons' initial modes and spatial anti-correlations in observed photon statistics. The experimental arrangement utilized highly focused signal beams and tiny optical tweezers to confine cold atoms, demonstrating the high level of precision and control in investigating non-contact nonlinear optics. Results exhibit strong agreement between theory and experiment across varying interaction strengths and distances, indicating the feasibility of implementing contactless effective photon-photon interactions in practical photonic devices. This contactless characteristic of interactions unveils new opportunities for scalable multi-channel photonic devices, exploration of strongly correlated many-body dynamics using light, and the development of advanced quantum technologies based on photon interactions mediated by Rydberg states.

B. Single-photon engineering

Rigid dipole blockade effect in Rydberg atoms allows one to attain efficient single-photon engineering, including single-photon generation and storage due to collectively enhanced strong couplings between single Rydberg superatoms and few-photon light pulses.²⁴⁵ In Ref. 247, Saffman and Walker conducted a detailed analysis of collective emission and proposed the protocol for realizing deterministic single-photon source using Rydberg superatom. Instead of using Rydberg EIT to store a single photon, they show that the Rydberg superatom can be coherently prepared by using two-photon excitation to drive a many-body Rabi oscillation, hence efficiently transferred into a highly directional single photon. Honer *et al.* further examined photon interactions with a Rydberg superatom under controlled dephasing conditions and discover that induced dephasing may dictate the absorption of a single photon from any probing field,²⁰⁴ which was recently employed in the controlled multi-photon subtraction process.³³²

A deterministic single-photon source based on Rydberg superatom was experimentally realized in 2012.²¹ As shown in Fig. 24, Dudin and Kuzmich performed 780 nm - 480 nm two-photon Rydberg excitation and photon retrieval in an ensemble of ⁸⁷Rb atoms confined within the blockade radius. When high-lying Rydberg states ($n \sim 100$) are used, the measured second-order-correlation function $g^2(0)$ of the retrieved photon approaches zero, indicating the successful preparation of a single photon. Further research in Rydberg single-photon source focused on analyzing and improving the quality of generated single photons.^{23-25,333} The state-of-the-art Rydberg single-photon sources feature near-unity purity and indistinguishability, which are comparable to those in other leading single-photon physical platforms³³⁴ and have been used to achieve a high-fidelity photonic quantum logic gate using linear optical approach.²⁵

In 2018, Petrosyan and Mølmer proposed a more efficient free space scheme to create deterministic single photons in a well-defined spatio-temporal mode.³³⁵ This is done by first excite a single source atom into a high-lying Rydberg state $|u\rangle$, which couples to an ensemble of ground state atoms via dipole-dipole exchange (DDE) interactions so that its transition to another Rydberg state $|d\rangle$ is accompanied by the creation of a spatially extended spin wave $S(\mathbf{r})$ of a single Rydberg excitation in the ensemble, as shown in Fig. 25. This collective single-Rydberg excitation can be converted to a propagating optical photon \mathcal{E} as a coherent control field Ω_c is switched on to form the ladder EIT configuration. This non-trivial scheme relies on neither the strong coupling of a single emitter to a resonant cavity nor the heralding of collective excitation or complete Rydberg blockade of multiple excitations in a mesoscopic atomic ensemble. Similarly, it is feasible to achieve reliable quantum memory at the single-photon level by absorbing all extra photons inside each blockade volume of the Rydberg superatoms.^{231,336-338}

The dipole blockade and exchange mechanisms described above used for generating single-photon sources can also be extended to design usually unattainable single-photon devices, including single-photon switch,³¹ transistor,^{32,339} and

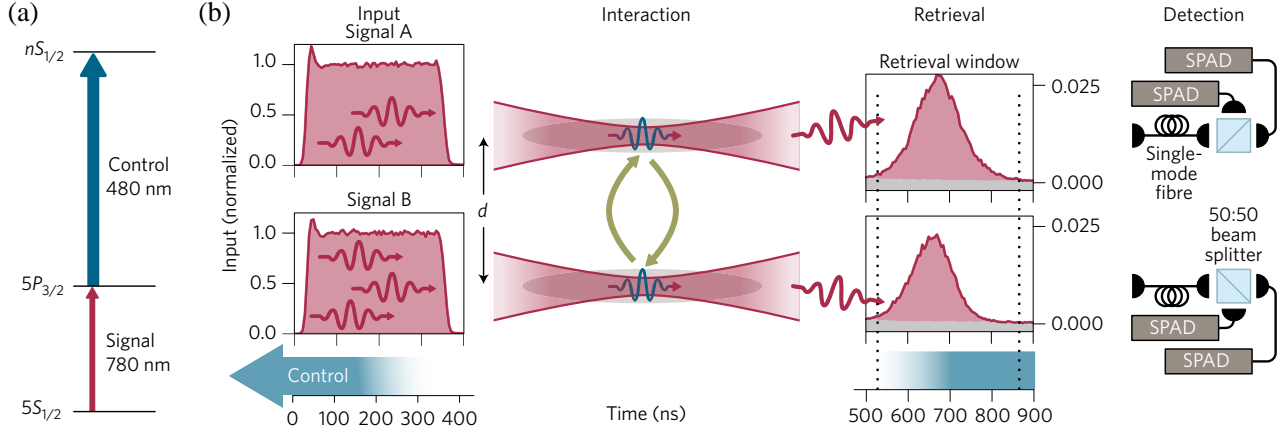


FIG. 23. Experimental realization of contactless nonlinear optics mediated by long-range Rydberg interactions. Reprinted with permission from Busche *et al.*, *Nature Physics* **13**(7), 655-658 (2017). Copyright 2017 Springer Nature.²⁶⁵

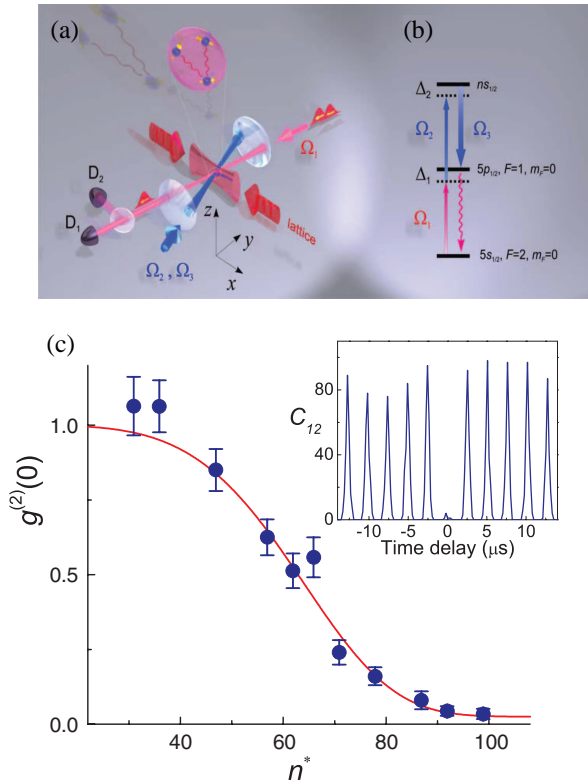


FIG. 24. Single-photon source with Rydberg superatom. (a) Illustration of experimental protocol. (b) Relevant atomic levels. (c) Measured second-order-correlation function $g^{(2)}(0)$ as a function of the effective principal quantum number. Reprinted with permission from Dudin *et al.*, *Science* **336**(6083), 887-889 (2012). Copyright 2012 The American Association for the Advancement of Science.²¹

absorber.²⁴⁵ For instance, one may store a gate light pulse containing only one photon on average as a collective Rydberg excitation in cold atoms, in the presence of which the transmission of the subsequent target pulse is largely suppressed due to dipole blockade.³¹ Such a single-photon switch offers

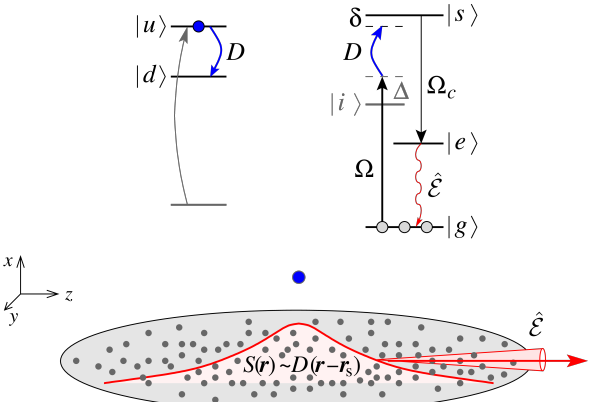


FIG. 25. Transition $|u\rangle \rightarrow |d\rangle$ of a source atom (top left) is coupled nonresonantly to transition $|i\rangle \rightarrow |s\rangle$ of the medium atoms (top right) via DDE interaction D . A laser pulse Ω couples ground state $|g\rangle$ to Rydberg state $|i\rangle$ and leads to the transition $|g\rangle \rightarrow |s\rangle$ with the help of DDE transition $|i\rangle|u\rangle \rightarrow |s\rangle|d\rangle$. The resulting single Rydberg excitation exhibits the profile $S(\mathbf{r}) \propto D(\mathbf{r} - \mathbf{r}_s)$ and can be converted into a propagating photon \mathcal{E} by applying the control field Ω_c . Reprinted with permission from Petrosyan *et al.*, *Phys. Rev. Lett.* **121**(12), 123605 (2018). Copyright 2018 American Physical Society.³³⁵

many interesting prospects ranging from quantum communication to quantum computing, such as heralding a successful quantum memory event, nondestructively detecting an optical photon, and building a photonic quantum-logic gate. Moreover, it is viable to realize an all-optical single-photon transistor by mapping gate and source (target) photons to strongly interacting Rydberg excitations with different principal quantum numbers³² or by suppressing and enhancing the transmission of target (source) photons through dipole blockade and Förster resonances, respectively.³³⁹

To be more specific, we can see from Figs. 26(a)-26(d) that an all-optical transistor can be achieved with the following two procedures. First, store photons in a gate field \mathcal{E}_g as collective Rydberg excitation in a sample of cold ^{87}Rb atoms by coupling the ground state $|g\rangle$ with the Rydberg state $|r\rangle$

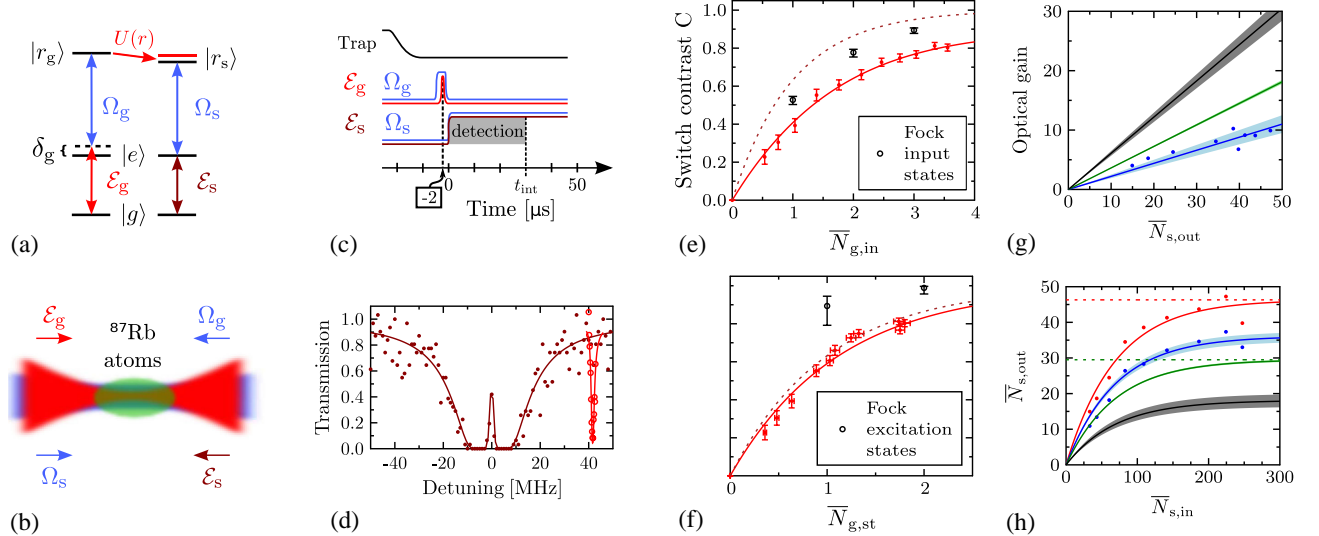


FIG. 26. (a) Level scheme, (b) simplified schematic, and (c) pulse sequence for the realization of an all-optical transistor with $U(r)$ denoting the dipole-dipole interaction between two atoms of distance r and in states $|r_g\rangle$ and $|r_s\rangle$, respectively. (d) Absorption spectrum of the source field (dots) exhibiting an EIT window at $\delta_g = 0$ and that of the gate field (circles) around $\delta_g = 40$ MHz. The contrast of the switches (red solid) against mean numbers of (e) incident and (f) stored gate photons in coherent states is presented with fundamental limits (pink dashed) set by the corresponding photon statistics. (g) Gate photon optical gain and (h) source photon transfer function with $\bar{N}_{g,\text{in}} = 0$ (red) and $\bar{N}_{g,\text{in}} = 0.75$ (blue) for coherent states, while $N_{\text{in,Fock}} = 1$ (green) and $N_{\text{st,Fock}} = 1$ (black) for Fock states. Reprinted with permission from Gorniaczyk *et al.*, Phys. Rev. Lett. **113**(5), 053601 (2014). Copyright 2014 American Physical Society.³²

through a control field Ω_g . Second, a source field \mathcal{E}_s is sent through the same medium at a reduced group velocity due to the resonant EIT provided by the control field Ω_s coupling to the Rydberg state $|r_s\rangle$. Then individual source photons can travel with little absorption through the atomic sample in the absence of a gate excitation for a low source photon rate or are strongly attenuated by the scattering from the intermediate state $|e\rangle$ in the blockade regime where Rydberg interactions between states $|r_g\rangle$ and $|r_s\rangle$ result in a two-level absorbing system. This realizes a transistor working at the single-photon level with its main performance illustrated in Figs. 26(e)-26(h). First, we can see from Fig. 26(e) that the switch contrast C plotted against the mean number of incident gate photons $\bar{N}_{g,\text{in}}$ is clearly below the fundamental limit set by the coherent-state photon statistics. Fig. 26(f) shows, however, that C plotted against $\bar{N}_{g,\text{st}}$ (the mean number of stored gate photons) gets much closer to the corresponding fundamental limit. It is more important to note that, on average, about 3 input or 2 stored gate photons are already enough to achieve a switch contrast over 0.8. Fig. 26(g) further shows that the optical gain is up to $20 \sim 30$ (limited by the self-blockade effect of the source photons) where a coherent input with $\bar{N}_{g,\text{in}} = 0.75(3)$ gate photons can be used to effectively control the transmission of $30 \sim 50$ source photons. Finally, we find in Fig. 26(h) a nonlinear saturation behavior due to self-blockade in terms of the source photon transfer function from $\bar{N}_{s,\text{in}}$ to $\bar{N}_{s,\text{out}}$. Hence a much higher optical gain is expected to occur provided the source photon loss due to self-blockade can be overcome.

C. Hybrid Rydberg system

Hybrid systems involving Rydberg atoms promise intriguing possibilities for quantum information processing. It was shown that a Jaynes-Cummings (JC) model could be realized in the optical domain for an ensemble of atoms by exploiting their collective couplings to a quantized cavity mode.^{340,341} This is realized by restricting the huge state space to the collective ground state $|G\rangle$ and the collective excited state $|E\rangle$ with a single Rydberg excitation due to dipole blockade. The main benefit is that the collectively enhanced coupling can be much larger than the decay rates, leading to the strong coupling regime of an effective JC model. Trapping some atoms in a volume smaller than the blockade sphere close to an atom chip, it is viable to attain a hybrid system consisting of a superatom coupled to a surface phonon polariton, which can be used to subtract individual photons from a beam of light.³⁴² Hybrid systems consisting of macroscopic mechanical oscillators coupled to a small ensemble of Rydberg atoms are also widely investigated to achieve ground state cooling, quantum state engineering, nontrivial nonlinear dynamics, bistable Rydberg excitation, and mechanical oscillation, etc.³⁴³⁻³⁴⁵ This depends especially on the collectively enhanced coupling arising from the dipole blockade effect of Rydberg superatoms.^{346,347} The strong coupling regime may also be realized between a Rydberg atomic ensemble and propagating surface phonon polaritons on a piezoelectric superlattice.³⁴⁸ These hybrid Rydberg systems provide a promising platform for extending the contents of nonlinear quantum optics and photonics, essential for developing future quantum control techniques. Moreover, when combined with

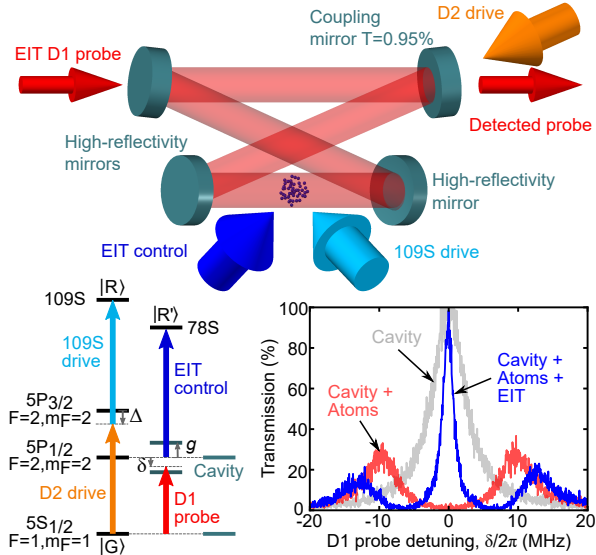


FIG. 27. The experimental setup involves measuring transmission, with EIT spectra depicted in blue (presence of EIT control) or red (absence of EIT control), normalized against the maximum transmission of an empty cavity (depicted in gray). Reprinted with permission from Vaneechout *et al.*, Phys. Rev. X **12**(2), 021034 (2022). Copyright 2022 American Physical Society, licensed under a Creative Commons Attribution 4.0 International license.³⁵¹

Floquet engineering techniques, polaritons, formed by photons entering a cavity and hybridized with atomic Rydberg excitations, can be efficiently manipulated to interact with each other.³⁴⁹ They can also be simulated to exhibit topological order, such as the Laughlin state.³⁵⁰

Below, we will explain the above discussions in more detail by focusing on recent experiments.^{28,351,352} As can be seen in Fig. 27, by placing a small cloud of ^{87}Rb atoms inside a cavity of finesse $\mathcal{F} = 590$, one observes the vacuum Rabi splitting of two transmission peaks located at $\delta/2\pi = \pm 10$ MHz, indicating a cavity-mode coupling constant ($g/2\pi = 10$ MHz) exceeding both cavity decay rate ($\kappa/2\pi = 2.9$ MHz) and atomic decay rate ($\gamma/2\pi = 3$ MHz). Exciting these atoms to a high Rydberg state $|R'\rangle$ by the EIT control and D1 probe beams, a narrower EIT window is found to open on resonance corresponding to a dark polariton state mixing a photon in the cavity and a Rydberg excitation in the atomic cloud. On the other hand, the 109S drive and D2 drive beams can drive these atoms to another high Rydberg state $|R\rangle$ via a two-photon Raman resonance so that they behave as a two-level superatom due to the blockade of multiple Rydberg excitations. Atoms in states $|R\rangle$ and $|R'\rangle$ further strongly interact via their dipoles as a result of the Förster resonance with another pair of Rydberg states. Then, by shifting the state $|R\rangle$ out of resonance, a superatom in the state $|R'\rangle$ destroys the EIT response to the D1 probe, which drives the photonic component of the $|R'\rangle$ polariton. This scheme has been exploited to realize the high-efficiency single shot optical detection of a Rydberg superatom, the superatom state-dependent π phase shift of light reflected by the cavity, and the deterministic preparation of freely propagating photonic qubits with negative Wigner

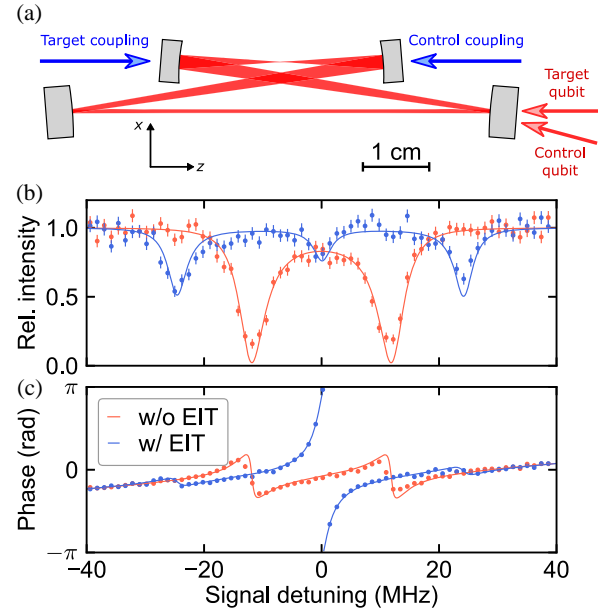


FIG. 28. (a) A bow-tie cavity composed of two concave mirrors and two convex mirrors. Relative intensity (b) and (c) phase of signal light as a function of signal detuning referring to cavity-enhanced Rydberg EIT spectra. Red (blue) data and lines are attained in the absence (presence) of coupling light. Reprinted with permission from Stolz *et al.*, Phys. Rev. X **12**(2), 021035 (2022). Copyright 2022 American Physical Society, licensed under a Creative Commons Attribution 4.0 International license.²⁸

functions,^{351,352} by taking advantage of two complementary approaches: i.e., cavity quantum electrodynamics and interacting atomic ensembles.³⁵³

It is also worth noting that a bow-tie cavity has been incorporated into a Rydberg EIT experiment for demonstrating a polarization CNOT gate between two optical pulses interacting with hundreds of trapped ^{87}Rb atoms at an average efficiency of about 41.7%, far exceeding that in previous experiments.²⁸ This atom-cavity system in a ring geometry minimizes dephasings resulting from the combination photon recoil of atomic motion and is characterized by $(g, \kappa, \gamma) = 2\pi \times (1.0, 2.3, 3.0)$ MHz, thus yielding finesse $\mathcal{F} = 350$ and a collective cooperativity of 21 facilitating the enhanced interaction of single photons and Rydberg atoms. The four-mirror bow-tie cavity is shown in Fig. 28(a) where the target and control coupling beams are guided into the cavity from different concave mirrors, while the target and control qubits are input from a common convex mirror. This ring resonator is necessary for converting the π conditional phase shift into a two-photon gate for polarization qubits. The relative intensity and phase of the target signal reflected from the cavity have been measured as a function of the signal detuning from the cavity resonance in Figs. 28(b) and 28(c), respectively. In the absence of an EIT coupling light, the intensity exhibits a normal-mode splitting, while the phase shows two dispersive features, one at a normal mode (see red data). As the EIT coupling light is on, a narrow EIT feature appears at resonance so that a 2π phase boost may occur as the signal detuning is tuned through

zero (see blue data) - the origin of a π conditional phase shift on which the CNOT gate could be built.

Another interesting hybrid setup involves polar molecules and Rydberg atoms trapped in optical tweezer arrays in which the Rydberg blockade due to the charge-dipole interaction is demonstrated.³⁵⁴ This setup is highly beneficial because quantum information can be encoded in the internal states of the molecule, and quantum gates can be performed by utilizing the strong Rydberg-Rydberg interactions of atoms, with little sensitivity to the motional states of the particles.³⁵⁵⁻³⁵⁷

VI. CONCLUSION AND OUTLOOK

In conclusion, Rydberg atoms have emerged as one of the most promising platforms for probing quantum physics and quantum technological applications. The essential elements necessary for understanding Rydberg physics are covered in the first part of this review article, particularly the optical excitation of Rydberg states and the emergence of different types of Rydberg-Rydberg interactions, such as van der Waals and dipolar interactions, including the tunability using external fields. The strong interatomic interactions lead to the emergence of superatoms in Rydberg gases via the Rydberg blockade. When driving by resonant lasers, many-body Rabi oscillations can be found. The superatom approach is an efficient way to describe the dynamics and collective states, while the underlying mechanism can be used to generate robust and scalable entanglement in neutral atoms. Further, the same mechanism can create the entanglement between atoms and photons and between two photons. In an atom array, Rydberg blockade and superatoms serve a mechanism to emulate many-body spin models to create various many-body states and intricate quantum dynamics.

The remarkable collective excitation properties of Rydberg atoms hold immense promise for advancing quantum information processing and quantum optics. It is expected that an increasing number of experimental achievements and theoretical proposals will be seen in the coming years. Future developments have a number of exciting perspectives. Quantum simulation, quantum computation and quantum optics applications are promising growing area. To fully unlock the potential of Rydberg atom systems, new schemes and experimental techniques are needed in order to mitigate limitations (such as spin wave dephasing) in existing experiments. Moreover, by combining different quantum systems, their individual properties can be leveraged in order to realize unique functionality. Recently, hybrid systems in which Rydberg excitations combine with Bose-Einstein condensates,^{199,358} trapped ions,^{50,359} polar molecules,^{354,356,357} mechanical oscillators,³⁶⁰ etc., pave the way for the exploration of novel applications and physics in the future.

ACKNOWLEDGMENTS

The authors would like to extend their sincere gratitude to F. Cesa, C. S. Adams, S. Dürr, S. Hofferberth, Y. O. Dudin,

and D. Petrosyan, for their valuable comments. This work was supported by the National Natural Science Foundation of China (NSFC) under Grant Nos. 12174048, 12274376, 12074061, 12374329, and U21A6006, and the National Key Research and Development Program of China under Grant No. 2021YFA1402003. R.N. acknowledges DST-SERB for Swarnajayanti fellowship File No. SB/SJF/2020-21/19, and the MATRICS grant (MTR/2022/000454) from SERB, Government of India. W.L. acknowledges support from the EPSRC through Grant No. EP/W015641/1 and the Going Global Partnerships Programme of the British Council (Contract No. IND/CONT/G/22-23/26).

AUTHOR DECLARATIONS

Conflict of Interest

The authors have no conflicts to disclose.

Author Contributions

Xiao-Qiang Shao: Funding acquisition (equal); Writing-original draft (equal); Writing-review & editing (equal). **Shi-Lei Su:** Funding acquisition (equal); Writing-original draft (equal); Writing-review & editing (equal). **Lin Li:** Funding acquisition (equal); Writing-original draft (equal); Writing-review & editing (equal). **Rejish Nath:** Funding acquisition (equal); Writing-original draft (equal); Writing-review & editing (equal). **Jin-Hui Wu:** Funding acquisition (equal); Writing-original draft (equal); Writing-review & editing (equal). **Weibin Li:** Funding acquisition (equal); Writing-original draft (equal); Writing-review & editing (equal).

DATA AVAILABILITY

The data of Figs. 1 and 5 generated in this review article are available from the corresponding authors upon reasonable request.

REFERENCES

- ¹T. F. Gallagher, "Rydberg atoms," *Reports on Progress in Physics* **51**, 143 (1988).
- ²T. F. Gallagher, *Rydberg Atoms* (Cambridge University Press, 1994).
- ³M. Saffman, T. G. Walker, and K. Mølmer, "Quantum information with rydberg atoms," *Rev. Mod. Phys.* **82**, 2313–2363 (2010).
- ⁴E. Urban, T. A. Johnson, T. Henage, L. Isenhower, D. Yavuz, T. Walker, and M. Saffman, "Observation of rydberg blockade between two atoms," *Nature Physics* **5**, 110–114 (2009).
- ⁵A. Gaëtan, Y. Miroshnychenko, T. Wilk, A. Chotia, M. Viteau, D. Comparat, P. Pillet, A. Browaeys, and P. Grangier, "Observation of collective

excitation of two individual atoms in the rydberg blockade regime,” *Nature Physics* **5**, 115–118 (2009).

⁶D. Jaksch, J. I. Cirac, P. Zoller, S. L. Rolston, R. Côté, and M. D. Lukin, “Fast quantum gates for neutral atoms,” *Phys. Rev. Lett.* **85**, 2208–2211 (2000).

⁷A. Browaeys and T. Lahaye, “Many-body physics with individually controlled rydberg atoms,” *Nature Physics* **16**, 132–142 (2020).

⁸O. Firstenberg, C. S. Adams, and S. Hofferberth, “Nonlinear quantum optics mediated by rydberg interactions,” *Journal of Physics B: Atomic, Molecular and Optical Physics* **49**, 152003 (2016).

⁹R. Heidemann, U. Raitzsch, V. Bendkowsky, B. Butscher, R. Löw, L. Santos, and T. Pfau, “Evidence for coherent collective rydberg excitation in the strong blockade regime,” *Phys. Rev. Lett.* **99**, 163601 (2007).

¹⁰Y. Dudin, L. Li, F. Bariani, and A. Kuzmich, “Observation of coherent many-body rabi oscillations,” *Nature Physics* **8**, 790–794 (2012).

¹¹J. Zeiher, P. Schauß, S. Hild, T. Macrì, I. Bloch, and C. Gross, “Microscopic characterization of scalable coherent rydberg superatoms,” *Phys. Rev. X* **5**, 031015 (2015).

¹²M. D. Lukin, M. Fleischhauer, R. Cote, L. M. Duan, D. Jaksch, J. I. Cirac, and P. Zoller, “Dipole blockade and quantum information processing in mesoscopic atomic ensembles,” *Phys. Rev. Lett.* **87**, 037901 (2001).

¹³T. Pohl, E. Demler, and M. D. Lukin, “Dynamical crystallization in the dipole blockade of ultracold atoms,” *Phys. Rev. Lett.* **104**, 043002 (2010).

¹⁴B. Olmos, R. González-Férez, and I. Lesanovsky, “Fermionic collective excitations in a lattice gas of rydberg atoms,” *Phys. Rev. Lett.* **103**, 185302 (2009).

¹⁵J. Honer, H. Weimer, T. Pfau, and H. P. Büchler, “Collective many-body interaction in rydberg dressed atoms,” *Phys. Rev. Lett.* **105**, 160404 (2010).

¹⁶H. Weimer, M. Müller, I. Lesanovsky, P. Zoller, and H. P. Büchler, “A rydberg quantum simulator,” *Nature Physics* **6**, 382–388 (2010).

¹⁷S. Ji, C. Ates, and I. Lesanovsky, “Two-dimensional rydberg gases and the quantum hard-squares model,” *Phys. Rev. Lett.* **107**, 060406 (2011).

¹⁸S. de Léséleuc, V. Lienhard, P. Scholl, D. Barredo, S. Weber, N. Lang, H. P. Büchler, T. Lahaye, and A. Browaeys, “Observation of a symmetry-protected topological phase of interacting bosons with rydberg atoms,” *Science* **365**, 775–780 (2019).

¹⁹J. D. Pritchard, D. Maxwell, A. Gauguet, K. J. Weatherill, M. P. A. Jones, and C. S. Adams, “Cooperative atom-light interaction in a blockaded rydberg ensemble,” *Phys. Rev. Lett.* **105**, 193603 (2010).

²⁰T. Peyronel, O. Firstenberg, Q.-Y. Liang, S. Hofferberth, A. V. Gorshkov, T. Pohl, M. D. Lukin, and V. Vuletić, “Quantum nonlinear optics with single photons enabled by strongly interacting atoms,” *Nature* **488**, 57–60 (2012).

²¹Y. O. Dudin and A. Kuzmich, “Strongly interacting rydberg excitations of a cold atomic gas,” *Science* **336**, 887–889 (2012).

²²F. Ripka, H. Kübler, R. Löw, and T. Pfau, “A room-temperature single-photon source based on strongly interacting rydberg atoms,” *Science* **362**, 446–449 (2018).

²³A. Padrón-Brito, J. Lowinski, P. Farrera, K. Theophilo, and H. de Riedmatten, “Probing the indistinguishability of single photons generated by rydberg atomic ensembles,” *Phys. Rev. Res.* **3**, 033287 (2021).

²⁴D. P. Ornelas-Huerta, A. N. Craddock, E. A. Goldschmidt, A. J. Hachtel, Y. Wang, P. Bienias, A. V. Gorshkov, S. L. Rolston, and J. V. Porto, “On-demand indistinguishable single photons from an efficient and pure source based on a rydberg ensemble,” *Optica* **7**, 813–819 (2020).

²⁵S. Shi, B. Xu, K. Zhang, G.-S. Ye, D.-S. Xiang, Y. Liu, J. Wang, D. Su, and L. Li, “High-fidelity photonic quantum logic gate based on near-optimal rydberg single-photon source,” *Nature Communications* **13**, 4454 (2022).

²⁶D. Tiarks, S. Schmidt, G. Rempe, and S. Dürr, “Optical π phase shift created with a single-photon pulse,” *Science Advances* **2**, e1600036 (2016).

²⁷D. Tiarks, S. Schmidt-Eberle, T. Stolz, G. Rempe, and S. Dürr, “A photon-photon quantum gate based on rydberg interactions,” *Nature Physics* **15**, 124–126 (2019).

²⁸T. Stolz, H. Hegels, M. Winter, B. Röhr, Y.-F. Hsiao, L. Husel, G. Rempe, and S. Dürr, “Quantum-logic gate between two optical photons with an average efficiency above 40%,” *Phys. Rev. X* **12**, 021035 (2022).

²⁹G.-S. Ye, B. Xu, Y. Chang, S. Shi, T. Shi, and L. Li, “A photonic entanglement filter with rydberg atoms,” *Nature Photonics* **17**, 538–543 (2023).

³⁰C. Tresp, C. Zimmer, I. Mirgorodskiy, H. Gorniaczyk, A. Paris-Mandoki, and S. Hofferberth, “Single-photon absorber based on strongly interacting rydberg atoms,” *Phys. Rev. Lett.* **117**, 223001 (2016).

³¹S. Baur, D. Tiarks, G. Rempe, and S. Dürr, “Single-photon switch based on rydberg blockade,” *Phys. Rev. Lett.* **112**, 073901 (2014).

³²H. Gorniaczyk, C. Tresp, J. Schmidt, H. Fedder, and S. Hofferberth, “Single-photon transistor mediated by interstate rydberg interactions,” *Phys. Rev. Lett.* **113**, 053601 (2014).

³³J. Lim, H.-g. Lee, and J. Ahn, “Review of cold Rydberg atoms and their applications,” *Journal of the Korean Physical Society* **63**, 867 (2013).

³⁴M. Nakagawa, N. Kawakami, and M. Ueda, “Non-hermitian kondo effect in ultracold alkaline-earth atoms,” *Phys. Rev. Lett.* **121**, 203001 (2018).

³⁵A. Cooper, J. P. Covey, I. S. Madjarov, S. G. Porsev, M. S. Safronova, and M. Endres, “Alkaline-earth atoms in optical tweezers,” *Phys. Rev. X* **8**, 041055 (2018).

³⁶R. Zhang, Y. Cheng, P. Zhang, and H. Zhai, “Controlling the interaction of ultracold alkaline-earth atoms,” *Nature Reviews Physics* **2**, 213–220 (2020).

³⁷F. Schäfer, T. Fukuhara, S. Sugawa, Y. Takasu, and Y. Takahashi, “Tools for quantum simulation with ultracold atoms in optical lattices,” *Nature Reviews Physics* **2**, 411–425 (2020).

³⁸A. M. Kaufman and K.-K. Ni, “Quantum science with optical tweezer arrays of ultracold atoms and molecules,” *Nature Physics* **17**, 1324–1333 (2021).

³⁹M. A. Norcia and F. Ferlaino, “Developments in atomic control using ultracold magnetic lanthanides,” *Nature Physics* **17**, 1349–1357 (2021).

⁴⁰R. Mukherjee, J. Millen, R. Nath, M. P. A. Jones, and T. Pohl, “Many-body physics with alkaline-earth rydberg lattices,” *Journal of Physics B: Atomic, Molecular and Optical Physics* **44**, 184010 (2011).

⁴¹J. T. Wilson, S. Saskin, Y. Meng, S. Ma, R. Dilip, A. P. Burgers, and J. D. Thompson, “Trapping alkaline earth rydberg atoms optical tweezer arrays,” *Phys. Rev. Lett.* **128**, 033201 (2022).

⁴²A. Piñeiro Orioli, J. K. Thompson, and A. M. Rey, “Emergent dark states from superradiant dynamics in multilevel atoms in a cavity,” *Phys. Rev. X* **12**, 011054 (2022).

⁴³A. Muni, L. Lachaud, A. Couto, M. Poirier, R. C. Teixeira, J. M. Raimond, M. Brune, and S. Gleyzes, “Optical coherent manipulation of alkaline-earth circular rydberg states,” *Nature Physics* **18**, 502–505 (2022).

⁴⁴Y. Wu, S. Kolkowitz, S. Puri, and J. D. Thompson, “Erasure conversion for fault-tolerant quantum computing in alkaline earth rydberg atom arrays,” *Nature communications* **13**, 4657 (2022).

⁴⁵M. Müller, L. Liang, I. Lesanovsky, and P. Zoller, “Trapped rydberg ions: from spin chains to fast quantum gates,” *New Journal of Physics* **10**, 093009 (2008).

⁴⁶T. Feldker, P. Bachor, M. Stappel, D. Kolbe, R. Gerritsma, J. Walz, and F. Schmidt-Kaler, “Rydberg excitation of a single trapped ion,” *Phys. Rev. Lett.* **115**, 173001 (2015).

⁴⁷W. Li and I. Lesanovsky, “Electronically excited cold ion crystals,” *Phys. Rev. Lett.* **108**, 023003 (2012).

⁴⁸G. Higgins, F. Pokorný, C. Zhang, Q. Bodart, and M. Hennrich, “Coherent control of a single trapped rydberg ion,” *Phys. Rev. Lett.* **119**, 220501 (2017).

⁴⁹F. M. Gambetta, I. Lesanovsky, and W. Li, “Exploring nonequilibrium phases of the generalized dicke model with a trapped rydberg-ion quantum simulator,” *Phys. Rev. A* **100**, 022513 (2019).

⁵⁰C. Zhang, F. Pokorný, W. Li, G. Higgins, A. Pöschl, I. Lesanovsky, and M. Hennrich, “Submicrosecond entangling gate between trapped ions via rydberg interaction,” *Nature* **580**, 345–349 (2020).

⁵¹F. M. Gambetta, C. Zhang, M. Hennrich, I. Lesanovsky, and W. Li, “Exploring the many-body dynamics near a conical intersection with trapped rydberg ions,” *Phys. Rev. Lett.* **126**, 233404 (2021).

⁵²T. Kazimierczuk, D. Fröhlich, S. Scheel, H. Stolz, and M. Bayer, “Giant rydberg excitons in the copper oxide cu₂o,” *Nature* **514**, 343–347 (2014).

⁵³M. Aßmann and M. Bayer, “Semiconductor rydberg physics,” *Advanced Quantum Technologies* **3**, 1900134 (2020).

⁵⁴J. Heckötter, M. Freitag, D. Fröhlich, M. Aßmann, M. Bayer, M. A. Semina, and M. M. Glazov, “Scaling laws of rydberg excitons,” *Phys. Rev. B* **96**, 125142 (2017).

⁵⁵M. J. Seaton, “Quantum defect theory,” *Reports on Progress in Physics* **46**, 167 (1983).

⁵⁶C.-J. Lorenzen and K. Niemax, “Quantum defects of the n2p1/2,3/2 levels in 39k i and 85rb i,” *Physica Scripta* **27**, 300 (1983).

⁵⁷P. Goy, J. M. Raimond, G. Vitrant, and S. Haroche, “Millimeter-wave spectroscopy in cesium rydberg states. quantum defects, fine- and hyperfine-structure measurements,” *Phys. Rev. A* **26**, 2733–2742 (1982).

⁵⁸C. J. Lorenzen and K. Niemax, “Precise quantum defects of ns, np and nd levels in cs i,” *Zeitschrift für Physik A Atoms and Nuclei* **315**, 127–133 (1984).

⁵⁹K.-H. Weber and C. J. Sansonetti, “Accurate energies of ns, np, nd, nf, and ng levels of neutral cesium,” *Phys. Rev. A* **35**, 4650–4660 (1987).

⁶⁰S. Dyubko, M. Efimenko, V. Efremov, and S. Podnos, “Microwave spectroscopy of s, p, and d states of sodium rydberg atoms,” *Phys. Rev. A* **52**, 514–517 (1995).

⁶¹W. Li, I. Mourachko, M. W. Noel, and T. F. Gallagher, “Millimeter-wave spectroscopy of cold rb rydberg atoms in a magneto-optical trap: Quantum defects of the ns, np, and nd series,” *Phys. Rev. A* **67**, 052502 (2003).

⁶²J. Han, Y. Jamil, D. V. L. Norum, P. J. Tanner, and T. F. Gallagher, “Rb nf quantum defects from millimeter-wave spectroscopy of cold ^{85}Rb rydberg atoms,” *Phys. Rev. A* **74**, 054502 (2006).

⁶³K. Afrousheh, P. Bohloli-Zanjani, J. A. Petrus, and J. D. D. Martin, “Determination of the ^{85}Rb ng-series quantum defect by electric-field-induced resonant energy transfer between cold rydberg atoms,” *Phys. Rev. A* **74**, 062712 (2006).

⁶⁴B. Sanguinetti, H. O. Majeed, M. L. Jones, and B. T. H. Varcoe, “Precision measurements of quantum defects in the np3/2 rydberg states of ^{85}Rb ,” *Journal of Physics B: Atomic, Molecular and Optical Physics* **42**, 165004 (2009).

⁶⁵M. Mack, F. Karlewski, H. Hattermann, S. Höckh, F. Jessen, D. Cano, and J. Fortágh, “Measurement of absolute transition frequencies of ^{87}Rb to nS and nD rydberg states by means of electromagnetically induced transparency,” *Phys. Rev. A* **83**, 052515 (2011).

⁶⁶J. Deiglmayr, H. Herburger, H. Saßmannshausen, P. Jansen, H. Schmutz, and F. Merkt, “Precision measurement of the ionization energy of cs i,” *Phys. Rev. A* **93**, 013424 (2016).

⁶⁷V. A. Sautenkov, S. A. Saakyan, E. V. Vilshanskaya, D. A. Murashkin, B. B. Zelener, and B. V. Zelener, “Quantum defects in rydberg nd states of optically cooled ^{7}Li atoms,” *Laser Physics* **26**, 115701 (2016).

⁶⁸M. Li, B. Li, X. Jiang, J. Qian, X. Li, and L. Liu, “Measurement of 85rb np-state transition frequencies via single-photon rydberg excitation spectroscopy,” *J. Opt. Soc. Am. B* **36**, 1850–1857 (2019).

⁶⁹S. Li, J. Yuan, L. Wang, L. Xiao, and S. Jia, “Measurement of the quantum defects of 85rb p and f-series via microwave-assisted electromagnetically induced transparency spectroscopy,” *Results in Physics* **29**, 104728 (2021).

⁷⁰J. Bai, Y. Jiao, R. Song, J. Fan, J. Zhao, S. Jia, and G. Raithel, “Quantum defects of nf_j levels of cs rydberg atoms,” *arXiv preprint arXiv:2304.07974* (2023).

⁷¹S. Weber, C. Tresp, H. Menke, A. Urvoy, O. Firstenberg, H. P. Büchler, and S. Hofferberth, “Calculation of rydberg interaction potentials,” *Journal of Physics B: Atomic, Molecular and Optical Physics* **50**, 133001 (2017).

⁷²N. Šibalić, J. Pritchard, C. Adams, and K. Weatherill, “Arc: An open-source library for calculating properties of alkali rydberg atoms,” *Computer Physics Communications* **220**, 319–331 (2017).

⁷³K. Prozument, A. P. Colombo, Y. Zhou, G. B. Park, V. S. Petrović, S. L. Coy, and R. W. Field, “Chirped-pulse millimeter-wave spectroscopy of rydberg-rydberg transitions,” *Phys. Rev. Lett.* **107**, 143001 (2011).

⁷⁴J. A. Gordon, C. L. Holloway, A. Schwarzkopf, D. A. Anderson, S. Miller, N. Thaicharoen, and G. Raithel, “Millimeter wave detection via Autler-Townes splitting in rubidium Rydberg atomsa,” *Applied Physics Letters* **105**, 024104 (2014).

⁷⁵J. M. Raimond, P. Goy, M. Gross, C. Fabre, and S. Haroche, “Statistics of millimeter-wave photons emitted by a rydberg-atom maser: An experimental study of fluctuations in single-mode superradiance,” *Phys. Rev. Lett.* **49**, 1924–1927 (1982).

⁷⁶L. Moi, P. Goy, M. Gross, J. M. Raimond, C. Fabre, and S. Haroche, “Rydberg-atom masers. i. a theoretical and experimental study of superradiant systems in the millimeter-wave domain,” *Phys. Rev. A* **27**, 2043–2064 (1983).

⁷⁷P. Goy, L. Moi, M. Gross, J. M. Raimond, C. Fabre, and S. Haroche, “Rydberg-atom masers. ii. triggering by external radiation and application to millimeter-wave detectors,” *Phys. Rev. A* **27**, 2065–2081 (1983).

⁷⁸A. B. Deb and N. Kjærgaard, “Radio-over-fiber using an optical antenna based on Rydberg states of atoms,” *Applied Physics Letters* **112**, 211106 (2018).

⁷⁹J. Yuan, T. Jin, L. Xiao, S. Jia, and L. Wang, “A rydberg atom-based receiver with amplitude modulation technique for the fifth-generation millimeter-wave wireless communication,” *IEEE Antennas and Wireless Propagation Letters* , 1–5 (2023).

⁸⁰J. D. Carter and J. D. D. Martin, “Coherent manipulation of cold rydberg atoms near the surface of an atom chip,” *Phys. Rev. A* **88**, 043429 (2013).

⁸¹M. Kiffner, A. Feizpour, K. T. Kaczmarek, D. Jaksch, and J. Nunn, “Two-way interconversion of millimeter-wave and optical fields in rydberg gases,” *New Journal of Physics* **18**, 093030 (2016).

⁸²D. D. Grimes, S. L. Coy, T. J. Barnum, Y. Zhou, S. F. Yelin, and R. W. Field, “Direct single-shot observation of millimeter-wave superradiance in rydberg-rydberg transitions,” *Phys. Rev. A* **95**, 043818 (2017).

⁸³C. G. Wade, N. Šibalić, N. R. de Melo, J. M. Kondo, C. S. Adams, and K. J. Weatherill, “Real-time near-field terahertz imaging with atomic optical fluorescence,” *Nature Photonics* **11**, 40–43 (2017).

⁸⁴M. Peper, J. Deiglmayr, F. Merkt, C. Sanna, and H. B. v. L. van den Heuvel, “Magic rydberg-rydberg transitions in electric fields,” *Phys. Rev. A* **100**, 032512 (2019).

⁸⁵A. Suleymanzade, A. Anferov, M. Stone, R. K. Naik, A. Oriani, J. Simon, and D. Schuster, “A tunable high-Q millimeter wave cavity for hybrid circuit and cavity QED experiments,” *Applied Physics Letters* **116**, 104001 (2020).

⁸⁶S. K. Kanungo, J. D. Whalen, Y. Lu, M. Yuan, S. Dasgupta, F. B. Dunning, K. R. A. Hazzard, and T. C. Killian, “Realizing topological edge states with rydberg-atom synthetic dimensions,” *Nature Communications* **13**, 972 (2022).

⁸⁷R. Legaie, G. Raithel, and D. A. Anderson, “A millimeter-wave atomic receiver,” *arXiv preprint arXiv:2306.17114* (2023).

⁸⁸C. E. Theodosiou, “Lifetimes of alkali-metal–atom rydberg states,” *Phys. Rev. A* **30**, 2881–2909 (1984).

⁸⁹G. Herzberg, “Rydberg molecules,” *Annual Review of Physical Chemistry* **38**, 27–56 (1987).

⁹⁰C. H. Greene, A. S. Dickinson, and H. R. Sadeghpour, “Creation of polar and nonpolar ultra-long-range rydberg molecules,” *Phys. Rev. Lett.* **85**, 2458–2461 (2000).

⁹¹V. Bendkowsky, B. Butscher, J. Nipper, J. P. Shaffer, R. Löw, and T. Pfau, “Observation of ultralong-range rydberg molecules,” *Nature* **458**, 1005–1008 (2009).

⁹²V. Bendkowsky, B. Butscher, J. Nipper, J. B. Balewski, J. P. Shaffer, R. Löw, T. Pfau, W. Li, J. Stanojevic, T. Pohl, and J. M. Rost, “Rydberg trimers and excited dimers bound by internal quantum reflection,” *Phys. Rev. Lett.* **105**, 163201 (2010).

⁹³M. Kiffner, H. Park, W. Li, and T. F. Gallagher, “Dipole-dipole-coupled double-rydberg molecules,” *Phys. Rev. A* **86**, 031401 (2012).

⁹⁴A. T. Krupp, A. Gaj, J. B. Balewski, P. Ilzhöfer, S. Hofferberth, R. Löw, T. Pfau, M. Kurz, and P. Schmelcher, “Alignment of d-state rydberg molecules,” *Phys. Rev. Lett.* **112**, 143008 (2014).

⁹⁵F. Camargo, J. D. Whalen, R. Ding, H. R. Sadeghpour, S. Yoshida, J. Burgdörfer, F. B. Dunning, and T. C. Killian, “Lifetimes of ultra-long-range strontium rydberg molecules,” *Phys. Rev. A* **93**, 022702 (2016).

⁹⁶W. Li, T. Pohl, J. M. Rost, S. T. Rittenhouse, H. R. Sadeghpour, J. Nipper, B. Butscher, J. B. Balewski, V. Bendkowsky, R. Löw, and T. Pfau, “A Homonuclear Molecule with a Permanent Electric Dipole Moment,” *334*, 1110–1114, 22116881.

⁹⁷M. T. Eiles and C. H. Greene, “Hamiltonian for the inclusion of spin effects in long-range rydberg molecules,” *Phys. Rev. A* **95**, 042515 (2017).

⁹⁸M. T. Eiles, H. Lee, J. Pérez-Ríos, and C. H. Greene, “Anisotropic blockade using pendular long-range rydberg molecules,” *Phys. Rev. A* **95**, 052708 (2017).

⁹⁹J. Shaffer, S. Rittenhouse, and H. Sadeghpour, “Ultracold rydberg molecules,” *Nature communications* **9**, 1965 (2018).

¹⁰⁰J. D. Whalen, S. K. Kanungo, Y. Lu, S. Yoshida, J. Burgdörfer, F. B. Dunning, and T. C. Killian, “Heteronuclear rydberg molecules,” *Phys. Rev. A* **101**, 060701 (2020).

¹⁰¹P. Giannakeas, M. T. Eiles, F. Robicheaux, and J. M. Rost, “Generalized local frame-transformation theory for ultralong-range rydberg molecules,” *Phys. Rev. A* **102**, 033315 (2020).

¹⁰²M. Peper and J. Deiglmayr, “Heteronuclear long-range rydberg molecules,” *Phys. Rev. Lett.* **126**, 013001 (2021).

¹⁰³F. H. Christian Fey and P. Schmelcher, "Ultralong-range rydberg molecules," *Molecular Physics* **118**, e1679401 (2020).

¹⁰⁴F. Hummel, M. T. Eiles, and P. Schmelcher, "Synthetic dimension-induced conical intersections in rydberg molecules," *Phys. Rev. Lett.* **127**, 023003 (2021).

¹⁰⁵I. I. Sobelman, *Atomic Spectra and Radiative Transitions* (Springer Berlin, Heidelberg, 1979).

¹⁰⁶J. Deiglmayr, M. Reetz-Lamour, T. Amthor, S. Westermann, A. de Oliveira, and M. Weidemüller, "Coherent excitation of rydberg atoms in an ultracold gas," *Optics Communications* **264**, 293–298 (2006).

¹⁰⁷C. Seiler, J. A. Agner, P. Pillet, and F. Merkt, "Radiative and collisional processes in translationally cold samples of hydrogen rydberg atoms studied in an electrostatic trap," *Journal of Physics B: Atomic, Molecular and Optical Physics* **49**, 094006 (2016).

¹⁰⁸I. Beterov, I. I. Ryabtsev, D. B. Tretyakov, and V. M. Entin, "Quasiclassical calculations of blackbody-radiation-induced depopulation rates and effective lifetimes of rydberg ns , np , and nd alkali-metal atoms with $n \leq 80$," *Phys. Rev. A* **79**, 052504 (2009).

¹⁰⁹R. G. Hulet and D. Kleppner, "Rydberg atoms in "circular" states," *Phys. Rev. Lett.* **51**, 1430–1433 (1983).

¹¹⁰T. L. Nguyen, J. M. Raimond, C. Sayrin, R. Cortiñas, T. Cantat-Moltrecht, F. Assemat, I. Dotsenko, S. Gleyzes, S. Haroche, G. Roux, T. Jolicoeur, and M. Brune, "Towards quantum simulation with circular rydberg atoms," *Phys. Rev. X* **8**, 011032 (2018).

¹¹¹A. Khadjavi, A. Lurio, and W. Happer, "Stark effect in the excited states of rb , cs , cd , and hg ," *Phys. Rev.* **167**, 128–135 (1968).

¹¹²M. Weissbluth, "Atoms and molecules," Academic Press, New York (1978).

¹¹³M. L. Zimmerman, M. G. Littman, M. M. Kash, and D. Kleppner, "Stark structure of the rydberg states of alkali-metal atoms," *Phys. Rev. A* **20**, 2251–2275 (1979).

¹¹⁴M. S. O'Sullivan and B. P. Stoicheff, "Scalar polarizabilities and avoided crossings of high rydberg states in rb ," *Phys. Rev. A* **31**, 2718–2720 (1985).

¹¹⁵Z. Lai, S. Zhang, Q. Gou, and Y. Li, "Polarizabilities of rydberg states of rb atoms with n up to 140," *Phys. Rev. A* **98**, 052503 (2018).

¹¹⁶J. Bai, S. Bai, X. Han, Y. Jiao, J. Zhao, and S. Jia, "Precise measurements of polarizabilities of cesium ns rydberg states in an ultra-cold atomic ensemble," *New Journal of Physics* **22**, 093032 (2020).

¹¹⁷A. Chakraborty and B. K. Sahoo, "High-precision electric dipole polarizabilities of the clock states in ^{133}Cs ," *Phys. Rev. A* **108**, 042818 (2023).

¹¹⁸J. A. Sedlacek, A. Schwettmann, H. Kübler, R. Löw, T. Pfau, and J. P. Shaffer, "Microwave electrometry with rydberg atoms in a vapour cell using bright atomic resonances," *Nature physics* **8**, 819–824 (2012).

¹¹⁹H. Q. Fan, S. Kumar, R. Daschner, H. Kübler, and J. P. Shaffer, "Subwavelength microwave electric-field imaging using rydberg atoms inside atomic vapor cells," *Opt. Lett.* **39**, 3030–3033 (2014).

¹²⁰H. Fan, S. Kumar, J. Sedlacek, H. Kübler, S. Karimkashi, and J. P. Shaffer, "Atom based rf electric field sensing," *Journal of Physics B: Atomic, Molecular and Optical Physics* **48**, 202001 (2015).

¹²¹D. A. Anderson, E. G. Paradis, and G. Raithel, "A vapor-cell atomic sensor for radio-frequency field detection using a polarization-selective field enhancement resonator," *Applied Physics Letters* **113**, 073501 (2018).

¹²²K. C. Cox, D. H. Meyer, F. K. Fatemi, and P. D. Kunz, "Quantum-limited atomic receiver in the electrically small regime," *Phys. Rev. Lett.* **121**, 110502 (2018).

¹²³D. H. Meyer, Z. A. Castillo, K. C. Cox, and P. D. Kunz, "Assessment of rydberg atoms for wideband electric field sensing," *Journal of Physics B: Atomic, Molecular and Optical Physics* **53**, 034001 (2020).

¹²⁴M. Jing, Y. Hu, J. Ma, H. Zhang, L. Zhang, L. Xiao, and S. Jia, "Atomic superheterodyne receiver based on microwave-dressed rydberg spectroscopy," *Nature Physics* **16**, 911–915 (2020).

¹²⁵S. E. Crawford, R. A. Shugayev, H. P. Paudel, P. Lu, M. Syamlal, P. R. Ohodnicki, B. Chorpeling, R. Gentry, and Y. Duan, "Quantum sensing for energy applications: Review and perspective," *Advanced Quantum Technologies* **4**, 2100049 (2021).

¹²⁶D. H. Meyer, C. O'Brien, D. P. Fahey, K. C. Cox, and P. D. Kunz, "Optimal atomic quantum sensing using electromagnetically-induced transparency readout," *Phys. Rev. A* **104**, 043103 (2021).

¹²⁷V. Calero, R. Fernández-Mateo, H. Morgan, P. García-Sánchez, and A. Ramos, "Stationary electro-osmotic flow driven by ac fields around inulators," *Phys. Rev. Appl.* **15**, 014047 (2021).

¹²⁸J. Hu, H. Li, R. Song, J. Bai, Y. Jiao, J. Zhao, and S. Jia, "Continuously tunable radio frequency electrometry with Rydberg atoms," *Applied Physics Letters* **121**, 014002 (2022).

¹²⁹B. Liu, L.-H. Zhang, Z.-K. Liu, Z.-Y. Zhang, Z.-H. Zhu, W. Gao, G.-C. Guo, D.-S. Ding, and B.-S. Shi, "Highly sensitive measurement of a megahertz rf electric field with a rydberg-atom sensor," *Phys. Rev. Appl.* **18**, 014045 (2022).

¹³⁰C. T. Fancher, K. L. Nicolich, K. M. Backes, N. Malvania, K. Cox, D. H. Meyer, P. D. Kunz, J. C. Hill, W. Holland, and B. L. Schmittberger Marlow, "A self-locking Rydberg atom electric field sensor," *Applied Physics Letters* **122**, 094001 (2023).

¹³¹B. Liu, L. Zhang, Z. Liu, Z. Deng, D. Ding, B. Shi, and G. Guo, "Electric field measurement and application based on rydberg atoms," *Electromagnetic Science* **1**, 1–16 (2023).

¹³²J. Yuan, W. Yang, M. Jing, H. Zhang, Y. Jiao, W. Li, L. Zhang, L. Xiao, and S. Jia, "Quantum sensing of microwave electric fields based on rydberg atoms," *Reports on Progress in Physics* **86**, 106001 (2023).

¹³³G. Günter, M. Robert-de Saint-Vincent, H. Schempp, C. S. Hofmann, S. Whitlock, and M. Weidemüller, "Interaction enhanced imaging of individual rydberg atoms in dense gases," *Phys. Rev. Lett.* **108**, 013002 (2012).

¹³⁴C. Gross, T. Vogt, and W. Li, "Ion imaging via long-range interaction with rydberg atoms," *Phys. Rev. Lett.* **124**, 053401 (2020).

¹³⁵R. Löw, H. Weimer, J. Nipper, J. B. Balewski, B. Butscher, H. P. Büchler, and T. Pfau, "An experimental and theoretical guide to strongly interacting rydberg gases," *Journal of Physics B: Atomic, Molecular and Optical Physics* **45**, 113001 (2012).

¹³⁶A. Browaeys, D. Barredo, and T. Lahaye, "Experimental investigations of dipole–dipole interactions between a few rydberg atoms," *Journal of Physics B: Atomic, Molecular and Optical Physics* **49**, 152001 (2016).

¹³⁷M. Saffman, "Quantum computing with atomic qubits and rydberg interactions: progress and challenges," *Journal of Physics B: Atomic, Molecular and Optical Physics* **49**, 202001 (2016).

¹³⁸P. Schauss, "Quantum simulation of transverse ising models with rydberg atoms," *Quantum Science and Technology* **3**, 023001 (2018).

¹³⁹S. Wüster and J.-M. Rost, "Rydberg aggregates," *Journal of Physics B: Atomic, Molecular and Optical Physics* **51**, 032001 (2018).

¹⁴⁰C. S. Adams, J. D. Pritchard, and J. P. Shaffer, "Rydberg atom quantum technologies," *Journal of Physics B: Atomic, Molecular and Optical Physics* **53**, 012002 (2019).

¹⁴¹I. I. Beterov, D. B. Tretyakov, V. M. Entin, E. A. Yakshina, I. I. Ryabtsev, M. Saffman, and S. Bergamini, "Application of adiabatic passage in rydberg atomic ensembles for quantum information processing," *Journal of Physics B: Atomic, Molecular and Optical Physics* **53**, 182001 (2020).

¹⁴²L. Henriet, L. Beguin, A. Signoles, T. Lahaye, A. Browaeys, G.-O. Raymond, and C. Jurczak, "Quantum computing with neutral atoms," *Quantum* **4**, 327 (2020).

¹⁴³M. Morgado and S. Whitlock, "Quantum simulation and computing with Rydberg-interacting qubits," *AVS Quantum Science* **3**, 023501 (2021).

¹⁴⁴X. Wu, X. Liang, Y. Tian, F. Yang, C. Chen, Y.-C. Liu, M. K. Tey, and L. You, "A concise review of rydberg atom based quantum computation and quantum simulation*," *Chinese Physics B* **30**, 020305 (2021).

¹⁴⁵X.-F. Shi, "Quantum logic and entanglement by neutral rydberg atoms: methods and fidelity," *Quantum Science and Technology* **7**, 023002 (2022).

¹⁴⁶A. Dalgarno and W. Davison, "The calculation of van der waals interactions," *Advances in Atomic and Molecular Physics* **2**, 1–32 (1966).

¹⁴⁷L. You and M. S. Chapman, "Quantum entanglement using trapped atomic spins," *Phys. Rev. A* **62**, 052302 (2000).

¹⁴⁸D. Barredo, H. Labuhn, S. Ravets, T. Lahaye, A. Browaeys, and C. S. Adams, "Coherent excitation transfer in a spin chain of three rydberg atoms," *Phys. Rev. Lett.* **114**, 113002 (2015).

¹⁴⁹S. de Léséleuc, D. Barredo, V. Lienhard, A. Browaeys, and T. Lahaye, "Optical control of the resonant dipole-dipole interaction between rydberg atoms," *Phys. Rev. Lett.* **119**, 053202 (2017).

¹⁵⁰V. Lienhard, P. Scholl, S. Weber, D. Barredo, S. de Léséleuc, R. Bai, N. Lang, M. Fleischhauer, H. P. Büchler, T. Lahaye, and A. Browaeys, "Realization of a density-dependent peierls phase in a synthetic, spin-orbit coupled rydberg system," *Phys. Rev. X* **10**, 021031 (2020).

¹⁵¹D. W. Schönleber, A. Eisfeld, M. Genkin, S. Whitlock, and S. Wüster, “Quantum simulation of energy transport with embedded rydberg aggregates,” *Phys. Rev. Lett.* **114**, 123005 (2015).

¹⁵²S. Geier, N. Thaicharoen, C. Hainaut, T. Franz, A. Salzinger, A. Tebben, D. Grimschandl, G. Zürn, and M. Weidemüller, “Floquet hamiltonian engineering of an isolated many-body spin system,” *Science* **374**, 1149–1152 (2021).

¹⁵³P. Scholl, H. J. Williams, G. Bornet, F. Wallner, D. Barredo, L. Henriet, A. Signoles, C. Hainaut, T. Franz, S. Geier, A. Tebben, A. Salzinger, G. Zürn, T. Lahaye, M. Weidemüller, and A. Browaeys, “Microwave engineering of programmable xxz hamiltonians in arrays of rydberg atoms,” *PRX Quantum* **3**, 020303 (2022).

¹⁵⁴C. Chen, G. Bornet, M. Bintz, G. Emperauger, L. Leclerc, V. S. Liu, P. Scholl, D. Barredo, J. Hauschild, S. Chatterjee, *et al.*, “Continuous symmetry breaking in a two-dimensional rydberg array,” *Nature* **616**, 691–695 (2023).

¹⁵⁵N. Nishad, A. Keselman, T. Lahaye, A. Browaeys, and S. Tsesses, “Quantum simulation of generic spin exchange models in floquet-engineered rydberg atom arrays,” *arXiv preprint arXiv:2306.07041* (2023).

¹⁵⁶C. Chen, G. Emperauger, G. Bornet, F. Caleca, B. Gély, M. Bintz, S. Chatterjee, V. Liu, D. Barredo, N. Y. Yao, *et al.*, “Spectroscopy of elementary excitations from quench dynamics in a dipolar xy rydberg simulator,” *arXiv preprint arXiv:2311.11726* (2023).

¹⁵⁷G. Bornet, G. Emperauger, C. Chen, F. Machado, S. Chern, L. Leclerc, B. Gély, D. Barredo, T. Lahaye, N. Y. Yao, *et al.*, “Enhancing a many-body dipolar rydberg tweezer array with arbitrary local controls,” *arXiv preprint arXiv:2402.11056* (2024).

¹⁵⁸X. X. Li, D. X. Li, and X. Q. Shao, “Generation of complete graph states in a spin-1/2 heisenberg chain with a globally optimized magnetic field,” *Phys. Rev. A* **109**, 042604 (2024).

¹⁵⁹T. G. Walker and M. Saffman, “Zeros of rydberg–rydberg förster interactions,” *Journal of Physics B: Atomic, Molecular and Optical Physics* **38**, S309 (2005).

¹⁶⁰I. I. Ryabtsev, D. B. Tretyakov, I. I. Beterov, and V. M. Entin, “Observation of the stark-tuned förster resonance between two rydberg atoms,” *Phys. Rev. Lett.* **104**, 073003 (2010).

¹⁶¹S. Ravets, H. Labuhn, D. Barredo, L. Béguin, T. Lahaye, and A. Browaeys, “Coherent dipole–dipole coupling between two single rydberg atoms at an electrically-tuned förster resonance,” *Nature Physics* **10**, 914–917 (2014).

¹⁶²S. Ravets, H. Labuhn, D. Barredo, T. Lahaye, and A. Browaeys, “Measurement of the angular dependence of the dipole-dipole interaction between two individual rydberg atoms at a förster resonance,” *Phys. Rev. A* **92**, 020701 (2015).

¹⁶³I. I. Beterov and M. Saffman, “Rydberg blockade, förster resonances, and quantum state measurements with different atomic species,” *Phys. Rev. A* **92**, 042710 (2015).

¹⁶⁴R. Faoro, B. Pelle, A. Zuliani, P. Cheinet, E. Arimondo, and P. Pillet, “Borromean three-body fret in frozen rydberg gases,” *Nature Communications* **6**, 8173 (2015).

¹⁶⁵D. B. Tretyakov, I. I. Beterov, E. A. Yakshina, V. M. Entin, I. I. Ryabtsev, P. Cheinet, and P. Pillet, “Observation of the borromean three-body förster resonances for three interacting rb rydberg atoms,” *Phys. Rev. Lett.* **119**, 173402 (2017).

¹⁶⁶I. I. Ryabtsev, I. I. Beterov, D. B. Tretyakov, E. A. Yakshina, V. M. Entin, P. Cheinet, and P. Pillet, “Coherence of three-body förster resonances in rydberg atoms,” *Phys. Rev. A* **98**, 052703 (2018).

¹⁶⁷I. I. Beterov, M. Saffman, E. A. Yakshina, D. B. Tretyakov, V. M. Entin, S. Bergamini, E. A. Kuznetsova, and I. I. Ryabtsev, “Two-qubit gates using adiabatic passage of the stark-tuned förster resonances in rydberg atoms,” *Phys. Rev. A* **94**, 062307 (2016).

¹⁶⁸I. I. Beterov, G. N. Hamzina, E. A. Yakshina, D. B. Tretyakov, V. M. Entin, and I. I. Ryabtsev, “Adiabatic passage of radio-frequency-assisted förster resonances in rydberg atoms for two-qubit gates and the generation of bell states,” *Phys. Rev. A* **97**, 032701 (2018).

¹⁶⁹X.-R. Huang, Z.-X. Ding, C.-S. Hu, L.-T. Shen, W. Li, H. Wu, and S.-B. Zheng, “Robust rydberg gate via landau-zener control of förster resonance,” *Phys. Rev. A* **98**, 052324 (2018).

¹⁷⁰Y. Chew, T. Tomita, T. P. Mahesh, S. Sugawa, S. de Léséleuc, and K. Ohmori, “Ultrafast energy exchange between two single rydberg atoms on a nanosecond timescale,” *Nature Photonics* **16**, 724–729 (2022).

¹⁷¹T. G. Walker and M. Saffman, “Consequences of zeeman degeneracy for the van der waals blockade between rydberg atoms,” *Phys. Rev. A* **77**, 032723 (2008).

¹⁷²L. Béguin, A. Vernier, R. Chicireanu, T. Lahaye, and A. Browaeys, “Direct measurement of the van der waals interaction between two rydberg atoms,” *Phys. Rev. Lett.* **110**, 263201 (2013).

¹⁷³D. Barredo, S. Ravets, H. Labuhn, L. Béguin, A. Vernier, F. Nogrette, T. Lahaye, and A. Browaeys, “Demonstration of a strong rydberg blockade in three-atom systems with anisotropic interactions,” *Phys. Rev. Lett.* **112**, 183002 (2014).

¹⁷⁴H. Bernien, S. Schwartz, A. Keesling, H. Levine, A. Omran, H. Pichler, S. Choi, A. S. Zibrov, M. Endres, M. Greiner, *et al.*, “Probing many-body dynamics on a 51-atom quantum simulator,” *Nature* **551**, 579–584 (2017).

¹⁷⁵V. Lienhard, S. de Léséleuc, D. Barredo, T. Lahaye, A. Browaeys, M. Schuler, L.-P. Henry, and A. M. Läuchli, “Observing the space- and time-dependent growth of correlations in dynamically tuned synthetic ising models with antiferromagnetic interactions,” *Phys. Rev. X* **8**, 021070 (2018).

¹⁷⁶S. de Léséleuc, S. Weber, V. Lienhard, D. Barredo, H. P. Büchler, T. Lahaye, and A. Browaeys, “Accurate mapping of multilevel rydberg atoms on interacting spin-1/2 particles for the quantum simulation of ising models,” *Phys. Rev. Lett.* **120**, 113602 (2018).

¹⁷⁷A. Keesling, A. Omran, H. Levine, H. Bernien, H. Pichler, S. Choi, R. Samajdar, S. Schwartz, P. Silvi, S. Sachdev, *et al.*, “Quantum kibble-zurek mechanism and critical dynamics on a programmable rydberg simulator,” *Nature* **568**, 207–211 (2019).

¹⁷⁸S. Ebadi, T. T. Wang, H. Levine, A. Keesling, G. Semeghini, A. Omran, D. Bluvstein, R. Samajdar, H. Pichler, W. W. Ho, *et al.*, “Quantum phases of matter on a 256-atom programmable quantum simulator,” *Nature* **595**, 227–232 (2021).

¹⁷⁹P. Scholl, M. Schuler, H. J. Williams, A. A. Eberharter, D. Barredo, K.-N. Schymik, V. Lienhard, L.-P. Henry, T. C. Lang, T. Lahaye, *et al.*, “Quantum simulation of 2d antiferromagnets with hundreds of rydberg atoms,” *Nature* **595**, 233–238 (2021).

¹⁸⁰V. Bharti, S. Sugawa, M. Mizoguchi, M. Kunimi, Y. Zhang, S. de Léséleuc, T. Tomita, T. Franz, M. Weidemüller, and K. Ohmori, “Picosecond-scale ultrafast many-body dynamics in an ultracold rydberg-excited atomic mott insulator,” *Phys. Rev. Lett.* **131**, 123201 (2023).

¹⁸¹K. Kim, F. Yang, K. Mølmer, and J. Ahn, “Realization of an extremely anisotropic heisenberg magnet in rydberg atom arrays,” *Phys. Rev. X* **14**, 011025 (2024).

¹⁸²A. Omran, H. Levine, A. Keesling, G. Semeghini, T. T. Wang, S. Ebadi, H. Bernien, A. S. Zibrov, H. Pichler, S. Choi, J. Cui, M. Rossignolo, P. Rembold, S. Montangero, T. Calarco, M. Endres, M. Greiner, V. Vuletić, and M. D. Lukin, “Generation and manipulation of schrödinger cat states in rydberg atom arrays,” *Science* **365**, 570–574 (2019).

¹⁸³A. W. Glaetzle, M. Dalmonte, R. Nath, I. Rousochatzakis, R. Moessner, and P. Zoller, “Quantum spin-ice and dimer models with rydberg atoms,” *Phys. Rev. X* **4**, 041037 (2014).

¹⁸⁴A. W. Glaetzle, M. Dalmonte, R. Nath, C. Gross, I. Bloch, and P. Zoller, “Designing frustrated quantum magnets with laser-dressed rydberg atoms,” *Phys. Rev. Lett.* **114**, 173002 (2015).

¹⁸⁵D. Bluvstein, A. Omran, H. Levine, A. Keesling, G. Semeghini, S. Ebadi, T. T. Wang, A. A. Michailidis, N. Maskara, W. W. Ho, S. Choi, M. Serbyn, M. Greiner, V. Vuletić, and M. D. Lukin, “Controlling quantum many-body dynamics in driven rydberg atom arrays,” *Science* **371**, 1355–1359 (2021).

¹⁸⁶G.-X. Su, H. Sun, A. Hudomal, J.-Y. Desaules, Z.-Y. Zhou, B. Yang, J. C. Halimeh, Z.-S. Yuan, Z. Papić, and J.-W. Pan, “Observation of many-body scarring in a bose-hubbard quantum simulator,” *Phys. Rev. Res.* **5**, 023010 (2023).

¹⁸⁷X. Q. Shao, F. Liu, X. W. Xue, W. L. Mu, and W. Li, “High-fidelity interconversion between greenberger-horne-zeilinger and w states through floquet-lindblad engineering in rydberg atom arrays,” *Phys. Rev. Appl.* **20**, 014014 (2023).

¹⁸⁸Y. Zhao, Y.-Q. Yang, W. Li, and X.-Q. Shao, “Dissipative stabilization of high-dimensional GHZ states for neutral atoms,” *Applied Physics Letters* **124**, 114001 (2024).

¹⁸⁹W. D. Knight, K. Clemenger, W. A. de Heer, W. A. Saunders, M. Y. Chou, and M. L. Cohen, “Electronic shell structure and abundances of sodium clusters,” *Phys. Rev. Lett.* **52**, 2141–2143 (1984).

¹⁹⁰T. Inoshita, S. Ohnishi, and A. Oshiyama, “Electronic structure of the superatom: A quasiatomic system based on a semiconductor heterostructure,” *Phys. Rev. Lett.* **57**, 2560–2563 (1986).

¹⁹¹S. N. Khanna and P. Jena, “Atomic clusters: Building blocks for a class of solids,” *Phys. Rev. B* **51**, 13705–13716 (1995).

¹⁹²Z. Luo and A. W. Castleman, “Special and general superatoms,” *Accounts of chemical research* **47**, 2931–2940 (2014).

¹⁹³A. C. Reber and S. N. Khanna, “Superatoms: electronic and geometric effects on reactivity,” *Accounts of Chemical Research* **50**, 255–263 (2017).

¹⁹⁴A. Castleman Jr and S. Khanna, “Clusters, superatoms, and building blocks of new materials,” *The Journal of Physical Chemistry C* **113**, 2664–2675 (2009).

¹⁹⁵E. A. Doud, A. Voevodin, T. J. Hochuli, A. M. Champsaur, C. Nuckolls, and X. Roy, “Superatoms in materials science,” *Nature Reviews Materials* **5**, 371–387 (2020).

¹⁹⁶F. Yu, J. Li, Z. Liu, R. Wang, Y. Zhu, W. Huang, Z. Liu, and Z. Wang, “From atomic physics to superatomic physics,” *Journal of Cluster Science* **34**, 1691–1708 (2023).

¹⁹⁷T. Vogt, M. Viteau, J. Zhao, A. Chotia, D. Comparat, and P. Pillet, “Dipole blockade at förster resonances in high resolution laser excitation of rydberg states of cesium atoms,” *Phys. Rev. Lett.* **97**, 083003 (2006).

¹⁹⁸Y. Zeng, P. Xu, X. He, Y. Liu, M. Liu, J. Wang, D. J. Papoular, G. V. Shlyapnikov, and M. Zhan, “Entangling two individual atoms of different isotopes via rydberg blockade,” *Phys. Rev. Lett.* **119**, 160502 (2017).

¹⁹⁹R. Heidemann, U. Raitzsch, V. Bendkowsky, B. Butscher, R. Löw, and T. Pfau, “Rydberg excitation of bose-einstein condensates,” *Phys. Rev. Lett.* **100**, 033601 (2008).

²⁰⁰N. Stiesdal, H. Busche, J. Kumlin, K. Kleinbeck, H. P. Büchler, and S. Hofferberth, “Observation of collective decay dynamics of a single rydberg superatom,” *Phys. Rev. Res.* **2**, 043339 (2020).

²⁰¹T. Pohl and P. R. Berman, “Breaking the dipole blockade: Nearly resonant dipole interactions in few-atom systems,” *Phys. Rev. Lett.* **102**, 013004 (2009).

²⁰²B. Vermersch, A. W. Glaetzle, and P. Zoller, “Magic distances in the blockade mechanism of rydberg *p* and *d* states,” *Phys. Rev. A* **91**, 023411 (2015).

²⁰³A. Derevianko, P. Kómár, T. Topcu, R. M. Kroese, and M. D. Lukin, “Effects of molecular resonances on rydberg blockade,” *Phys. Rev. A* **92**, 063419 (2015).

²⁰⁴J. Honer, R. Löw, H. Weimer, T. Pfau, and H. P. Büchler, “Artificial atoms can do more than atoms: Deterministic single photon subtraction from arbitrary light fields,” *Phys. Rev. Lett.* **107**, 093601 (2011).

²⁰⁵V. Srivastava, A. Niranjan, and R. Nath, “Dynamics and quantum correlations in two independently driven rydberg atoms with distinct laser fields,” *Journal of Physics B: Atomic, Molecular and Optical Physics* **52**, 184001 (2019).

²⁰⁶W. Dür, G. Vidal, and J. I. Cirac, “Three qubits can be entangled in two inequivalent ways,” *Phys. Rev. A* **62**, 062314 (2000).

²⁰⁷A. Cabello, “Bell’s theorem with and without inequalities for the three-qubit greenberger-horne-zeilinger and w states,” *Phys. Rev. A* **65**, 032108 (2002).

²⁰⁸R. Horodecki, P. Horodecki, M. Horodecki, and K. Horodecki, “Quantum entanglement,” *Rev. Mod. Phys.* **81**, 865–942 (2009).

²⁰⁹M. Kim, K. Kim, J. Hwang, E.-G. Moon, and J. Ahn, “Rydberg quantum wires for maximum independent set problems,” *Nature Physics* **18**, 755 (2022).

²¹⁰W. Xu, A. V. Venkatramani, S. H. Cantú, T. Šumarač, V. Klüsener, M. D. Lukin, and V. Vuletić, “Fast preparation and detection of a rydberg qubit using atomic ensembles,” *Phys. Rev. Lett.* **127**, 050501 (2021).

²¹¹N. L. R. Spong, Y. Jiao, O. D. W. Hughes, K. J. Weatherill, I. Lesanovsky, and C. S. Adams, “Collectively encoded rydberg qubit,” *Phys. Rev. Lett.* **127**, 063604 (2021).

²¹²C. Ates, T. Pohl, T. Pattard, and J. M. Rost, “Antiblockade in rydberg excitation of an ultracold lattice gas,” *Phys. Rev. Lett.* **98**, 023002 (2007).

²¹³T. Amthor, C. Giese, C. S. Hofmann, and M. Weidemüller, “Evidence of antiblockade in an ultracold rydberg gas,” *Phys. Rev. Lett.* **104**, 013001 (2010).

²¹⁴N. Henkel, R. Nath, and T. Pohl, “Three-dimensional roton excitations and supersolid formation in rydberg-excited bose-einstein condensates,” *Phys. Rev. Lett.* **104**, 195302 (2010).

²¹⁵G. Pupillo, A. Micheli, M. Boninsegni, I. Lesanovsky, and P. Zoller, “Strongly correlated gases of rydberg-dressed atoms: Quantum and classical dynamics,” *Phys. Rev. Lett.* **104**, 223002 (2010).

²¹⁶J. E. Johnson and S. L. Rolston, “Interactions between rydberg-dressed atoms,” *Phys. Rev. A* **82**, 033412 (2010).

²¹⁷W. Li, L. Hamadeh, and I. Lesanovsky, “Probing the interaction between rydberg-dressed atoms through interference,” *Phys. Rev. A* **85**, 053615 (2012).

²¹⁸J. B. Balewski, A. T. Krupp, A. Gaj, S. Hofferberth, R. Löw, and T. Pfau, “Rydberg dressing: understanding of collective many-body effects and implications for experiments,” *New Journal of Physics* **16**, 063012 (2014).

²¹⁹Y.-Y. Jau, A. Hankin, T. Keating, I. H. Deutsch, and G. Biedermann, “Entangling atomic spins with a rydberg-dressed spin-flip blockade,” *Nature Physics* **12**, 71–74 (2016).

²²⁰X. Q. Shao, D. X. Li, Y. Q. Ji, J. H. Wu, and X. X. Yi, “Ground-state blockade of rydberg atoms and application in entanglement generation,” *Phys. Rev. A* **96**, 012328 (2017).

²²¹A. Cidrim, T. S. do Espírito Santo, J. Schachenmayer, R. Kaiser, and R. Bachelard, “Photon blockade with ground-state neutral atoms,” *Phys. Rev. Lett.* **125**, 073601 (2020).

²²²D. X. Li and X. Q. Shao, “Unconventional rydberg pumping and applications in quantum information processing,” *Phys. Rev. A* **98**, 062338 (2018).

²²³X.-Q. Shao, “Selective rydberg pumping via strong dipole blockade,” *Phys. Rev. A* **102**, 053118 (2020).

²²⁴D. J. Bradley, P. Ewart, J. V. Nicholas, and J. R. D. Shaw, “Excited state absorption spectroscopy of alkaline earths selectively pumped by tunable dye lasers. i. barium arc spectra,” *Journal of Physics B: Atomic and Molecular Physics* **6**, 1594 (1973).

²²⁵R. Stebbings and F. Dunning, *Rydberg States of Atoms and Molecules* (Cambridge University Press, 1983).

²²⁶B. K. Teo, D. Feldbaum, T. Cubel, J. R. Guest, P. R. Berman, and G. Raithel, “Autler-townes spectroscopy of the $5S_{1/2}-5p_{3/2}-4d$ cascade of cold ^{85}Rb atoms,” *Phys. Rev. A* **68**, 053407 (2003).

²²⁷I. S. Madjarov, J. P. Covey, A. L. Shaw, J. Choi, A. Kale, A. Cooper, H. Pichler, V. Schkolnik, J. R. Williams, and M. Endres, “High-fidelity entanglement and detection of alkaline-earth rydberg atoms,” *Nature Physics* **16**, 857–861 (2020).

²²⁸J. Wang, J. Bai, J. He, and J. Wang, “Single-photon cesium rydberg excitation spectroscopy using 318.6-nm uv laser and room-temperature vapor cell,” *Opt. Express* **25**, 22510–22518 (2017).

²²⁹P. Thoumany, T. Hänsch, G. Stania, L. Urbonas, and T. Becker, “Optical spectroscopy of rubidium rydberg atoms with a 297 nm frequency-doubled dye laser,” *Opt. Lett.* **34**, 1621–1623 (2009).

²³⁰A. M. Hankin, Y.-Y. Jau, L. P. Parazzoli, C. W. Chou, D. J. Armstrong, A. J. Landahl, and G. W. Biedermann, “Two-atom rydberg blockade using direct $6s$ to np excitation,” *Phys. Rev. A* **89**, 033416 (2014).

²³¹L. Li and A. Kuzmich, “Quantum memory with strong and controllable rydberg-level interactions,” *Nature Communications* **7**, 13618 (2016).

²³²H. Levine, A. Keesling, A. Omran, H. Bernien, S. Schwartz, A. S. Zibrov, M. Endres, M. Greiner, V. Vuletić, and M. D. Lukin, “High-fidelity control and entanglement of rydberg-atom qubits,” *Phys. Rev. Lett.* **121**, 123603 (2018).

²³³L. Li, W. Huie, N. Chen, B. DeMarco, and J. P. Covey, “Active cancellation of servo-induced noise on stabilized lasers via feedforward,” *Phys. Rev. Appl.* **18**, 064005 (2022).

²³⁴I. I. Ryabtsev, I. I. Beterov, D. B. Tretyakov, V. M. Entin, and E. A. Yakshina, “Doppler- and recoil-free laser excitation of rydberg states via three-photon transitions,” *Phys. Rev. A* **84**, 053409 (2011).

²³⁵Z. Fu, P. Xu, Y. Sun, Y.-Y. Liu, X.-D. He, X. Li, M. Liu, R.-B. Li, J. Wang, L. Liu, and M.-S. Zhan, “High-fidelity entanglement of neutral atoms via a rydberg-mediated single-modulated-pulse controlled-phase gate,” *Phys. Rev. A* **105**, 042430 (2022).

²³⁶S. J. Evered, D. Bluvstein, M. Kalinowski, S. Ebadi, T. Manovitz, H. Zhou, S. H. Li, A. A. Geim, T. T. Wang, N. Maskara, H. Levine, G. Semeghini, M. Greiner, V. Vuletić, and M. D. Lukin, “High-fidelity parallel entangling gates on a neutral-atom quantum computer,” *Nature* **622**, 268–272 (2023).

²³⁷S. de Léséleuc, D. Barredo, V. Lienhard, A. Browaeys, and T. Lahaye, “Analysis of imperfections in the coherent optical excitation of single atoms to rydberg states,” *Phys. Rev. A* **97**, 053803 (2018).

²³⁸Y.-X. Chao, Z.-X. Hua, X.-H. Liang, Z.-P. Yue, L. You, and M. K. Tey, “Pound-drever-hall feedforward: Laser phase noise suppression beyond feedback,” *arXiv preprint arXiv:2309.09759* (2023).

²³⁹J. Kumlin, C. Braun, C. Tresp, N. Stiesdal, S. Hofferberth, and A. Paris-Mandoki, “Quantum optics with rydberg superatoms,” *Journal of Physics Communications* **7**, 050201 (2023).

²⁴⁰I. I. Rabi, S. Millman, P. Kusch, and J. R. Zacharias, “The molecular beam resonance method for measuring nuclear magnetic moments. The magnetic moments of ${}^3\text{Li}^6$, ${}^3\text{Li}^7$ and ${}^9\text{F}^{19}$,” *Phys. Rev.* **55**, 526–535 (1939).

²⁴¹R. H. Dicke, “Coherence in spontaneous radiation processes,” *Phys. Rev.* **93**, 99–110 (1954).

²⁴²F. W. Cummings and A. Dorri, “Exact solution for spontaneous emission in the presence of N atoms,” *Phys. Rev. A* **28**, 2282–2285 (1983).

²⁴³L. Isenhower, E. Urban, X. L. Zhang, A. T. Gill, T. Henage, T. A. Johnson, T. G. Walker, and M. Saffman, “Demonstration of a neutral atom controlled-not quantum gate,” *Phys. Rev. Lett.* **104**, 010503 (2010).

²⁴⁴M. Ebert, A. Gill, M. Gibbons, X. Zhang, M. Saffman, and T. G. Walker, “Atomic fock state preparation using rydberg blockade,” *Phys. Rev. Lett.* **112**, 043602 (2014).

²⁴⁵A. Paris-Mandoki, C. Braun, J. Kumlin, C. Tresp, I. Mirgorodskiy, F. Christaller, H. P. Büchler, and S. Hofferberth, “Free-space quantum electrodynamics with a single rydberg superatom,” *Phys. Rev. X* **7**, 041010 (2017).

²⁴⁶H. Labuhn, D. Barredo, S. Ravets, S. De Léséleuc, T. Macrì, T. Lahaye, and A. Browaeys, “Tunable two-dimensional arrays of single Rydberg atoms for realizing quantum Ising models,” *Nature* **534**, 667–670 (2016).

²⁴⁷M. Saffman and T. G. Walker, “Creating single-atom and single-photon sources from entangled atomic ensembles,” *Phys. Rev. A* **66**, 065403 (2002).

²⁴⁸V. Vuletić, “When superatoms talk photons,” *Nat. Phys.* **2**, 801–802 (2006).

²⁴⁹O. Firstenberg, T. Peyronel, Q.-Y. Liang, A. V. Gorshkov, M. D. Lukin, and V. Vuletić, “Attractive photons in a quantum nonlinear medium,” *Nature* **502**, 71–75 (2013).

²⁵⁰J. D. Thompson, T. L. Nicholson, Q.-Y. Liang, S. H. Cantu, A. V. Venkatramani, S. Choi, I. A. Fedorov, D. Viscor, T. Pohl, M. D. Lukin, and V. Vuletić, “Symmetry-protected collisions between strongly interacting photons,” *Nature* **542**, 206–209 (2017).

²⁵¹Z. Bai, C. S. Adams, G. Huang, and W. Li, “Self-induced transparency in warm and strongly interacting rydberg gases,” *Phys. Rev. Lett.* **125**, 263605 (2020).

²⁵²P. Berman and V. Malinovsky, *Principles of Laser Spectroscopy and Quantum Optics* (Princeton University Press, 2011).

²⁵³Y. O. Dudin, L. Li, and A. Kuzmich, “Light storage on the time scale of a minute,” *Phys. Rev. A* **87**, 031801 (2013).

²⁵⁴S. Zhang, F. Robicheaux, and M. Saffman, “Magic-wavelength optical traps for rydberg atoms,” *Phys. Rev. A* **84**, 043408 (2011).

²⁵⁵M. Saffman and T. G. Walker, “Analysis of a quantum logic device based on dipole-dipole interactions of optically trapped rydberg atoms,” *Phys. Rev. A* **72**, 022347 (2005).

²⁵⁶L. Li, Y. O. Dudin, and A. Kuzmich, “Entanglement between light and an optical atomic excitation,” *Nature* **498**, 466–469 (2013).

²⁵⁷J. Lampen, H. Nguyen, L. Li, P. R. Berman, and A. Kuzmich, “Long-lived coherence between ground and rydberg levels in a magic-wavelength lattice,” *Phys. Rev. A* **98**, 033411 (2018).

²⁵⁸Y. Mei, Y. Li, H. Nguyen, P. R. Berman, and A. Kuzmich, “Trapped alkali-metal rydberg qubit,” *Phys. Rev. Lett.* **128**, 123601 (2022).

²⁵⁹S. Schmidt-Eberle, T. Stolz, G. Rempe, and S. Dürr, “Dark-time decay of the retrieval efficiency of light stored as a rydberg excitation in a noninteracting ultracold gas,” *Phys. Rev. A* **101**, 013421 (2020).

²⁶⁰S. Kurzyna, B. Niewelt, M. Mazelanik, W. Wasilewski, and M. Parniak, “Long-lived collective rydberg excitations in atomic gas achieved via a stark lattice modulation,” (2024), *arXiv:2402.06513 [quant-ph]*.

²⁶¹F. Bariani, Y. O. Dudin, T. A. B. Kennedy, and A. Kuzmich, “Dephasing of multiparticle rydberg excitations for fast entanglement generation,” *Phys. Rev. Lett.* **108**, 030501 (2012).

²⁶²J. Stanojevic, V. Parigi, E. Bimbard, A. Ourjoumtsev, P. Pillet, and P. Grangier, “Generating non-gaussian states using collisions between rydberg polaritons,” *Phys. Rev. A* **86**, 021403 (2012).

²⁶³Y. Li, Y. Mei, H. Nguyen, P. R. Berman, and A. Kuzmich, “Dynamics of collective-dephasing-induced multiatom entanglement,” *Phys. Rev. A* **106**, L051701 (2022).

²⁶⁴P. R. Berman and A. Kuzmich, “Interplay of the dipole blockade and interaction-induced dephasing in rydberg single-photon sources,” *Phys. Rev. A* **109**, 013710 (2024).

²⁶⁵H. Busche, P. Huillery, S. W. Ball, T. Ilieva, M. P. A. Jones, and C. Adams, “Contactless nonlinear optics mediated by long-range rydberg interactions,” *Nature Physics* **13**, 655–658 (2017).

²⁶⁶C. Gaul, B. J. DeSalvo, J. A. Aman, F. B. Dunning, T. C. Killian, and T. Pohl, “Resonant rydberg dressing of alkaline-earth atoms via electromagnetically induced transparency,” *Phys. Rev. Lett.* **116**, 243001 (2016).

²⁶⁷H. Jo, Y. Song, M. Kim, and J. Ahn, “Rydberg atom entanglements in the weak coupling regime,” *Phys. Rev. Lett.* **124**, 033603 (2020).

²⁶⁸M. Reetz-Lamour, T. Amthor, J. Deiglmayr, and M. Weidemüller, “Rabi oscillations and excitation trapping in the coherent excitation of a mesoscopic frozen rydberg gas,” *Phys. Rev. Lett.* **100**, 253001 (2008).

²⁶⁹K. J. Weatherill, J. D. Pritchard, R. P. Abel, M. G. Bason, A. K. Mohapatra, and C. S. Adams, “Electromagnetically induced transparency of an interacting cold rydberg ensemble,” *Journal of Physics B: Atomic, Molecular and Optical Physics* **41**, 201002 (2008).

²⁷⁰M. Müller, I. Lesanovsky, H. Weimer, H. P. Büchler, and P. Zoller, “Mesoscopic rydberg gate based on electromagnetically induced transparency,” *Phys. Rev. Lett.* **102**, 170502 (2009).

²⁷¹A. Micheli, A. J. Daley, D. Jaksch, and P. Zoller, “Single atom transistor in a 1d optical lattice,” *Phys. Rev. Lett.* **93**, 140408 (2004).

²⁷²B. T. Seaman, M. Krämer, D. Z. Anderson, and M. J. Holland, “Atomtronics: Ultracold-atom analogs of electronic devices,” *Phys. Rev. A* **75**, 023615 (2007).

²⁷³G. F. Xu, J. Zhang, D. M. Tong, E. Sjöqvist, and L. C. Kwek, “Nonadiabatic holonomic quantum computation in decoherence-free subspaces,” *Phys. Rev. Lett.* **109**, 170501 (2012).

²⁷⁴P. Z. Zhao, X. Wu, T. H. Xing, G. F. Xu, and D. M. Tong, “Nonadiabatic holonomic quantum computation with rydberg superatoms,” *Phys. Rev. A* **98**, 032313 (2018).

²⁷⁵P. Maity and M. Purkait, “Implementation of a holonomic 3-qubit gate using rydberg superatoms in a microwave cavity,” *The European Physical Journal Plus* **137**, 1299 (2022).

²⁷⁶C.-Y. Guo, L.-L. Yan, S. Zhang, S.-L. Su, and W. Li, “Optimized geometric quantum computation with a mesoscopic ensemble of rydberg atoms,” *Phys. Rev. A* **102**, 042607 (2020).

²⁷⁷M. Ebert, M. Kwon, T. G. Walker, and M. Saffman, “Coherence and rydberg blockade of atomic ensemble qubits,” *Phys. Rev. Lett.* **115**, 093601 (2015).

²⁷⁸I. I. Beterov, M. Saffman, E. A. Yakshina, D. B. Tretyakov, V. M. Entin, G. N. Hamzina, and I. I. Ryabtsev, “Simulated quantum process tomography of quantum gates with rydberg superatoms,” *Journal of Physics B: Atomic, Molecular and Optical Physics* **49**, 114007 (2016).

²⁷⁹P. Scholl, A. L. Shaw, R. B.-S. Tsai, R. Finkelstein, J. Choi, and M. Endres, “Erasure conversion in a high-fidelity rydberg quantum simulator,” *Nature* **622**, 273–278 (2023).

²⁸⁰S. Ma, G. Liu, P. Peng, B. Zhang, S. Jandura, J. Claes, A. P. Burgers, G. Pupillo, S. Puri, and J. D. Thompson, “High-fidelity gates and mid-circuit erasure conversion in an atomic qubit,” *Nature* **622**, 279–284 (2023).

²⁸¹J. C. Garcia-Escartin and P. Chamorro-Posada, “Counterfactual rydberg gate for photons,” *Phys. Rev. A* **85**, 032309 (2012).

²⁸²D. Paredes-Barato and C. S. Adams, “All-optical quantum information processing using rydberg gates,” *Phys. Rev. Lett.* **112**, 040501 (2014).

²⁸³Y. M. Hao, G. W. Lin, K. Xia, X. M. Lin, Y. P. Niu, and S. Q. Gong, “Quantum controlled-phase-flip gate between a flying optical photon and a rydberg atomic ensemble,” *Scientific Reports* **5**, 10005 (2015).

²⁸⁴S. Das, A. Grankin, I. Iakourov, E. Brion, J. Borregaard, R. Boddeda, I. Usmani, A. Ourjoumtsev, P. Grangier, and A. S. Sørensen, “Photonic controlled-phase gates through rydberg blockade in optical cavities,” *Phys. Rev. A* **93**, 040303 (2016).

²⁸⁵L. Sárkány, J. Fortágh, and D. Petrosyan, “Long-range quantum gate via rydberg states of atoms in a thermal microwave cavity,” *Phys. Rev. A* **92**, 030303 (2015).

²⁸⁶F. Cesa and H. Pichler, “Universal quantum computation in globally driven rydberg atom arrays,” *Phys. Rev. Lett.* **131**, 170601 (2023).

²⁸⁷R. Prevedel, G. Cronenberg, M. S. Tame, M. Paternostro, P. Walther, M. S. Kim, and A. Zeilinger, “Experimental realization of dicke states of up to six qubits for multiparty quantum networking,” *Phys. Rev. Lett.* **103**, 020503 (2009).

²⁸⁸W. Wieczorek, R. Krischek, N. Kiesel, P. Michelberger, G. Tóth, and H. Weinfurter, “Experimental entanglement of a six-photon symmetric dicke state,” *Phys. Rev. Lett.* **103**, 020504 (2009).

²⁸⁹H. Häffner, W. Hänsel, C. F. Roos, J. Benhelm, D. Chek-al kar, M. Chwalla, T. Körber, U. D. Rapol, M. Riebe, P. O. Schmidt, C. Becher, O. Gühne, W. Dür, and R. Blatt, “Scalable multiparticle entanglement of trapped ions,” *Nature* **438**, 643–646 (2005).

²⁹⁰M. Zwierz and P. Kok, “High-efficiency cluster-state generation with atomic ensembles via the dipole-blockade mechanism,” *Phys. Rev. A* **79**, 022304 (2009).

²⁹¹M. Khazali, “Progress towards macroscopic spin and mechanical superposition via rydberg interaction,” *Phys. Rev. A* **98**, 043836 (2018).

²⁹²M. Gärttner, “Heralded *w*-state preparation using laser-designed superatoms,” *Phys. Rev. A* **92**, 013629 (2015).

²⁹³Y. Ji, Y. Liu, H. Li, X. Zhou, R. Xiao, L. Dong, and X.-M. Xiu, “Fast preparation of bell state and *w* state with rydberg superatom,” *Quantum Information Processing* **19**, 1–12 (2020).

²⁹⁴Y.-L. Liu, Y.-Q. Ji, X. Han, W.-X. Cui, S. Zhang, and H.-F. Wang, “Fast conversion of three-particle dicke states to four-particle dicke states with rydberg superatoms,” *Advanced Quantum Technologies* **6**, 2200173 (2023).

²⁹⁵W. Y. Zhang, Y. L. Liu, Y. Q. Ji, L. Dong, and X. M. Xiu, “Fusing atomic *w* states with rydberg superatom,” *Laser Physics Letters* **19**, 055206 (2022).

²⁹⁶J. Li, M.-T. Zhou, C.-W. Yang, P.-F. Sun, J.-L. Liu, X.-H. Bao, and J.-W. Pan, “Semideterministic entanglement between a single photon and an atomic ensemble,” *Phys. Rev. Lett.* **123**, 140504 (2019).

²⁹⁷P.-F. Sun, Y. Yu, Z.-Y. An, J. Li, C.-W. Yang, X.-H. Bao, and J.-W. Pan, “Deterministic time-bin entanglement between a single photon and an atomic ensemble,” *Phys. Rev. Lett.* **128**, 060502 (2022).

²⁹⁸W. Heisenberg and H. Euler, “Folgerungen aus der diracschen theorie des positrons,” *Zeitschrift für Physik* **98**, 714–732 (1936).

²⁹⁹J.-W. Pan, Z.-B. Chen, C.-Y. Lu, H. Weinfurter, A. Zeilinger, and M. Żukowski, “Multiphoton entanglement and interferometry,” *Rev. Mod. Phys.* **84**, 777–838 (2012).

³⁰⁰H.-S. Zhong, Y. Li, W. Li, L.-C. Peng, Z.-E. Su, Y. Hu, Y.-M. He, X. Ding, W. Zhang, H. Li, L. Zhang, Z. Wang, L. You, X.-L. Wang, X. Jiang, L. Li, Y.-A. Chen, N.-L. Liu, C.-Y. Lu, and J.-W. Pan, “12-photon entanglement and scalable scattershot boson sampling with optimal entangled-photon pairs from parametric down-conversion,” *Phys. Rev. Lett.* **121**, 250505 (2018).

³⁰¹K. M. Gheri, C. Saavedra, P. Törmä, J. I. Cirac, and P. Zoller, “Entanglement engineering of one-photon wave packets using a single-atom source,” *Phys. Rev. A* **58**, R2627–R2630 (1998).

³⁰²C. Schön, E. Solano, F. Verstraete, J. I. Cirac, and M. M. Wolf, “Sequential generation of entangled multiqubit states,” *Phys. Rev. Lett.* **95**, 110503 (2005).

³⁰³C.-W. Yang, Y. Yu, J. Li, B. Jing, X.-H. Bao, and J.-W. Pan, “Sequential generation of multiphoton entanglement with a rydberg superatom,” *Nature Photonics* **16**, 658–661 (2022).

³⁰⁴H. Weimer, “Variational analysis of driven-dissipative rydberg gases,” *Phys. Rev. A* **91**, 063401 (2015).

³⁰⁵W. Lechner and P. Zoller, “Spatial patterns in rydberg excitations from logarithmic pair interactions,” *Phys. Rev. Lett.* **115**, 125301 (2015).

³⁰⁶D. Ding, Z. Bai, Z. Liu, B. Shi, G. Guo, W. Li, and C. S. Adams, “Ergodicity breaking from Rydberg clusters in a driven-dissipative many-body system,” **10**, eadl5893.

³⁰⁷B. Sun and F. Robicheaux, “Numerical study of two-body correlation in a 1d lattice with perfect blockade,” *New Journal of Physics* **10**, 045032 (2008).

³⁰⁸B. Olmos, M. Müller, and I. Lesanovsky, “Thermalization of a strongly interacting 1d rydberg lattice gas,” *New Journal of Physics* **12**, 013024 (2010).

³⁰⁹R. M. W. van Bijnen, S. Smit, K. A. H. van Leeuwen, E. J. D. Vredenbregt, and S. J. J. M. F. Kokkelmans, “Adiabatic formation of rydberg crystals with chirped laser pulses,” *Journal of Physics B: Atomic, Molecular and Optical Physics* **44**, 184008 (2011).

³¹⁰F. Letscher, D. Petrosyan, and M. Fleischhauer, “Many-body dynamics of holes in a driven, dissipative spin chain of rydberg superatoms,” *New Journal of Physics* **19**, 113014 (2017).

³¹¹M. Kim, Y. Song, J. Kim, and J. Ahn, “Quantum ising hamiltonian programming in trio, quartet, and sextet qubit systems,” *PRX Quantum* **1**, 020323 (2020).

³¹²A. Byun, M. Kim, and J. Ahn, “Finding the maximum independent sets of platonic graphs using rydberg atoms,” *PRX Quantum* **3**, 030305 (2022).

³¹³S. Jeong, M. Kim, M. Hhan, J. Park, and J. Ahn, “Quantum programming of the satisfiability problem with rydberg atom graphs,” *Phys. Rev. Res.* **5**, 043037 (2023).

³¹⁴I. I. Beterov, T. Andrijauskas, D. B. Tretyakov, V. M. Entin, E. A. Yakshina, I. I. Ryabtsev, and S. Bergamini, “Jaynes-cummings dynamics in mesoscopic ensembles of rydberg-blockaded atoms,” *Phys. Rev. A* **90**, 043413 (2014).

³¹⁵M. Fleischhauer, A. Imamoglu, and J. P. Marangos, “Electromagnetically induced transparency: Optics in coherent media,” *Rev. Mod. Phys.* **77**, 633–673 (2005).

³¹⁶D. E. Chang, V. Vuletić, and M. D. Lukin, “Quantum nonlinear optics—photon by photon,” *Nature Photonics* **8**, 685–694 (2014).

³¹⁷D. Petrosyan, J. Otterbach, and M. Fleischhauer, “Electromagnetically induced transparency with rydberg atoms,” *Phys. Rev. Lett.* **107**, 213601 (2011).

³¹⁸Y.-M. Liu, D. Yan, X.-D. Tian, C.-L. Cui, and J.-H. Wu, “Electromagnetically induced transparency with cold rydberg atoms: Superatom model beyond the weak-probe approximation,” *Phys. Rev. A* **89**, 033839 (2014).

³¹⁹J.-H. Wu, M. Artoni, and G. C. La Rocca, “Polarization-selective optical nonlinearities in cold rydberg atoms,” *Phys. Rev. A* **92**, 063805 (2015).

³²⁰Y.-M. Liu, X.-D. Tian, X. Wang, D. Yan, and J.-H. Wu, “Cooperative nonlinear grating sensitive to light intensity and photon correlation,” *Opt. Lett.* **41**, 408–411 (2016).

³²¹S. Asghar, Ziauddin, S. Qamar, and S. Qamar, “Electromagnetically induced grating with rydberg atoms,” *Phys. Rev. A* **94**, 033823 (2016).

³²²M. Gärttner, S. Whitlock, D. W. Schönleber, and J. Evers, “Semianalytical model for nonlinear absorption in strongly interacting rydberg gases,” *Phys. Rev. A* **89**, 063407 (2014).

³²³Z. Bai and G. Huang, “Enhanced third-order and fifth-order kerr nonlinearities in a cold atomic system via rydberg-rydberg interaction,” *Opt. Express* **24**, 4442–4461 (2016).

³²⁴Z. Bai, W. Li, and G. Huang, “Stable single light bullets and vortices and their active control in cold rydberg gases,” *Optica* **6**, 309–317 (2019).

³²⁵D.-D. Zheng, H.-M. Zhao, X.-J. Zhang, and J.-H. Wu, “Correlation-enhanced goos-hänchen shift in rydberg atomic gases,” *Phys. Rev. A* **106**, 043119 (2022).

³²⁶H.-M. Zhao, X.-J. Zhang, M. Artoni, G. C. L. Rocca, and J.-H. Wu, “Biphoton generation enhanced by nonlocal nonlinearity via rydberg interactions,” *Opt. Lett.* **48**, 5105–5108 (2023).

³²⁷E. Distante, A. Padrón-Brito, M. Cristiani, D. Paredes-Barato, and H. de Riedmatten, “Storage enhanced nonlinearities in a cold atomic rydberg ensemble,” *Phys. Rev. Lett.* **117**, 113001 (2016).

³²⁸X.-D. Tian, Y.-M. Liu, Q.-Q. Bao, J.-H. Wu, M. Artoni, and G. C. La Rocca, “Nonclassical storage and retrieval of a multiphoton pulse in cold rydberg atoms,” *Phys. Rev. A* **97**, 043811 (2018).

³²⁹A. V. Gorshkov, R. Nath, and T. Pohl, “Dissipative many-body quantum optics in rydberg media,” *Phys. Rev. Lett.* **110**, 153601 (2013).

³³⁰E. Zeuthen, M. J. Gullans, M. F. Maghrebi, and A. V. Gorshkov, “Correlated photon dynamics in dissipative rydberg media,” *Phys. Rev. Lett.* **119**, 043602 (2017).

³³¹L. Yang, B. He, J.-H. Wu, Z. Zhang, and M. Xiao, “Interacting photon pulses in a rydberg medium,” *Optica* **3**, 1095–1103 (2016).

³³²N. Stiesdal, H. Busche, K. Kleinbeck, J. Kumlin, M. G. Hansen, H. P. Büchler, and S. Hofferberth, “Controlled multi-photon subtraction with cascaded rydberg superatoms as single-photon absorbers,” *Nature Communications* **12**, 4328 (2021).

³³³J. Lampen, A. Duspayev, H. Nguyen, H. Tamura, P. R. Berman, and A. Kuzmich, “Hanbury brown-twiss correlations for a driven superatom,” *Phys. Rev. Lett.* **123**, 203603 (2019).

³³⁴I. Aharonovich, D. Englund, and M. Toth, “Solid-state single-photon emitters,” *Nat. Photon.* **10**, 631–641 (2016).

³³⁵D. Petrosyan and K. Mølmer, “Deterministic free-space source of single photons using rydberg atoms,” *Phys. Rev. Lett.* **121**, 123605 (2018).

³³⁶W. Li, D. Viscor, S. Hofferberth, and I. Lesanovsky, “Electromagnetically induced transparency in an entangled medium,” *Phys. Rev. Lett.* **112**, 243601 (2014).

³³⁷E. Distante, P. Farrera, A. Padrón-Brito, D. Paredes-Barato, G. Heinze, and H. De Riedmatten, “Storing single photons emitted by a quantum memory on a highly excited rydberg state,” *Nature communications* **8**, 14072 (2017).

³³⁸H. Zhang, J. Wu, M. Artoni, and G. C. La Rocca, “Single-photon-level light storage with distributed rydberg excitations in cold atoms,” *Frontiers of Physics* **17**, 22502 (2022).

³³⁹D. Tiarks, S. Baur, K. Schneider, S. Dürr, and G. Rempe, “Single-photon transistor using a förster resonance,” *Phys. Rev. Lett.* **113**, 053602 (2014).

³⁴⁰C. Guerlin, E. Brion, T. Esslinger, and K. Mølmer, “Cavity quantum electrodynamics with a rydberg-blocked atomic ensemble,” *Phys. Rev. A* **82**, 053832 (2010).

³⁴¹X.-Q. Shao, J.-H. Wu, and X.-X. Yi, “Dissipative stabilization of quantum-feedback-based multipartite entanglement with rydberg atoms,” *Phys. Rev. A* **95**, 022317 (2017).

³⁴²H. Kübler, D. Booth, J. Sedlacek, P. Zabawa, and J. P. Shaffer, “Exploiting the coupling between a rydberg atom and a surface phonon polariton for single-photon subtraction,” *Phys. Rev. A* **88**, 043810 (2013).

³⁴³D. Yan, Z.-H. Wang, C.-N. Ren, H. Gao, Y. Li, and J.-H. Wu, “Duality and bistability in an optomechanical cavity coupled to a rydberg superatom,” *Phys. Rev. A* **91**, 023813 (2015).

³⁴⁴F. Bariani, J. Otterbach, H. Tan, and P. Meystre, “Single-atom quantum control of macroscopic mechanical oscillators,” *Phys. Rev. A* **89**, 011801 (2014).

³⁴⁵A. Carnele, B. Vogell, K. Stannigel, and P. Zoller, “Opto-nanomechanics strongly coupled to a rydberg superatom: coherent versus incoherent dynamics,” *New Journal of Physics* **16**, 063042 (2014).

³⁴⁶N. Stiesdal, J. Kumlin, K. Kleinbeck, P. Lunt, C. Braun, A. Paris-Mandoki, C. Tresp, H. P. Büchler, and S. Hofferberth, “Observation of three-body correlations for photons coupled to a rydberg superatom,” *Phys. Rev. Lett.* **121**, 103601 (2018).

³⁴⁷C.-W. Yang, J. Li, M.-T. Zhou, X. Jiang, X.-H. Bao, and J.-W. Pan, “Deterministic measurement of a rydberg superatom qubit via cavity-enhanced single-photon emission,” *Optica* **9**, 853–858 (2022).

³⁴⁸J. Sheng, Y. Chao, and J. P. Shaffer, “Strong coupling of rydberg atoms and surface phonon polaritons on piezoelectric superlattices,” *Phys. Rev. Lett.* **117**, 103201 (2016).

³⁴⁹L. W. Clark, N. Jia, N. Schine, C. Baum, A. Georgakopoulos, and J. Simon, “Interacting floquet polaritons,” *Nature* **571**, 532–536 (2019).

³⁵⁰L. W. Clark, N. Schine, C. Baum, N. Jia, and J. Simon, “Observation of Laughlin states made of light,” *Nature* **582**, 41–45 (2020).

³⁵¹J. Vaneechloo, S. Garcia, and A. Ourjoumtsev, “Intracavity rydberg superatom for optical quantum engineering: Coherent control, single-shot detection, and optical π phase shift,” *Phys. Rev. X* **12**, 021034 (2022).

³⁵²V. Magro, J. Vaneechloo, S. Garcia, and A. Ourjoumtsev, “Deterministic freely propagating photonic qubits with negative wigner functions,” *Nature Photonics* **17**, 688–693 (2023).

³⁵³S. Kumar, J. Sheng, J. A. Sedlacek, H. Fan, and J. P. Shaffer, “Collective state synthesis in an optical cavity using rydberg atom dipole blockade,” *Journal of Physics B: Atomic, Molecular and Optical Physics* **49**, 064014 (2016).

³⁵⁴A. Guttridge, D. K. Ruttle, A. C. Baldock, R. González-Férez, H. R. Sadeghpour, C. S. Adams, and S. L. Cornish, “Observation of rydberg blockade due to the charge-dipole interaction between an atom and a polar molecule,” *Phys. Rev. Lett.* **131**, 013401 (2023).

³⁵⁵E. Kuznetsova, S. T. Rittenhouse, H. R. Sadeghpour, and S. F. Yelin, “Rydberg atom mediated polar molecule interactions: a tool for molecular-state conditional quantum gates and individual addressability,” *Phys. Chem. Chem. Phys.* **13**, 17115–17121 (2011).

³⁵⁶K. Wang, C. P. Williams, L. R. Picard, N. Y. Yao, and K.-K. Ni, “Enriching the quantum toolbox of ultracold molecules with rydberg atoms,” *PRX Quantum* **3**, 030339 (2022).

³⁵⁷C. Zhang and M. Tarbutt, “Quantum computation in a hybrid array of molecules and rydberg atoms,” *PRX Quantum* **3**, 030340 (2022).

³⁵⁸S. Rammohan, A. K. Chauhan, R. Nath, A. Eisfeld, and S. Wüster, “Tailoring bose-einstein-condensate environments for a rydberg impurity,” *Phys. Rev. A* **103**, 063307 (2021).

³⁵⁹A. Mokhberi, M. Hennrich, and F. Schmidt-Kaler, “Chapter four - trapped rydberg ions: A new platform for quantum information processing,” *Advances In Atomic, Molecular, and Optical Physics* **69**, 233 (2020).

³⁶⁰M. Antezza, C. Braggio, G. Carugno, A. Noto, R. Passante, L. Rizzato, G. Ruoso, and S. Spagnolo, “Optomechanical rydberg-atom excitation via dynamic casimir-polder coupling,” *Phys. Rev. Lett.* **113**, 023601 (2014).